
Report No. FHWA-KS-08-8
FINAL REPORT

**ACCELERATED TESTING FOR STUDYING
PAVEMENT DESIGN AND PERFORMANCE (FY 2004):
THIN BONDED RIGID OVERLAY ON PCCP AND HMA
(CISL EXPERIMENT NO. 13)**

Stefan Roamnoschi, Ph.D., P.E.*

Cristian Dumitru

Paul Lewis

Mustaque Hossain, Ph.D., P.E.

Kansas State University

Manhattan, Kansas

*Currently affiliated with the University of Texas at Arlington

March 2009

KANSAS DEPARTMENT OF TRANSPORTATION

**Division of Operations
Bureau of Materials and Research**



1 Report No. FHWA-KS-08-8	2 Government Accession No.	3 Recipient Catalog No.	
4 Title and Subtitle Accelerated Testing for Studying Pavement Design and Performance (FY 2004): Thin Bonded Rigid Overlay on PCCP and HMA (CISL Experiment No. 13)		5 Report Date March 2009	6 Performing Organization Code
		8 Performing Organization Report No.	
7 Author(s) Stefan Romanoschi, Ph.D., P.E.*, Cristian Dumitru, Paul Lewis, Mustaque Hossain, Ph.D., P.E. *currently affiliated with the University of Texas at Arlington		10 Work Unit No. (TR AIS)	
9 Performing Organization Name and Address Kansas State University Department of Civil Engineering 2118 Fiedler Hall Manhattan, Kansas 66506		11 Contract or Grant No. C1436	
		13 Type of Report and Period Covered Final Report August 2003 - July 2008	
12 Sponsoring Agency Name and Address Kansas Department of Transportation Bureau of Materials and Research 700 SW Harrison Street Topeka, Kansas 66603-3745		14 Sponsoring Agency Code RE-0328-01	
		15 Supplementary Notes For more information write to address in block 9.	
16 Abstract <p>The thirteenth full-scale Accelerated Pavement Test (APT) experiment at the Civil Infrastructure Laboratory (CISL) of Kansas State University aimed to determine the response and the failure mode of thin concrete overlays. Four pavement structures were built and tested in this experiment: two Thin Concrete Overlays (TCO) pavements, with 4-inch and 6-inch thick overlays constructed on a 5-inch thick PCCP and two Thin Whitetopping (TWT) pavements, with 4-inch and 6-inch thick PCC overlays constructed on a 5-inch hot-mix asphalt layer. The pavements were instrumented to measure the strains at selected locations in each PCC overlay. Each of the four pavements was loaded with approximately two million passes of the CISL APT machine, under in-door ambient temperature condition. No moisture was added to the pavements. Response measurements and performance evaluations were performed at about every 100,000 passes.</p> <p>The TCO overlays failed due to the loss of support underneath the concrete slab which caused transverse cracks to develop in both 4- and 6-inch PCC overlays. No loss of bond between the PCC overlay and the supporting slab was observed. The 4-inch TWT exhibited a transverse crack at the middle of the slab, while the 6-inch TWT exhibited no cracks at the end of testing.</p> <p>The theoretical strains in the concrete overlays at the locations where instrumentation was installed were computed with the ANSYS Finite Element Method (FEM) software. It was found that the magnitude and shape of computed strains matched well with those of the strains measured before any APT loads were applied. It was, therefore, concluded that the three-dimensional finite element model built and the assumption made (linear elastic materials, fully bonded overlays) can accurately estimate the response of TWT and TCO pavements under wheel loading. In addition, the FEM can be used to estimate the evolution of lineal extent of the loss of support under the joints by comparing the measured strains with the corresponding computed strains.</p>			
17 Key Words PCCP, HMA, Accelerated Pavement Test, APT, Civil Infrastructure Laboratory, CISL,		18 Distribution Statement No restrictions. This document is available to the public through the National Technical Information Service, Springfield, Virginia 22161	
19 Security Classification (of this report) Unclassified	20 Security Classification (of this page) Unclassified	21 No. of pages 132	22 Price

**ACCELERATED TESTING FOR STUDYING
PAVEMENT DESIGN AND PERFORMANCE
(FY 2004): THIN BONDED RIGID OVERLAY ON
PCCP AND HMA (CISL EXPERIMENT NO. 13)**

Final Report

Prepared by
Stefan Romanoschi, Ph.D., P.E.*
Cristian Dumitru
Paul Lewis
Mustaque Hossain, Ph.D., P.E.

*Currently affiliated with the University of Texas at Arlington

A Report on Research Sponsored By

THE KANSAS DEPARTMENT OF TRANSPORTATION
TOPEKA, KANSAS

March 2009

© Copyright 2009, **Kansas Department of Transportation**

NOTICE

The authors and the state of Kansas do not endorse products or manufacturers. Trade and manufacturers' names appear herein solely because they are considered essential to the object of this report.

This information is available in alternative accessible formats. To obtain an alternative format, contact the Office of Transportation Information, Kansas Department of Transportation, 700 SW Harrison Street, Topeka, Kansas 66603-3745 or phone (785) 296-3585 (Voice) (TDD).

DISCLAIMER

The contents of this report reflect the views of the authors who are responsible for the facts and accuracy of the data presented herein. The contents do not necessarily reflect the views or the policies of the state of Kansas. This report does not constitute a standard, specification or regulation.

ABSTRACT

The thirteenth full-scale Accelerated Pavement Test (APT) experiment at the Civil Infrastructure Laboratory (CISL) of Kansas State University aimed to determine the response and the failure mode of thin concrete overlays. Four pavement structures were built and tested in this experiment: two Thin Concrete Overlays (TCO) pavements, with 4-inch and 6-inch thick overlays constructed on a 5-inch thick PCCP and two Thin Whitetopping (TWT) pavements, with 4-inch and 6-inch thick PCC overlays constructed on a 5-inch hot-mix asphalt layer. The pavements were instrumented to measure the strains at selected locations in each PCC overlay. Each of the four pavements was loaded with approximately two million passes of the CISL APT machine, under in-door ambient temperature condition. No moisture was added to the pavements. Response measurements and performance evaluations were performed at about every 100,000 passes.

The TCO overlays failed due to the loss of support underneath the concrete slab which caused transverse cracks to develop in both 4 and 6-inch PCC overlays. No loss of bond between the PCC overlay and the supporting slab was observed. The 4-inch TWT exhibited a transverse crack at the middle of the slab, while the 6-inch TWT exhibited no cracks at the end of testing.

The theoretical strains in the concrete overlays at the locations where instrumentation was installed were computed with the ANSYS Finite Element Method (FEM) software. It was found that the magnitude and shape of computed strains matched well with those of the strains measured before any APT loads were applied. It was, therefore, concluded that the three-dimensional finite element model built and the

assumption made (linear elastic materials, fully bonded overlays) can accurately estimate the response of TWT and TCO pavements under wheel loading. In addition, the FEM can be used to estimate the evolution of lineal extent of the loss of support under the joints by comparing the measured strains with the corresponding computed strains.

TABLE OF CONTENTS

ABSTRACT	iii
TABLE OF CONTENTS.....	v
LIST OF TABLES	vii
LIST OF FIGURES.....	viii
Chapter 1 - INTRODUCTION	1
Chapter 2 - BACKGROUND	5
2.1 Thin Bonded Overlays on PCC Pavements	5
2.2 Thin Whitetopping.....	10
2.3 DESCRIPTION OF THE APT FACILITY AT KSU	21
Chapter 3 - CONSTRUCTION, TESTING AND EVALUATION OF TWT PAVEMENTS	25
3.1 CONSTRUCTION OF TWT EXPERIMENTAL PAVEMENTS	25
3.2 INSTRUMENTATION USED IN THE TWT PAVEMENTS.....	31
3.3 APT TESTING OF THE TWT PAVEMENTS	35
3.4 PERFORMANCE OF THE TWT OVERLAYS.....	38
3.5 Measured Horizontal Strains in Concrete Layer.....	40
3.6 TWT PAVEMENT MODELING	45
3.6.1 Geometry Definition	45
3.6.2 Material Properties	47
3.6.3 Model Mesh Generation.....	52
3.6.4 Boundary Conditions and Loads.....	54
3.7 Analysis of Response Data of Twt PAVEMENTS.....	56

3.7.1 Results of the Modeling of 4-inch TWT Pavement	57
3.7.2 Results of Modeling of 6-inch TWT Pavement.....	65
Chapter 4 - CONSTRUCTION, TESTING and evaluation OF TCO PAVEMENTS.....	73
4.1 CONSTRUCTION of TCO ON PCCP PAVEMENTS	73
4.2 INSTRUMENTATION INSTALLED IN THE TCO PAVEMENTS	81
4.3 APT Testing OF THE TCO ON PCCP	83
4.4 PERFORMANCE OF TCO PAVEMENTS	83
4.5 Horizontal Strains in Concrete Overlay.....	84
4.6 TCO PAVEMENT MODELING	89
4.6.1 Geometry Definition	89
4.6.2 Materials Properties	90
4.6.3 Model Meshing	90
4.6.4 Boundary Condition and Loading.....	92
4.7 Analysis of the Response Data of the TCO Pavements.....	93
4.7.1 Results of the Modeling of 6-inch TCO on PCCP Pavement	93
4.7.2 Results of the Modeling of 4-inch TCO on PCCP Pavement	101
Chapter 5 - CONCLUSIONS AND RECOMMENDATIONS	111
REFERENCES.....	117

LIST OF TABLES

Table 2.1: Guidelines for whitetopping pre-overaly repair (ACPA, 1998).....	11
Table 2.2: ACPA Recommended Joint Spacing (ACPA, 1998).....	13
Table 2.3: ACPA Recommended Dowel Bar Size and Spacing (ACPA, 1998).....	13
Table 2.4: Interface Shear Strength at the Colorado Sections (Tarr et al., 1998)...	13
Table 3.1: Nuclear Density Measurements on South Pit.....	27
Table 3.2: Design of the Concrete Mix used for TWT.....	31
Table 3.3: Strain Gage Technical Characteristics (TML Tokio Sokki Kenkyujo) ...	33
Table 3.4: Testing of the TWT pavements: Activity Log	37
Table 3.5: Maximum and Minimum Measured Strains: 6-inch TWT	43
Table 3.6: Maximum and Minimum Measured Strains: 4-inch TWT	44
Table 3.7: Input Data for Material Characterization	57
Table 4.1: Nuclear Density Measurements on North Pit	75
Table 4.2: Concrete Mix Design for the TCO Pavements.....	76
Table 4.3: Activity Log for the Distressing and APT Loading of the TCO Pavements	80
Table 4.4: Maximum and Minimum Strains Values: 6-inch TCO	86
Table 4.5: Maximum and Minimum Strains Values: 4-inch TCO	87

LIST OF FIGURES

Figure 1.1: Bonded PCC overlay (Smith et al., 2002)	2
Figure 1.2: Unbonded PCC overlay (Smith et al., 2002)	3
Figure 1.3: Whitetopping - PCC overlay on HMA pavements (Smith et al., 2002).....	3
Figure 2.1: Comparative performance of interface shear strength for several surface preparation methods (Smith et al., 2002)	7
Figure 2.2: Differences between Conventional Two Layer System and Three Layer System Models (ACPA, 1998).....	16
Figure 2.4: Effect of Slab Size over Stress (redrawn after ACPA, 1998).....	17
Figure 2.3: Effect of Composite Action over Stress (redrawn after ACPA, 1998).....	17
Figure 2.5: Effect of Slab Size over Curling Stress (redrawn after ACPA, 1998) ...	18
Figure 2.6: Framework of the Colorado DOT Design Procedure.....	20
Figure 2.7: Insulated Environmental Pit.....	23
Figure 2.8: Steady State Pulse Loading Assembly	24
Figure 3.1: CISL #13 TWT Sections	26
Figure 3.3: TWT Pavement Sections - Joint Spacing.....	30
Figure 3.2: Saw Cuts in the HMA Layer.....	30
Figure 3.4: Instrumentation for the Thin Whitetopping Pavements.....	34
Figure 3.5: Strain Gages and Fixtures Setting.....	35
Figure 3.6: Distribution Function for the Lateral Wheel Wander.....	36
Figure 3.7: Cracks Recorded at the End of Loading: 4-inch TWT Pavement.....	39
Figure 3.8: Typical Shape of Measured Longitudinal Strain	41
Figure 3.9: Typical Shape of Measured Transverse Strain.....	41
Figure 3.10: Typical Shape of Measured 45 ⁰ Corner Strain.....	42
Figure 3.11: Location of Transverse Strain Gages.....	46
Figure 3.12: Transverse Strain above the Saw Cut in the HMA: 6-inch TWT at 0K	46
Figure 3.13: Transverse Strain above the Saw Cut in the HMA: 4-inch TWT at 0K	47
Figure 3.14: Back-Estimated Modulus of the Asphalt Layer	49
Figure 3.15: Segment Used For Asphalt Modulus Estimation	49

Figure 3.16: Strain and Stress Distribution in Composite Section	50
Figure 3.17: SOLID186 and SOLID45 Geometry	53
Figure 3.18: Model of the 6-inch TWT (Expanded for Symmetry)	54
Figure 3.19: Load Model	56
Figure 3.20: Computed Longitudinal Strains for the 4-inch TWT Pavement.....	60
Figure 3.21: Computed Transverse Strains: 4-inch TWT Pavement.....	61
Figure 3.22: Measured vs. Computed Transverse Strains: 4-inch TWT Pavement	61
Figure 3.23: Evolution of Maximum Measured Transverse Strains: 4-inch TWT Pavement	62
Figure 3.24: Measured vs. Computed Longitudinal Strains: 4-inch TWT Pavement	62
Figure 3.25: Evolution of Maximum Measured Transverse Strains: 4-inch TWT Pavement	63
Figure 3.26: Influence of Loss of Support Distance over Longitudinal Strain: 4-inch TWT Pavement.....	63
Figure 3.27: Maximum Tensile Longitudinal Strain vs. Loss of Support Length: 4-inch TWT Pavement.....	64
Figure 3.28: Loss of Support Length vs. Number of Load Repetitions: 4-inch TWT Pavement	64
Figure 3.29: Measured vs. Computed Longitudinal Strains: 4-inch TWT Pavement	65
Figure 3.30: Computed Longitudinal Strains: 6-inch TWT Pavement.....	68
Figure 3.31: Computed Transverse Strains: 6-inch TWT Pavement.....	68
Figure 3.32: Measured vs. Computed Transverse Strains: 6-inch TWT Pavement	69
Figure 3.33: Evolution of Maximum Measured Transverse Strains: 6-inch TWT Pavement	69
Figure 3.34: Measured vs. Computed Longitudinal Strains: 6-inch TWT Pavement	70
Figure 3.35: Evolution of Maximum Measured Transverse Strains: 6-inch TWT Pavement	70
Figure 3.36: Influence of Loss of Support Length over Longitudinal Strain: 6- inch TWT Pavement	71
Figure 3.37: Maximum Tensile Longitudinal Strain vs. Loss of Support Length: 6-inch TWT Pavement.....	71

Figure 3.38: Loss of Support Length vs. Number of Load Repetitions: 6-inch TWT Pavement	72
Figure 3.39: Measured vs. Computed Longitudinal Strains: 6-inch TWT Pavement	72
Figure 4.1: Configuration of the TCO Pavement Structures.....	73
Figure 4.2: TCO on PCCP Joint Location.....	77
Figure 4.3: TCO on PCCP Slab Crack Mapping	78
Figure 4.4: TCO on PCC- Pavement Instrumentation.....	82
Figure 4.5: TCO - Overlay Crack Mapping.....	84
Figure 4.6: Typical Shape of Measured Longitudinal Strain	88
Figure 4.7: Typical Shape of Measured Transverse Strain.....	88
Figure 4.8: Typical Shape of Measured 45⁰ Corner Strain.....	89
Figure 4.9: FEM Mesh of the Model Used for the 6-Inch TCO Pavement.....	92
Figure 4.10: Computed Longitudinal Strains: 6-inch TCO Pavement.....	96
Figure 4.11: Computed Transverse Strains: 6-inch TCO pavement	96
Figure 4.12: Measured vs. Computed Transverse Strains: 6-inch TCO pavement	97
Figure 4.13: Evolution of Maximum Measured Transverse Strains: 6-inch TCO pavement	97
Figure 4.14: Measured vs. Computed Longitudinal Strains: 6-inch TCO pavement	98
Figure 4.15: Evolution of Maximum Measured Transverse Strains: 6-inch TCO pavement	98
Figure 4.16: Influence of Loss of Support Length over Longitudinal Strain: 6-inch TCO pavement	99
Figure 4.17: Maximum Tensile Longitudinal Strain vs. Loss of Support Length	99
Figure 4.18: Loss of Support Length vs. Number of Load Repetitions	100
Figure 4.19: Measured vs. Computed Longitudinal Strains at 1.1M Passes	100
Figure 4.20: Correlation between Maximum Tensile Strain and Slab Cracking...	101
Figure 4.21: Computed Longitudinal Strains: 4-inch TCO Pavement.....	104
Figure 4.22: Computed Transverse Strains: 4-inch TCO Pavement	105
Figure 4.23: Measured vs. Computed Transverse Strains: 4-inch TCO Pavement	105
Figure 4.24: Evolution of Maximum Measured Transverse Strains: 4-inch TCO Pavement	106

Figure 4.26: Transverse Crack in the Concrete Slab Underneath the 4-inch TCO Pavement.....	107
Figure 4.25: Measured vs. Computed Longitudinal Strains: 4-inch TCO Pavement	107
Figure 4.27: Evolution of Maximum Measured Longitudinal Strains: 4-inch TCO Pavement.....	108
Figure 4.28: Influence of Loss of Support Length on Longitudinal Strains: 4-inch TCO Pavement	108
Figure 4.29: Maximum Tensile Longitudinal Strain vs. Loss of Support Length	109
Figure 4.30: Loss of Support Length vs. Number of Load Repetitions	109
Figure 4.31: Comparison of Measured vs. Computed Longitudinal Strains	110

CHAPTER 1 - INTRODUCTION

Despite fifty years of collective experience with the construction of Portland Cement Concrete (PCC) overlays on existing distressed rigid and flexible pavements, research is needed to determine optimum construction and design procedures for these overlays. Two major PCC overlay types that are used to rehabilitate distressed PCC pavements are bonded and unbonded overlays. Unbonded overlays are effectively used to strengthen highly distressed Jointed Plain Concrete Pavement (JPCP) and Continuously Reinforced Concrete Pavements (CRCP). These overlays are designed with the assumption that no bond exists between the overlay and the underlying existing pavement. Figure 1.1 shows the schematic of an unbonded overlay.

Bonded overlays are used when the underlying rigid pavement does not exhibit severe structural distresses and are designed basing on the assumption that the overlay and the underlying concrete slab are fully bonded and form a monolithic layer. Thus, bonded overlays are typically thinner than the unbonded overlays. Figure 1.2 illustrates the schematic of an unbonded PCC overlay.

The process of rehabilitating distressed hot-mix asphalt (HMA) pavements using a PCC overlay is called "whitetopping." Conventional whitetopping has a thickness between 6 and 12 inches (150 and 305 mm). The design of PCC overlay is the same as for a new rigid pavement, with the HMA layer assumed to be a base layer with high stiffness underneath the concrete slab as shown in Figure 1.3. The composite stiffness/support capacity of the existing pavement and the underlying subgrade is used to compute the design thickness of the PCC overlay (AASHTO, 1993). However, despite some other design methods assume low friction between the PCC overlay and

the existing HMA layer, some partial bonding, which can contribute to the performance of the overlaid pavement, may occur (Smith et al., 2002).

A more recent but increasingly popular technology is the ultra-thin whitetopping (UTW), where the thickness of the PCC overlay is between 2 and 4 inches (50 and 100 mm). UTW is used on structurally sound asphalt pavements that exhibit mainly surface rutting. The overlay thickness is designed based on the assumption that the PCC overlay bonds well to the distressed HMA layer. Milling of the distressed HMA layer is normally done to ensure a good bond. The use of UTW is relatively new but has grown rapidly in the last decade, with over 200 projects built in 35 states since 1992 (Smith et al., 2002).

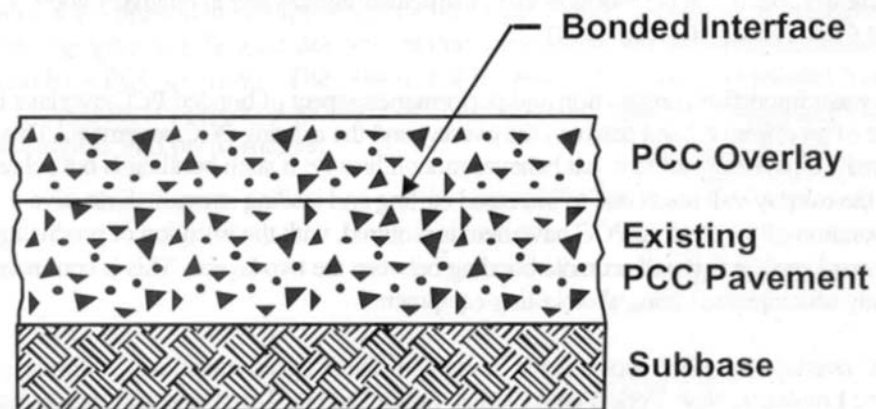


Figure 1.1: Bonded PCC overlay (Smith et al., 2002)

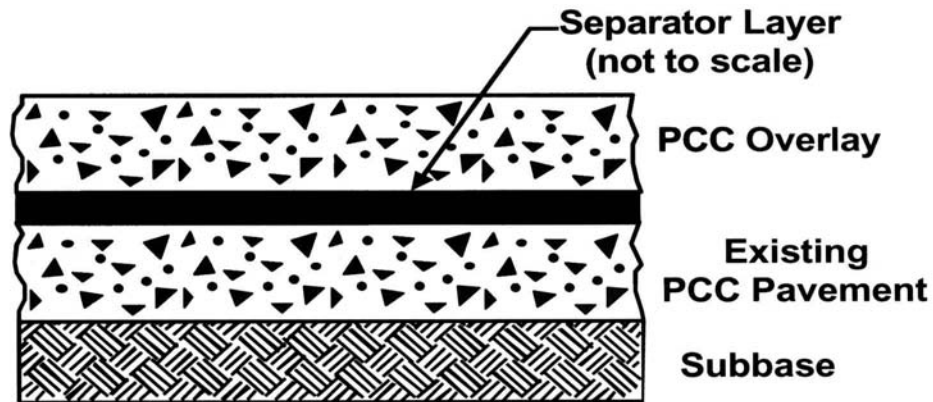


Figure 1.2: Unbonded PCC overlay (Smith et al., 2002)

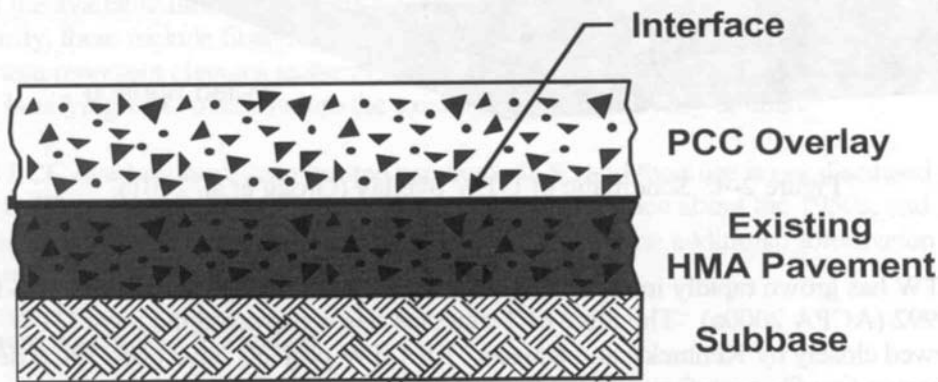


Figure 1.3: Whitetopping - PCC overlay on HMA pavements (Smith et al., 2002)

More recently, a new class of whitetopping, called thin whitetopping, has been used primarily on state highways. The thickness of this PCC overlay ranges from 4 to 8 inches (100 - 200 mm). The joint spacing ranges between 6 and 12 ft (1.8 – 3.6 m). The overlay is designed assuming full bonding between the existing HMA pavements and the new overlay (Tarr et al., 1998; Sheehan et al., 2002; Rasmussen, 2002). This assumption minimizes the need for additional thickness (Rasmussen, 2002).

The research study described in this report aimed to evaluate the performance of thin bonded PCC overlays on existing PCC and HMA pavements through accelerated pavement testing (APT) and to determine the failure modes and the parameters that affect the performance of these pavement structures. The advantage of using

accelerated pavement test when compared to in-situ field tests is that the results of the comparative APT study can be obtained in a few months. In in-situ field tests, the results are obtained after observing the behavior of the road test sections for a period of minimum five years. Also, on in-situ field tests, some of the environmental factors and traffic loadings cannot be controlled. However, pavement performance evaluation using APT has two major limitations: a) the effect of the environment cannot be simulated well even though temperature can be controlled, and b) APT loading may differ from the vehicle loading provided by in-service traffic, in terms of speed and frequency (headway) of loading, lateral wheel wander, load spectra. The effects of long term exposure to water and extreme temperatures (e.g. freezing and thawing, water damage) and long term changes in material properties (e.g. aging of asphalt binders) cannot be reproduced in an APT test.

With these benefits and limitations in mind, the proposed study was conducted at the Civil Infrastructure Systems Laboratory (CISL) of Kansas State University (KSU). The Department of Civil Engineering at KSU, in cooperation with KDOT, has developed the Accelerated Testing Laboratory (ATL) (Melhem, 1997). The lab was renamed CISL in 2001. The facility allows full-scale accelerated tests on pavement structures using the APT machine as the loading device. The loading device is placed on a full-scale road structure constructed in a pit. A full-size truck axle passes over the pavement at about every five seconds, applying a total single or tandem axle load between 18,000 and 36,000 lbs (9 and 18 kN) depending upon axle type. Both single and dual tires, single and tandem axles can be accommodated in this system. A detailed description of the facility is given by Melhem (1997).

CHAPTER 2 - BACKGROUND

2.1. Thin Bonded Overlays on PCC Pavements

Bonded PCC overlays are typically 3 to 6 inches (75 to 150 mm) concrete overlays bonded to the existing rigid pavement to function as a monolithic layer. Their purpose is to increase the structural capacity and/or to improve the ride quality of existing PCC pavements. Bonded overlays are an effective rehabilitation strategy for rigid pavements that are in good condition, but are in need of structural capacity enhancements. Typically the extra structural capacity is needed by an unexpected increase in traffic level or by signs of structural deficiency (e.g. corner cracks, transverse cracking). These overlays should not be used on severely distressed pavements, pavements with severe “D” cracking or reactive aggregate problems. Bonded overlays are typically used to correct functional deficiencies, such as, surface roughness, insufficient surface friction or a pavement surface that is excessively noisy.

The construction of bonded overlays requires the following operations:

- Pre-overlay repairs;
- cold milling or shot blasting of the existing pavement to produce a rough surface for bonding to take place;
- air, water, shot blasting or sand blasting of the milled surface to obtain a clean surface;
- optional placement of a bonding agent;
- placing, finishing and curing of the PCC overlay;
- sawing of joints in the overlay to overlap the joints in the existing pavement.

Bonded overlays have provided good performance on many projects and have been shown to be an effective way of improving the structural capacity of existing rigid overlays (Zollinger et al., 2001). The condition for successful rehabilitation is that the rigid pavements must be in an acceptable condition before the bonded overlay is placed. Otherwise, there is a high potential that the unrepaired, working cracks in the old pavement will reflect through the overlay. Therefore, the pre-overlay repairs are necessary to achieve long life for the of the bonded PCC overlay. The pre-overlay repairs may consist of replacing shattered slabs, cross-stitching of cracks in the wheelpath and placing of crack control cages.

Achievement of an adequate bond between the overlay and the underlying pavement is essential for a good performance of the overlay, since the design of these overlays is based on the assumption that the existing concrete slab and the overlay form a monolithic slab. Debonding can lead to rapid deterioration of bonded overlays, mainly due to the construction method used, the climatic condition during construction or the bonding agent (Zollinger et al. 2001). The HIPERPAV program developed by McCullough and Rasmussen (1999) predicts the interface bond stresses and strengths during the first 72 hours after the PCC placement function of the PCC mix composition and the climatic conditions during construction.

Past experience has not clearly indicated the best bonding method to be used. Research conducted in Texas showed that the spraying of cement grout right before placement of the overlay may not increase the performance of the overlay. It was also found that better interface shear strength may be achieved when shot blasting is used instead of milling during surface removal as shown in Figure 2.1.

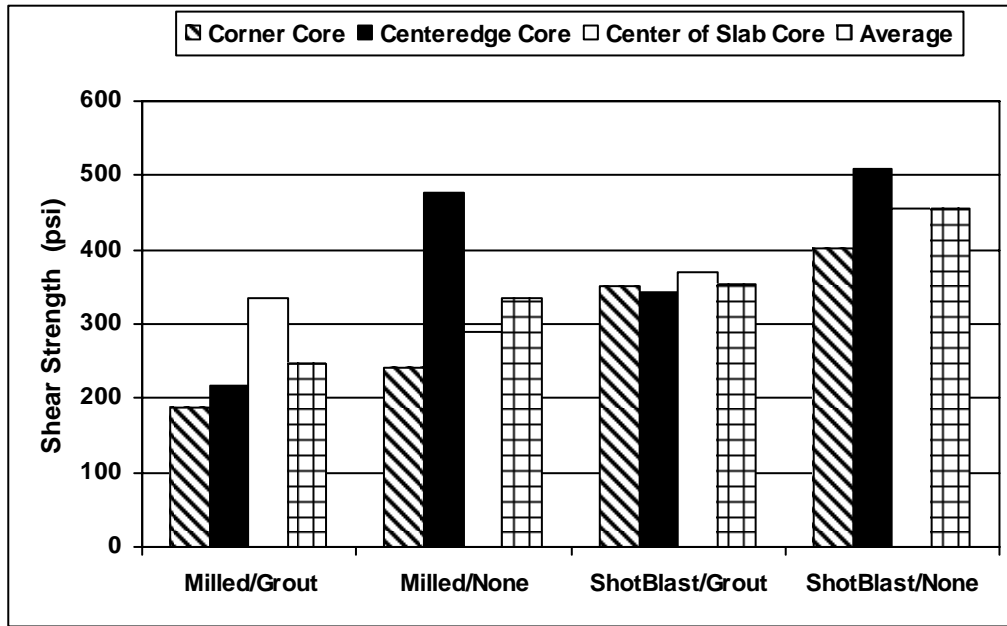


Figure 2.1: Comparative performance of interface shear strength for several surface preparation methods (Smith et al., 2002)

Similar conclusions were reached by Rowden (1996) after conducting an extensive field and laboratory study on thin bonded concrete overlays in Illinois. Rowden (1996) found that the surface preparation is essential for obtaining a good overlay and that the bond strength of the overlay did not vary significantly either with or without grout, and that placement of grout was cumbersome and slowed down the paving process. A typical cement grout for this application consists of a mix of water and cement in a ratio by weight between 0.33 and 0.62. The grout is placed on the dry surface, right in front of the slip-form paver, before the concrete mix is placed.

The basic concept of the 1993 AASHTO Design Guide PCCP overlay design is that the overlay thickness should be the difference between the required pavement thickness and the effective thickness of the concrete slab [Eq. 2-1] (Huang, 2003). The first step in overlay design is the assessment of the pavement condition: slab thickness, type of load transfer, type of shoulder, effective modulus of subgrade reaction, joint load

transfer and mechanical characteristics of PCC slab. The next step consists of computing the required slab thickness of a new rigid pavement corresponding to the forecasted future traffic (D_f). The third step is assessing the effective thickness of the existing slab (D_{eff}). This can be done in two ways:

- From a condition survey;
- From remaining life calculation.

$$D_{OL} = D_f - D_{eff} \quad \text{Equation 2-1}$$

Where:

- D_{OL} - required thickness of un-bonded rigid overlay
- D_f - slab thickness required to carry all future traffic
- D_{eff} - effective thickness of the existing slab

For computing the effective thickness of the existing slab from a condition survey, the following equation is used to adjust the actual existing slab thickness [Eq. 2-2]:

$$D_{eff} = F_{jc} \times F_{dur} \times F_{fat} \times D \quad \text{Equation 2-2}$$

Where:

- D_{eff} - effective thickness of the existing slab
- F_{jc} - joints and cracks adjustment factor - accounts for the extra loss of serviceable life caused by deteriorated reflection cracks in the overlay that will result from any unrepaired distresses in the existing pavement.

F_{dur} - durability adjustment factor - accounts for the extra loss in serviceability caused by any durability problems (such as "D" cracking) in the existing pavement.

F_{fat} - fatigue damage adjustment factor (accounts for past fatigue damage in the existing pavement).

D - thickness of the existing slab

For computing effective thickness of the existing slab from a remaining life calculation, Equation 2-3 determines the remaining life as a percentage of total life based on present damage accumulated due to the present traffic. The effective thickness of the slab is computed based on the remaining life percentage [Eq. 2-4].

$$RL = 100 \left[1 - \frac{N_p}{N_{1.5}} \right] \quad \text{Equation 2-3}$$

Where:

RL - remaining life, as a percentage of total life

N_p - total loads to date in ESALs

$N_{1.5}$ - total loads to failure in ESALs. To be consistent with AASHO Road Test data, "failure" is assumed to occur at PSI = 1.5 and reliability = 50%.

$$D_{eff} = F_{jcu} \times D \quad \text{Equation 2-4}$$

Where:

D_{eff} - effective thickness of the existing slab

F_{jcu} - joints and cracks adjustment factor, accounts for the extra loss of serviceable life caused by deteriorated transverse joints and cracks in the existing pavement.

D - existing slab thickness, maximum value is 250 mm (10 inch) even if the existing slab is thicker

2.2 Thin Whitetopping

The overlay thickness for thin whitetopping ranges from 4 to 8 inches (100 to 200 mm). The general design considerations are: (a) Existing pavement condition, (b) Overlay pavement type, and (c) Pre-overlay repair (Smith et al., 2002). In general, whitetopping overlays are most appropriate for HMA pavements that are extensively deteriorated, such as, those with excessive rutting, shoving, or alligator cracking. The most common whitetopping overlay type is JPCP. Pre-overlay repair of the existing HMA pavements for thin whitetopping should ensure that uniform support is provided for the PCC surface. ACPA (1998) has provided guidelines for pre-overlay repairs of conventional whitetopping, as shown in Table 2.1.

Three surface preparation methods are commonly used for whitetopping: (a) direct placement, (b) milling and (c) placement of leveling course. Direct placement has been used extensively by the Iowa counties. However, milling has been found to increase the interface shear strength (Tarr et. al., 1998).

The thickness design procedure for thin white topping had been based on the new PCC pavement design with the existing HMA pavement as a stabilized base. Thus existing design procedures for new pavements, such as, the 1993 AASHTO Design Guide or the 1998 Supplemental procedure could be used. ACPA (1998) also provided simple design charts for selecting PCC overlay thickness for whitetopping. Most recently Colorado DOT has developed a mechanistic design procedure based on field instrumentation and observation of several thin whitetopping projects in Colorado (Tarr et al., 2000). TransTec Group is also developing a new procedure for designing whitetopping overlays (Rasmussen et al., 2002).

Table 2.1: Guidelines for whitetopping pre-overaly repair (ACPA, 1998)

General Pavement Condition	Recommended Repair*
Rutting (<50mm [2 in.])	None or milling**
Rutting (>50mm [2 in.])	Milling or leveling
Shoving	Milling
Potholes	Fill with crushed stone cold mix or hot mix
Subgrade failure	Remove and replace or repair
Alligator cracking	None
Block cracking	None
Transverse cracking	None
Longitudinal cracking	None
Raveling	None
Bleeding	None

* Other factors to consider: adding edge drains; costs of direct placement vs. milling or leveling.

** Consider increasing the joint sawing depth

ACPA (1998) recommends that satisfactory whitetopping design should consider four factors:

- (1) Quality concrete considering both strength and durability;
- (2) Adequate slab thickness to limit the load stresses;
- (3) Joint design that will control unwanted cracking and provide adequate load transfer; and
- (4) Use of concrete with the 28-day compressive strength of at least 4,000 psi (30 MPa).

For structural design, the recommended methodology considers the strength of the existing asphalt pavement, flexural strength of the concrete, design period and traffic. The other features in design are joint spacing to control cracking and load transfer across the joints. Tables 2.2 and 2.3 show the ACPA recommended joint

spacing and dowel bar sizes and spacing. The maximum joint spacing recommended for conventional whitetopping constructed as JPCP is 21 times the slab thickness (in inches). However, a Colorado study has found that the effect of joint spacing is not significant (Tarr et al., 1998). This observation is being revisited in another study (Sheehan et al, 2002).

In the design of conventional whitetopping overlays, the effects of any bonding between the PCC overlay and the underlying HMA layers are typically ignored. However, past research has shown that some degree of bonding does occur between the two layers. The recent design methodology for thin whitetopping developed by Colorado DOT takes this into account (Tarr et al., 2000).

The issue of the bond between the two layers also brings into the picture the method of surface preparation. A study in Iowa (Grove et al., 1993) found that tack coat may reduce the bond. Milling and air blasting generally produced enhanced bond. Also, cement and water grout demonstrated no significant advantage in bond strength. A study in Colorado showed that milling significantly enhanced interlayer bond over surface with no special preparation (Tarr et al., 1998). The degradation of this interface bond is intuitively expected due to environmental factors (curling, shrinkage, and moisture damage of the HMA layer) and associated normal loading from the traffic. However, in the Colorado study the bond strength was found to increase after one year as shown in Table 2.4 (Tarr et al., 1998). The increase is higher for the thin whitetopping pavement where milling was used in surface preparation. The possible explanation for this is that the shear stresses induced at the interface between PCC and HMA by temperature variation are smaller for thinner overlays.

Table 2.2: ACPA Recommended Joint Spacing (ACPA, 1998)

Slab Thickness, mm (in.)	Maximum joint spacing, ¹ m (ft)
100 (4)	2.1 (7)
150 (6)	3.2 (10.5)
200 (8)	4.3 (14)
250 (10)	5.3 (17.5)
300 (12)	6.4 (21)
350 or more (14 or more)	7.6 (25)

¹ Joint spacing may also be based on local experience for pavements that have provided good service

Table 2.3: ACPA Recommended Dowel Bar Size and Spacing (ACPA, 1998)

Slab Thickness, mm (in.)	Dowel diameter, mm (in.)	Dowel length, mm (in.)	Dowel spacing, mm (in.)
Plain (unreinforced) pavements			
< 200 (<8)	Dowels not required		
200 (8)	32 (1.25)	450 (18)	300 (12)
225 (9)	32 (1.25)	450 (18)	300 (12)
250 (10)	32 (1.25)	450 (18)	300 (12)
280 (11)	38 (1.50)	450 (18)	300 (12)
300 (12)	38 (1.50)	450 (18)	300 (12)
350 (14)	44 (1.75)	500 (20)	380 (15)
400 (16)	50 (2.00)	600 (24)	450 (18)
Reinforced pavements			
150 (6)	20 (0.75)	350 (14)	300 (12)
175 (7)	25 (1.00)	400 (16)	300 (12)
> 200 (>8)	Same dowel size and spacing as above		

Table 2.4: Interface Shear Strength at the Colorado Sections (Tarr et al., 1998)

Site	Test Slab	Longitudinal Joint Spacing, in.	Transverse Joint Spacing, in.	AC Surface Condition	28-day Interface Shear Strength, psi	365-day Interface Shear Strength, psi
Santa Fe	1	60	60	New	45	80
	2	60	60	New	30	60
	3	60	60	New Milled	10	80
Longmont	1	72	72	Existing	100	****
	2	120	144	New	60	105
	3	72	72	New	70	105
	4	72	144	Existing Milled	65	100
	5	144	144	Existing Milled	****	155
Lamar	B	144	120	Existing Milled	80	****
	E	72	72	Existing Milled	90	****
	F	72	72	Existing Milled	110	****

Although the values of the coefficient of thermal expansion are quite dissimilar [5 to $6 \times 10^{-6}/^{\circ}\text{F}$ (9 to $10.8 \times 10^{-6}/^{\circ}\text{C}$) for PCC, and 1.2 to $1.4 \times 10^{-5}/^{\circ}\text{F}$ ($2.0 \times 10^{-5}/^{\circ}\text{C}$) for HMA], the expansion and/or contraction in the HMA layer probably roughly equals that of the PCC overlay due to lower temperature gradient in HMA. In fact, Tarr et al. (1998) observed that slab upward warping effects due to moisture differentials (surface drier than the bottom) were greater than measured downward temperature curling effects. However, stripping would be a very detrimental factor as was evident on a conventional whitetopping project on I-70 in Kansas (Gisi, 1985; Gisi, 2003). In thin whitetopping pavement, stripping could happen due to the saturated interface of the two layers in presence of a significant thermal gradient and loading due to the traffic.

Other important factors are the thickness and properties of the existing HMA pavement. A minimum HMA thickness of 2 inches (50 mm) (after milling) has been recommended for conventional whitetopping overlays by Grogg et al. (2001). However, Tarr et al. (1998) recommends a minimum HMA layer thickness of 5 inches (127 mm) for thin whitetopping overlays. They also recommended a minimum subgrade modulus of reaction (k) value of 150 pci for thin whitetopping projects.

Thickness design of TWT is a very complex procedure because of the particular aspects of this technology:

- The bond between concrete overlay and asphalt creates a composite structure lowering the neutral axis reducing substantially the stress
- The short joint spacing reduces substantially load and curling stresses
- The asphalt layer provides a non erodible support for the concrete
- The concrete used has a higher strength than in conventional concrete pavements

For these reasons, the conventional design, which does assume the bonding between layers, and consider the asphalt layer as a granular subbase, would overestimate the thicknesses of the concrete overlay. The results are very sensitive to the model: the critical stress at the bottom of the concrete layer computed on a composite three layer model is half of that computed for an un-bonded two layer pavement model (ACPA, 1998). The difference between a conventional two layer system and a three layer system models is shown in Figure 2.2.

The degree of composite action is also very important in modeling the TWT pavement. Function of the percent of composite action, defined as the ratio between the moment of inertia of the existing section and the moment of inertia of the fully bonded section, the stresses at the bottom of the asphalt layer can decrease up to 5 times. Figure 2.3 shows the effect on composite action versus stress for a 4-inch concrete over a 4-inch asphalt layer on a 100 pci subgrade.

A mechanistic analysis of TWT should also include the effect of slab size. As shown in Figure 2.4, for a composite pavement consisting of 4 inch concrete over 4 inch

asphalt, there is a substantial reduction in load stresses as slab size decreases. The effect is the same on curling and warping stresses that occur due to temperature and moisture gradients in the concrete slab (Figure 2.5).

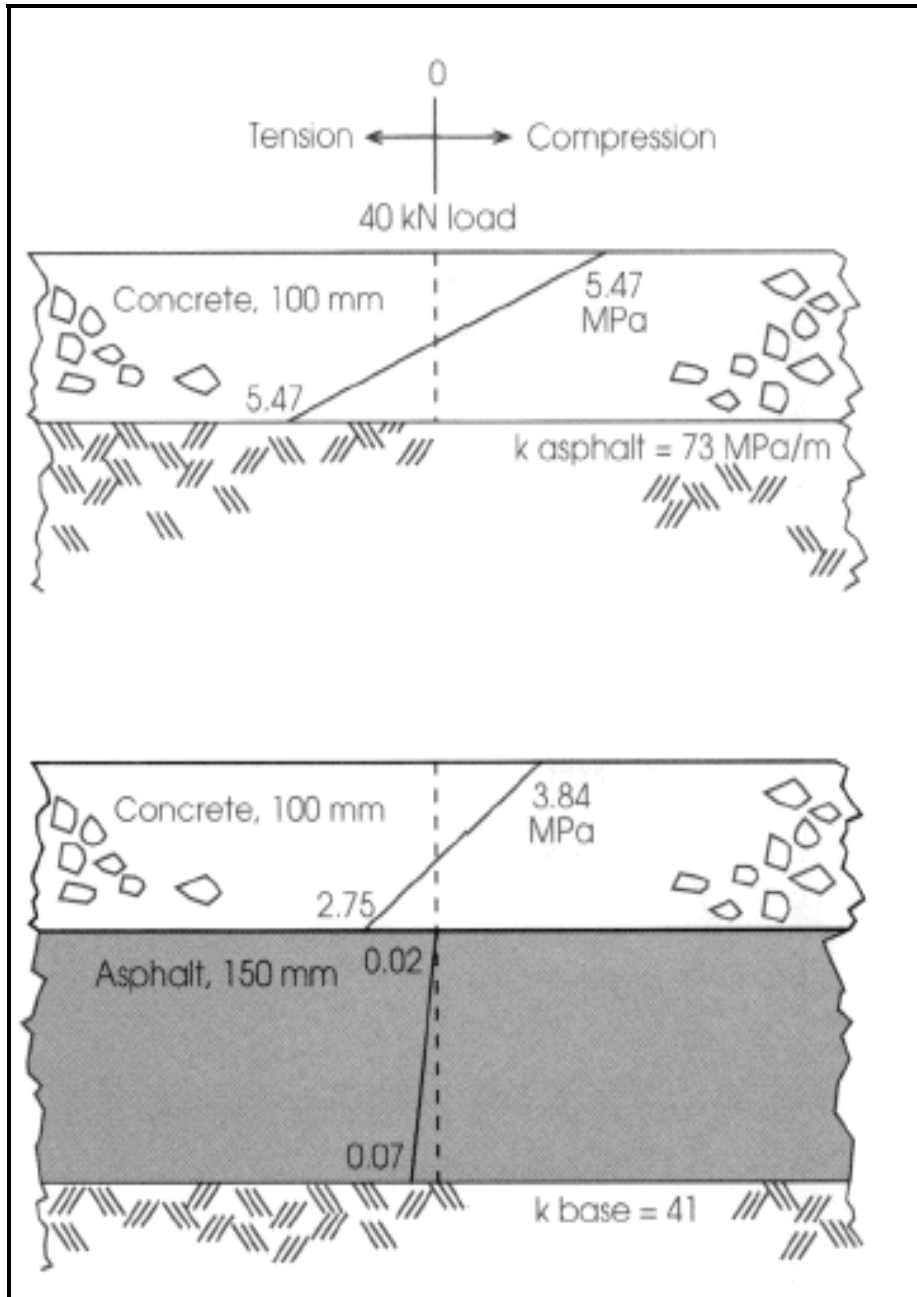


Figure 2.2: Differences between Conventional Two Layer System and Three Layer System Models (ACPA, 1998)

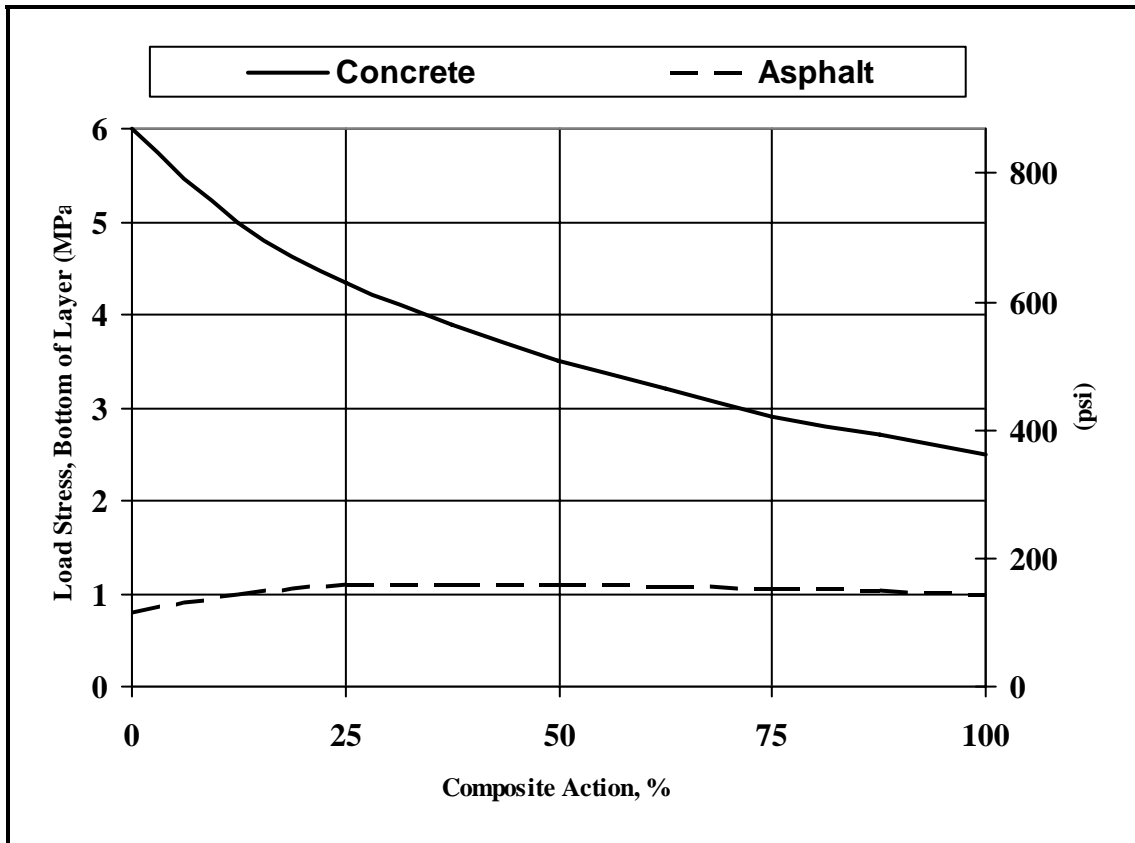


Figure 2.3: Effect of Composite Action over Stress (redrawn after ACPA, 1998)

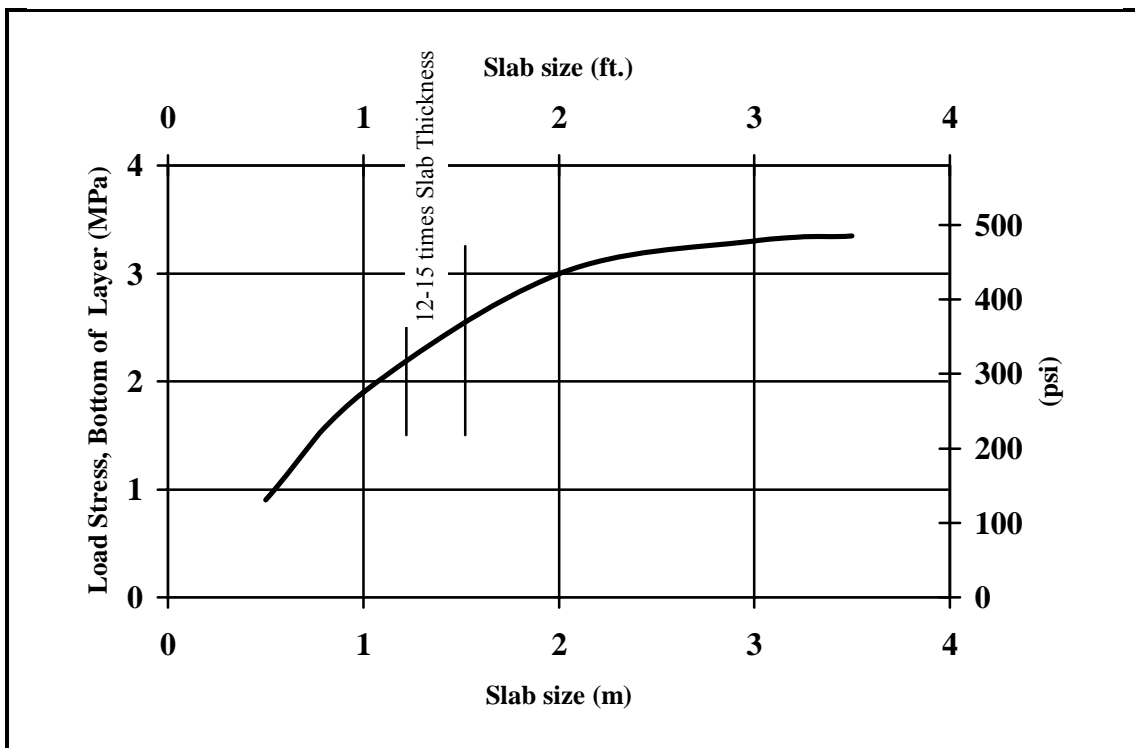


Figure 2.4: Effect of Slab Size over Stress (redrawn after ACPA, 1998)

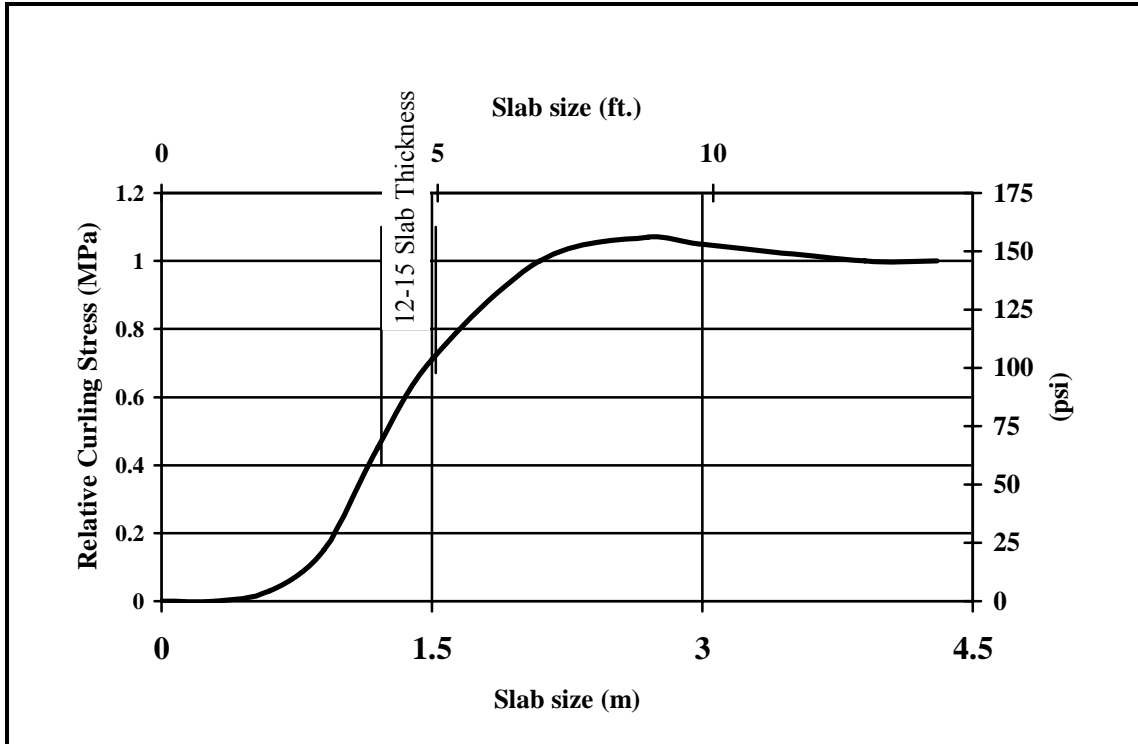


Figure 2.5: Effect of Slab Size over Curling Stress (redrawn after ACPA, 1998)

Currently, the Colorado Design Procedure (Sheehan et al, 2004) is the most advanced procedure for the thickness design. They developed theoretical design equations for prediction of critical stresses and strains. The location of the critical stress from axle loads is at the middle of the free edge joint. The critical stress is computed based on the relation between the free edge and tied edge stress using a correlation equation [Eq. 2-5]. In addition, thermal stress is the second critical stress, but the methodology doesn't present any model for computing the stress from temperature gradient.

$$\sigma_{FE} = 1.87\sigma_{TE} \quad \text{Equation 2-5}$$

Where:

σ_{FE} -longitudinal free edge load induced stress

σ_{TE} -longitudinal tied edge load induced stress

The comparison between theoretically computed stresses and the measured stresses showed that the measured stresses are greater than the computed stresses. This difference is caused mainly by the imperfect bonding between the asphalt layer and the concrete layer. For this reason the correlation equation [2-6] was developed to determine the design values for stresses.

$$\sigma_{EX} = 1.51\sigma_{TH} \quad \text{Equation 2-6}$$

Where:

σ_{EX} -measured partially bonded interfacial stresses

σ_{TH} -theoretically fully bonded interfacial stresses

The strains at the bottom of the concrete layer and the top of the asphalt layer were measured and compared in order to assess the bonding between layers. Because the strains on the asphalt layer are smaller than the strains on the concrete layer, Equation 2-7 was developed based on the measurements.

$$\epsilon_{AC} = 0.897\epsilon_{PCC} - 0.776 \quad \text{Equation 2-7}$$

Where:

ϵ_{AC} -strains at the top of the asphalt layer

ϵ_{PCC} -strains at the bottom of the concrete layer

The framework of the procedure is shown in Figure 2-6. Stresses from 20 kip (90 KN) single axle load and 40 kip (180 KN) tandem axes load are computed using given design equations. The failure criteria are based on concrete and hot mix asphalt fatigue relations. Thus, the traffic volume can be computed as a function of critical stresses and the failure criteria.

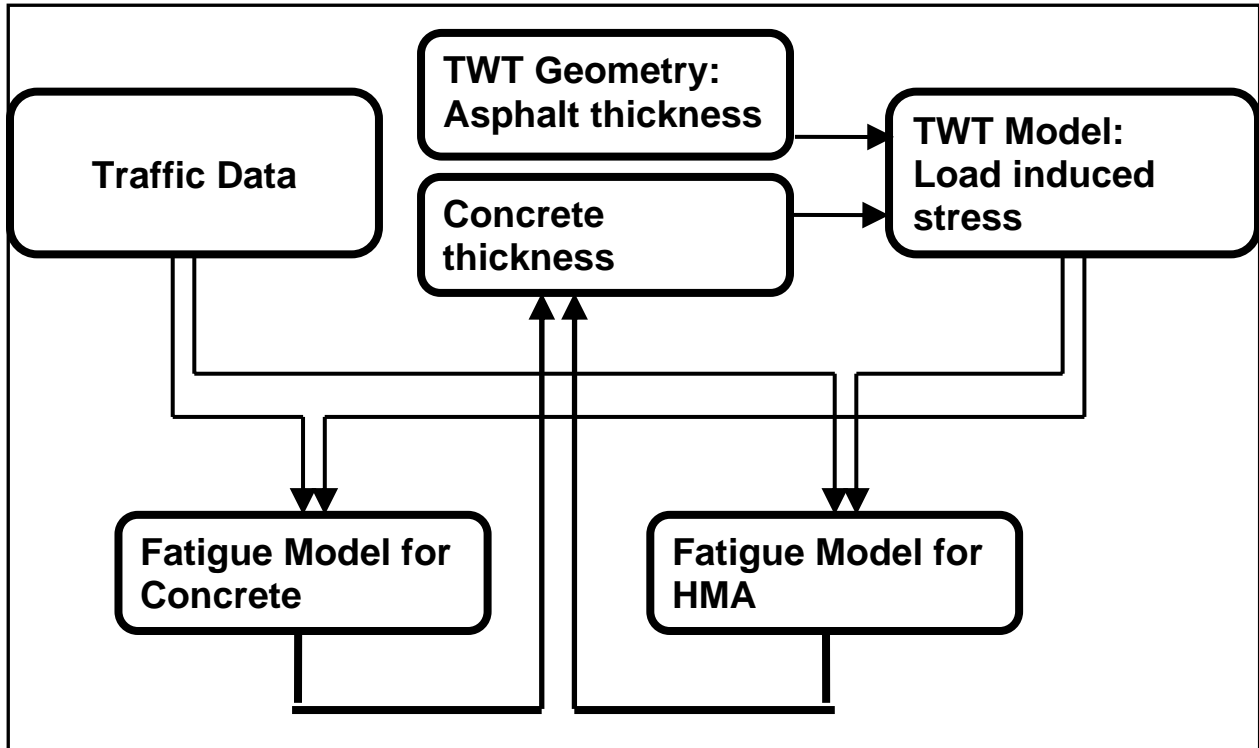


Figure 2.6: Framework of the Colorado DOT Design Procedure

2.3 DESCRIPTION OF THE APT FACILITY AT KSU

The Civil Infrastructure Systems Laboratory (CISL) of KSU is an indoor facility with about 7,000 ft² floor space, and consists of a main research hall containing three pits for pavement testing, an FWD calibration room, and a mechanical and electrical room for the cooling and heating equipment.

The APT test pavements are built in specially constructed pits. The largest pit is 32 ft x 20 ft x 6 ft and is divided in two smaller pits. The smaller pit is 20 ft x 12 ft x 6 ft and is equipped with a system of copper pipes that circulates a heated or cooled glycol solution (Figure 2.7) to control the temperature of the subgrade. This pit has a thermal insulation and can maintain a steady temperature of the subgrade between +5⁰ F and +72⁰ F.

The APT loading device is a steel frame that can move between testing pits on a rail embedded in the concrete floor. The loading frame has two main 42 ft (12.8 m) center-to-center span girders. A carriage rolling along the girders carries the loading bogie. While loading in one direction, the carriage can lift the bogie for unidirectional traffic testing. At the both ends of the traveled way, the carriage hits an energy absorption and releasing system (spring and damper system) that transform the kinetic energy into potential energy and back to kinetic energy to reverse its direction of travel. The driving force accelerates the carriage to reach a steady-state speed of 5 mph (8 km/h) in a minimum distance of 14 feet (4.3 m). The distance traveled by the carriage is longer than the test pavements; the acceleration and deceleration are outside of the test pavements so the speed of the applied load doesn't change while the bogie travels the pavement.

The carriage assembly takes approximately 2.75 seconds to complete its travel distance for the 20 ft (6.1 m) long test section in one direction. The carriage completes an entire two way travel cycle in approximately 11 seconds. This way, approximately 100,000 load passes are applied to the pavement in a week when bidirectional loading is used.

The main component of the carriage is a conventional truck axle. However, the airbag- type suspension has been replaced by a hydraulic cylinder. The pressure control is done in open loop mode using load cells. The maximum applied load is 40,000 lbs (178 KN). The load magnitude is controlled manually by setting the pressure in the hydraulic circuit.

The machine is equipped with a lateral wandering device that moves the entire structure in the lateral direction and allows the bogie to apply loading at several lateral offsets from the centerline of the wheel path. The lateral offset ranges between maximum limits of ± 24 inch (± 610 mm); the movement is done in steps of 0.5 inch (12.5 mm). The lateral position of the frame is controlled by an electronic controller.

Alternative to applying moving loads the ATL machine can be used for steady state pulse loads. In this loading configuration, two hydraulic cylinders are fixed on the machine girders through a steel beam and load the pavement through a set of hydraulic cylinders (Figure 2.8). The loading is monitored by a programmable logic controller that adjusts the hydraulic pressure given by the hydraulic pump to the cylinders using a servo-valve. The controller can use external LVDT's, pressure or force cells as feedback for the loading process.

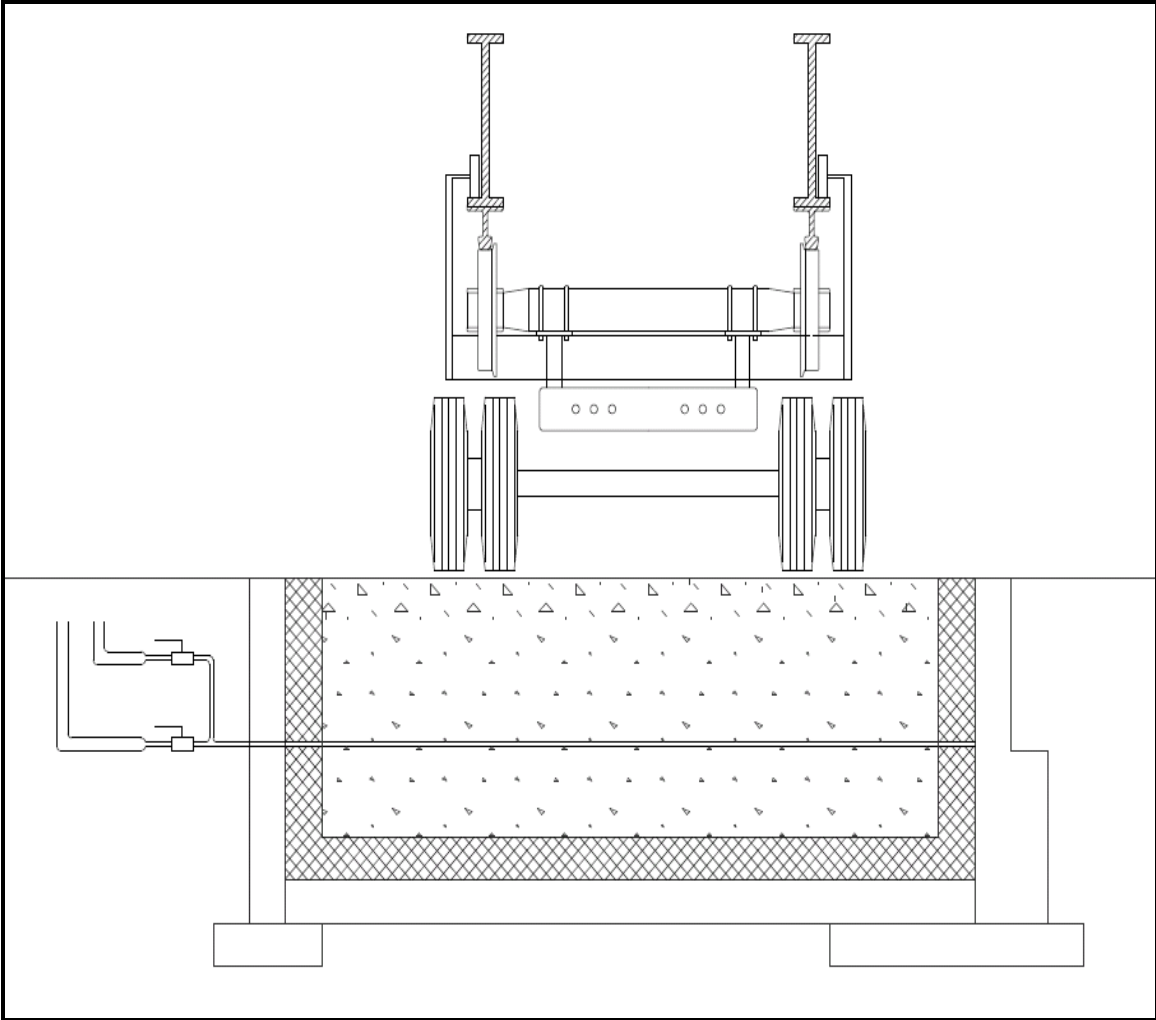


Figure 2.7: Insulated Environmental Pit

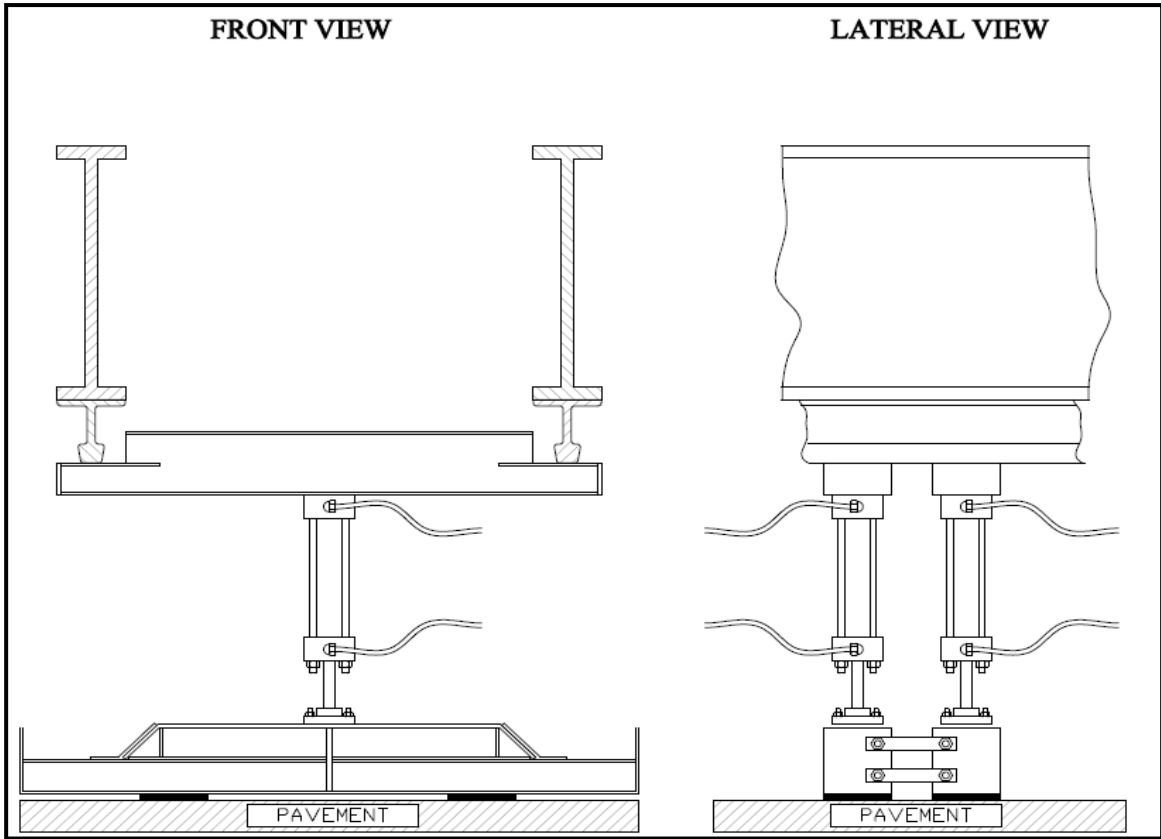


Figure 2.8: Steady State Pulse Loading Assembly

CHAPTER 3 - CONSTRUCTION, TESTING AND EVALUATION OF TWT PAVEMENTS

3.1 CONSTRUCTION OF TWT EXPERIMENTAL PAVEMENTS

Four experimental pavement sections were constructed for the CISL # 13 experiment. The two TWT sections were constructed on the two lanes in the South pit (SS and SN lanes). Two TCO over PCCP were constructed on the two lanes in the North pit (NS and NN lanes).

To evaluate the TWT behavior, two pavement structures, having different thicknesses of concrete overlays, were constructed. The first experimental section consisted of a 6-inch whitetopping placed on a 5-inch HMA pavement, and the second consisted of a 4-inch whitetopping on a 5-inch HMA pavement. The final pavement configuration is shown in Figure 3.1.

Both pavements were 20 feet long and 7 feet wide, and were constructed side-by-side in the South pit on the same subgrade soil (A-7-6). The compaction of the subgrade to the required depth was done in 6-inch lifts with a vibratory compactor (jumping jack-type). After compaction, the excessive soil of the subgrade was trimmed to the final design level. The level of compaction was verified for six locations, three for each lane. The measurements were made with a Nuclear Gauge. The results of nuclear density measurements are presented in Table 3.1.

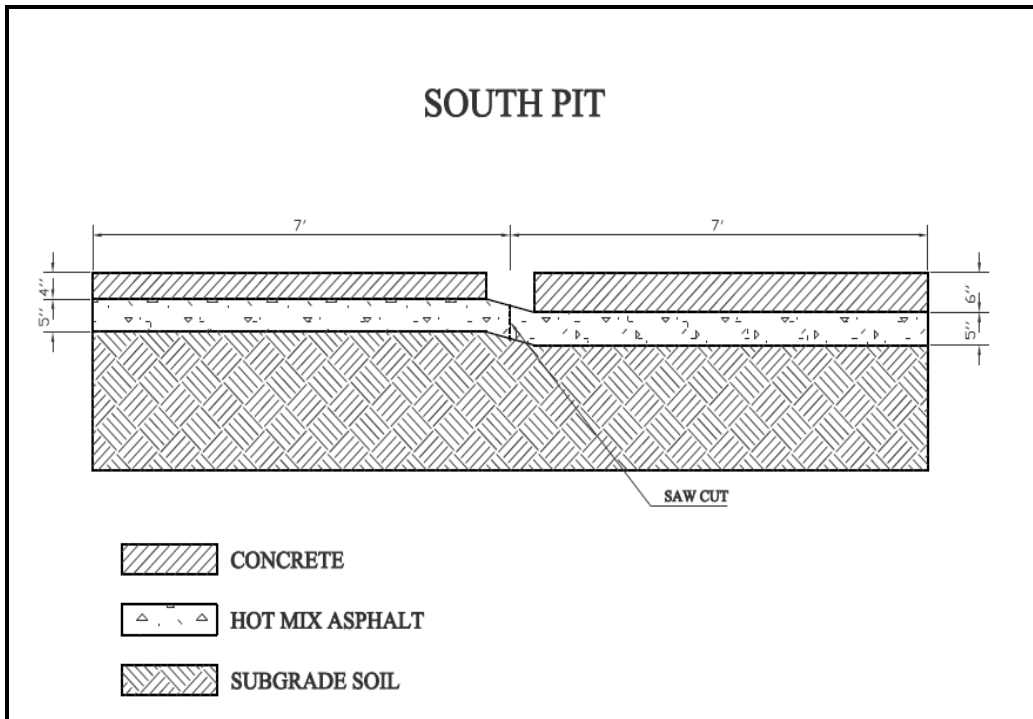


Figure 3.1: CISL #13 TWT Sections

Table 3.1: Nuclear Density Measurements on South Pit

		Date:		11/11/03	
		Time:		1440	
		Depth		12"	
		Optimum Density		1582	
		Optimum Moisture		21.3	
		Density Standard		687	
		Moisture Standard		2970	
	% Proctor	Wet	Dry	Moisture	% Moisture
Station #1					
A	93.5	1826	1480	346.3	23.4
B	94.4	1824	1493	330.8	22.2
C	93.2	1818	1475	343.5	23.3
Average	93.7	1822.67	1482.67	340.20	22.97
Station #2					
A	94.9	1825	1501	323.7	21.6
B	94.7	1826	1498	327.9	21.9
C	94.7	1826	1498	327.9	21.9
Average	94.77	1825.67	1499.00	326.50	21.80
Station #3					
A	102.3	1909	1619	289.9	17.9
B	101.4	1907	1604	302.5	18.9
C	101.4	1906	1603	302.5	18.9
Average	101.7	1907.33	1608.67	298.30	18.57
Station #4					
A	97.7	1860	1546	313.8	20.3
B	97.3	1860	1539	320.9	20.9
C	96.8	1859	1531	327.9	21.4
Average	97.27	1859.67	1538.67	320.87	20.87
Station #5					
A	101.9	1936	1612	323.7	20.1
B	100.9	1936	1596	339.2	21.2
C	101.3	1927	1603	323.7	20.2
Average	101.37	1933.00	1603.67	328.87	20.50
Station #6					
A	96.8	1860	1532	327.9	21.4
B	96	1556	1519	336.4	22.1
C	96.7	1860	1529	330.8	21.6
Average	96.5	1758.67	1526.67	331.70	21.70

The HMA layer was placed on the compacted subgrade for both TWT lanes. Initially, the asphalt layer was constructed one inch thicker than the design thickness (5-inch). To avoid the influence between the two pavements, the asphalt layer was cut longitudinally before placement of the concrete layer, as shown in Figure 3.2.

To obtain an HMA layer that could represent a severely distressed layer, the asphalt layer was compacted at the lowest acceptable limit (92%). Also, full depth saw cuts were made in the asphalt layer under the central concrete slab. The location of the saw cuts is presented in Figure 3.2 and was done as follows:

- Two transverse cuts parallel to the concrete joints at a distance of 8 inch;
- One longitudinal cut in the center of the wheelpath.

The performance of TWT is very sensitive to the bonding between the concrete and asphalt layer so the preparation of the interface was carefully performed. The HMA layer was milled one inch; then the surface was cleaned with a broom and with compressed air. The macro-texture of the interface was achieved by milling, while the micro-texture was achieved by abrasive blasting (shot blasting). Before the concrete placement, the surface was again air blasted and wetted. Based on the previous studies and common practices for whitetopping, no other preparation or treatment of the surface was performed (i.e. grouting prior to concrete laying, etc.).

The concrete layers were poured keeping a 4-inch gap between the lanes by placing vertical wood forms between the lanes. This gap was not only used for the structural separation between lanes, but also for the placement of the fixtures for the curling measurement. The pit walls were separated and treated against adhesion to the pavement. The vibration of the concrete was done with a small vibratory compactor; the

finishing was done with a vibratory screed; the texture was created by manual brooming of the surface. The joints of concrete slabs on both lanes were sawn to one third of the depth, to obtain the final dimensions of the two slabs of 10 x 7 feet for the central slab, and 5 feet x 7 feet for the end slabs (Figure 3.3).

The concrete mix was designed for $4\pm 1\%$ entrained air and a 28 day compressive strength of 4,000 psi. Because TWT has a higher exposed surface to volume ratio than the regular concrete pavement and the final concrete strength is very sensitive to curing, proper curing was ensured by spraying water on the finished surface and covering the pavement with a plastic sheet for 28 days. The design of the concrete mix is given in Table 3.2.

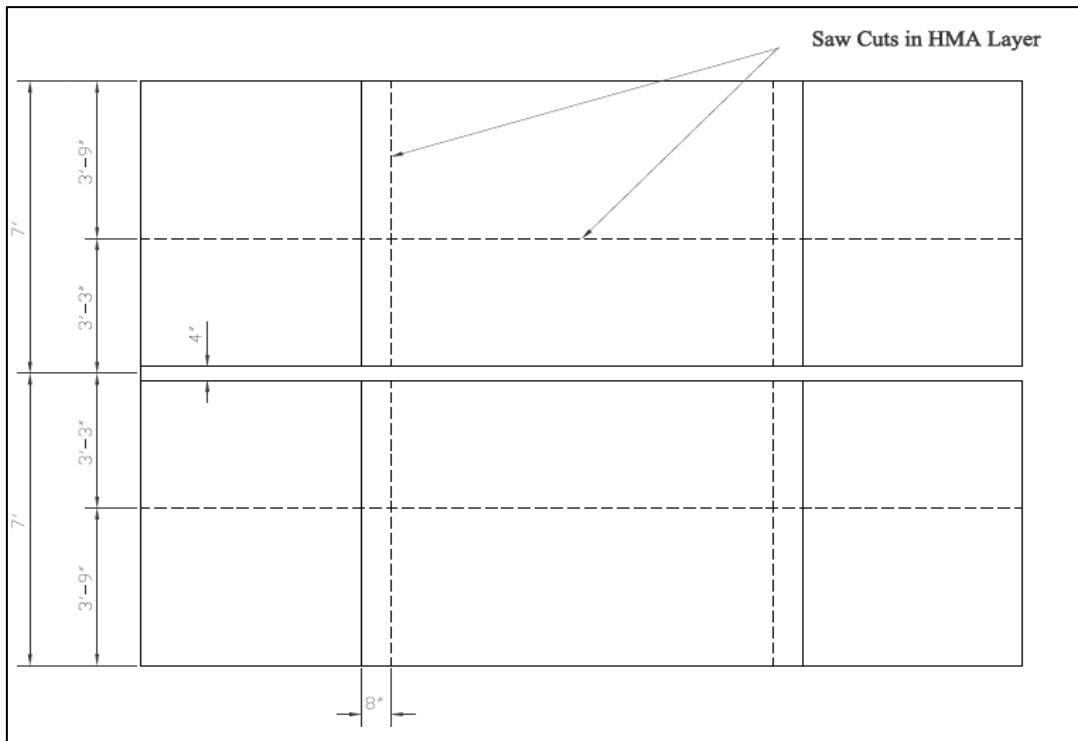


Figure 3.2: Saw Cuts in the HMA Layer.

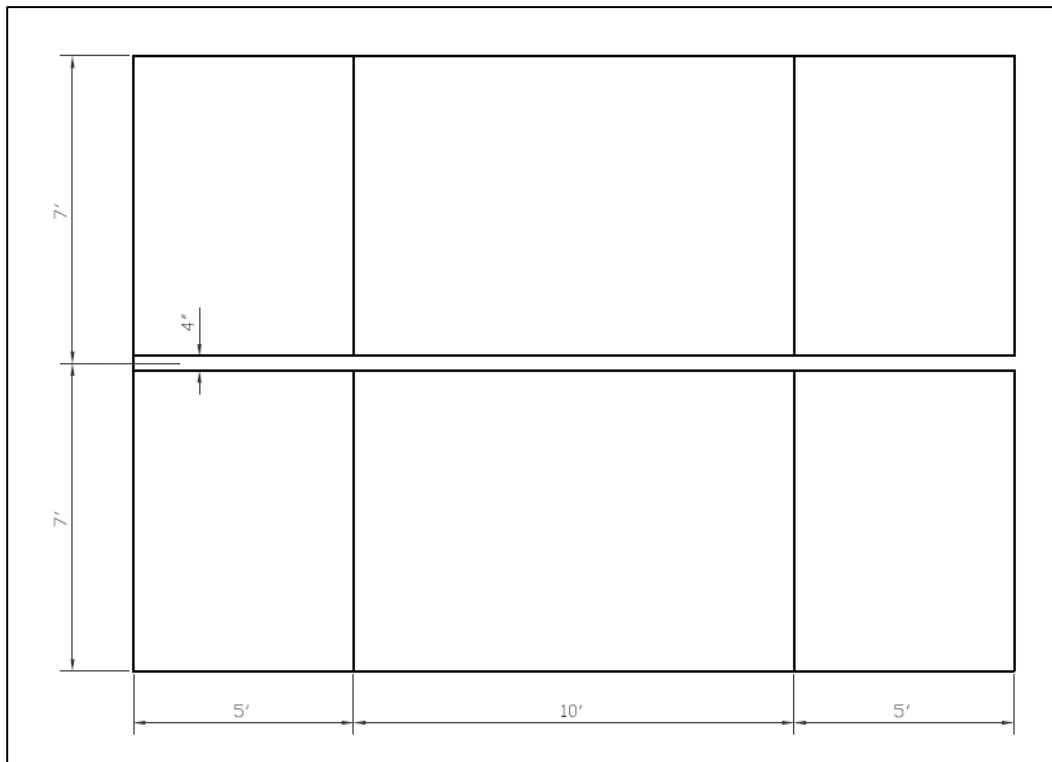


Figure 3.3: TWT Pavement Sections - Joint Spacing

Table 3.2: Design of the Concrete Mix used for TWT

Material	Design Quantity (per cu. yd)
Sand	1029 lb.
CA-6	846 lb.
Type I/II cement	611 lb.
A/E	2.00 oz
Dara65	24.00 oz.
Water	35.1 gal
Hot Water	100 %

3.2 INSTRUMENTATION USED IN THE TWT PAVEMENTS

One of the objectives of the CISL Experiment #13 was to evaluate the behavior of the thin concrete overlays by measuring the response of the pavement to the real loads, and to compare the measured response with that computed by a linear elastic theoretical model. Thus, the pavement was equipped with instrumentation to measure the strains at critical points of the overlay.

Strain gages and thermocouples were embedded in the pavement to monitor the response of the pavement, as shown in Figure 3.4. The instrumentation was installed only in the central slabs. The TWT pavement structure was not subjected to any special heating or cooling cycles, all APT testing in TWT sections was performed at room temperature.

The strain gages were installed at the same positions in both TWT sections, corresponding to critical strain location: at the middle of the tied and untied joints, and at the corner of the slab (Figure 3.4). The placement of the strain gages was done before concrete paving; the strain gages were set in wire fixtures, as shown in Figure 3.5. Two

gages were installed in each location: one gage at one inch from the top of the PCC slab, and one gage at one inch from the bottom of the concrete slab, as follows:

- In the middle of the wheel path and parallel to the western tied joint, with the gages positioned parallel to the joint at two inches inward from the joint.;
- In the middle of the untied joint, two inches from the joint. The gages are parallel to the joint and the wheelpath;
- Twelve inch from the tied joint and twelve inches from the untied joint. The gages are inclined 45° to the joint and the wheelpath.

Strain gages manufactured by Tokyo Sokkai were used based on previous experience. The technical characteristics are shown in Table 3.3.

Table 3.3: Strain Gage Technical Characteristics (TML Tokio Sokki Kenkyujo)

MOLD STRAIN GAGE		SERIES "PM"		Operational temperature: -20°C to 60°C					
Concrete Mortar Material Use									
Gauge pattern	Lead-wire pre-attached	Type	Gauge size (mm)		Backing (mm)				Resistance (ohm)
			l	w	a	b	c	d	
Single element 0.3 mm ² heat resistive vinyl lead-wire pre-attached Total resistance per meter: 0.1 Ohm	2 wire Parallel 2 meter long	PML-60-2L	60	1	125	13	5	4	120

Three thermocouples were placed at each strain measurement locations in horizontal plane, but at different depths: at the middle of the asphalt layer, at the middle of the concrete layer, and at the interface between concrete and asphalt. These thermocouples were fabricated in-house, because similar thermocouples were previously used with good results in past CISL projects.

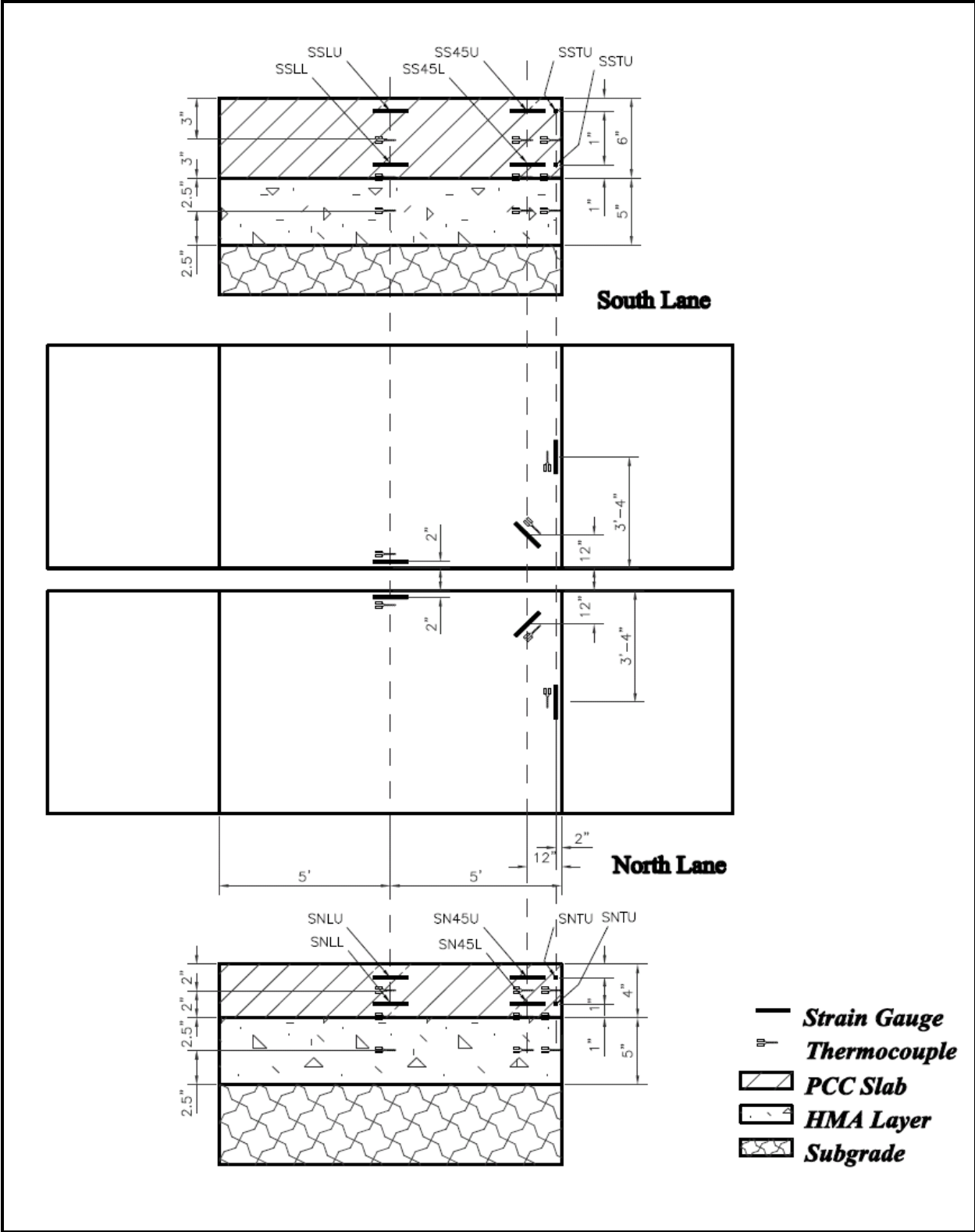


Figure 3.4: Instrumentation for the Thin Whitetopping Pavements



Figure 3.5: Strain Gages and Fixtures Setting

3.3 APT TESTING OF THE TWT PAVEMENTS

The APT testing was conducted under following conditions:

- The lateral wander applied in this experiment followed a truncated normal distribution (Figure 3.6), with the “0” position corresponding to the center of the wheelpath.
- The applied single axle load was approximately 26 kips, equally distributed between the two pavements (13 kips on each pavement). The wheel load was monitored with load cells installed on each wheel.

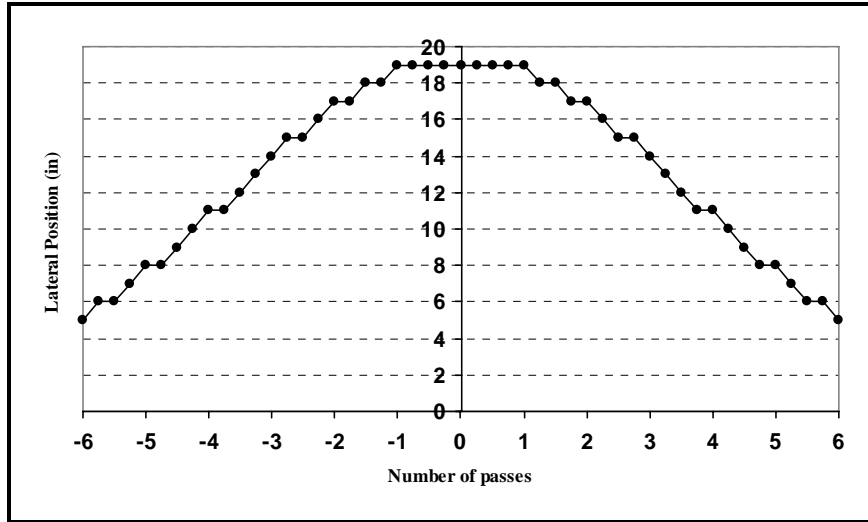


Figure 3.6: Distribution Function for the Lateral Wheel Wander

A total of 2,000,000 passes were applied to the TWT pavements. The activity log for the testing of the TWT pavements is given in Table 3.4.

Table 3.4: Testing of the TWT pavements: Activity Log

Date	Load Repetitions	Comments
04/12/04	Initial	Start Wheel Loading
04/20/04	100k	Take Data and Restart
04/27/04	200k	Take Data and Restart
05/04/04	300k	Take Data and Restart
05/11/04	400k	Take Data and Restart
05/18/04	500k	Take Data and Restart
05/25/04	600k	Service air cylinder seals Take Data and Restart
06/01/04	700k	Take Data and Restart
06/08/04	800k	Take Data and Restart
06/15/04	900k	Take Data and Restart
06/24/04	1M	Machine maintenance and lubrication Take Data and Restart
07/01/04	1.1M	Take Data and Restart
07/08/04	1.2M	Take Data and Restart
07/15/04	1.3M	Take Data and Restart
07/22/04	1.4M	Take Data and Restart
07/29/04	1.5M	Take Data and Restart
08/06/04	1.6M	Take Data and Restart
08/13/04	1.7M	Take Data and Restart
08/20/04	1.8M	Take Data and Restart
08/30/04	1.9M	Measurements for single axle Take Data and Restart
09/15/04	2M	End of Loading. Take Final Data

The testing was performed at ambient temperature. No water was added to the pavements during the APT loading of the two pavement structures.

3.4 PERFORMANCE OF THE TWT OVERLAYS

The TWT pavement sections performed well under the loading by the APT machine. It is important to note that loading was applied at ambient temperature and no water was added to the pavements during the test. Therefore, no severe daily or seasonal changes in temperature in the upper layers, or severe changes in the moisture content in the subgrade soil, were imposed on the tested pavement sections during the experiment.

The 4 inch TWT pavement section exhibited cracking. One transverse crack developed in the central slab, close to the middle of the slab, at about 400,000 passes of the APT machine.

Cracks also developed in the west end slabs of this pavement section. However, the visual observation of the wheels during travel as well as the wheel load data profile recorded suggested that the failure of the end slab did not affect the loading of this section. Figure 3.7 shows the schematic diagram of the cracks recorded on the 4-inch TWT pavement section (SN lane) at the end of loading (2 million passes of the APT machine). No significant joint faulting was recorded.

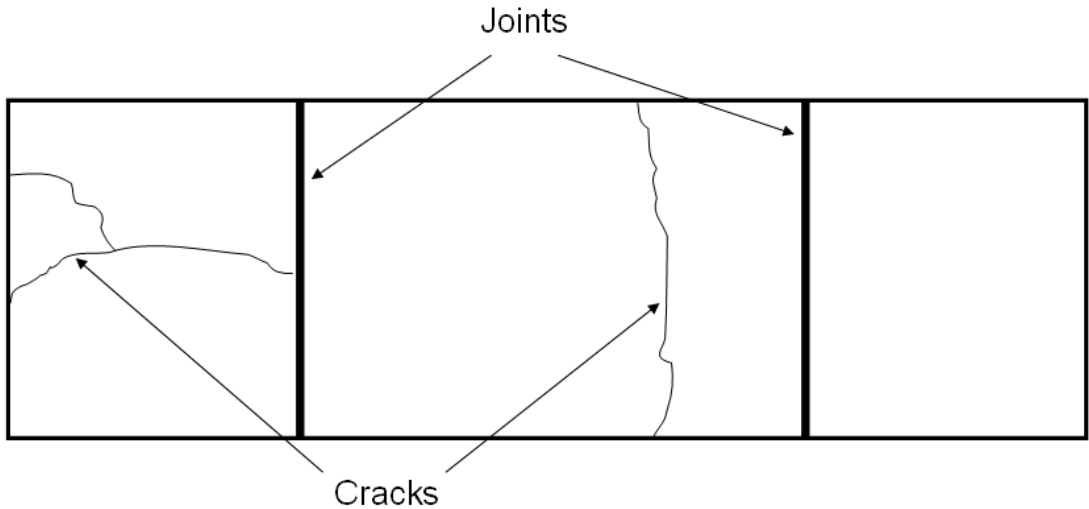


Figure 3.7: Cracks Recorded at the End of Loading: 4-inch TWT Pavement

At the end of loading (2 million passes), the 6-inch TWT pavement section (SS lane) exhibited no cracking or significant joint faulting. Due to budget and time constraints it was decided to stop loading on the TWT sections, even though the 6-inch TWT section showed no distresses.

3.5 Measured Horizontal Strains in Concrete Layer

The strains were measured when the wheel assembly was in the middle of the wheel path (corresponding to “0” position of the wandering device), at a sampling rate of 100 readings per second for four complete cycles (8 passes) of the APT bogie. The measurements were performed at an interval of 100,000 passes of the APT machine. The data was recorded and stored in spreadsheet format together with the data for the axle magnitude and position.

Because the applied load was not precisely constant in time, the measured values of the strain were normalized to a 26-kip single axle load. Figures 3.8, 3.9 and 3.10 present the typical shapes of the strain signals for the typical locations of the gages (tied joint, untied joint and respectively corner) for the 6-inch TWT section. The strains recorded for the 4-inch TWT section have the same general aspect. Values for the peak values of strains are listed in Tables 3.5 and 3.6.

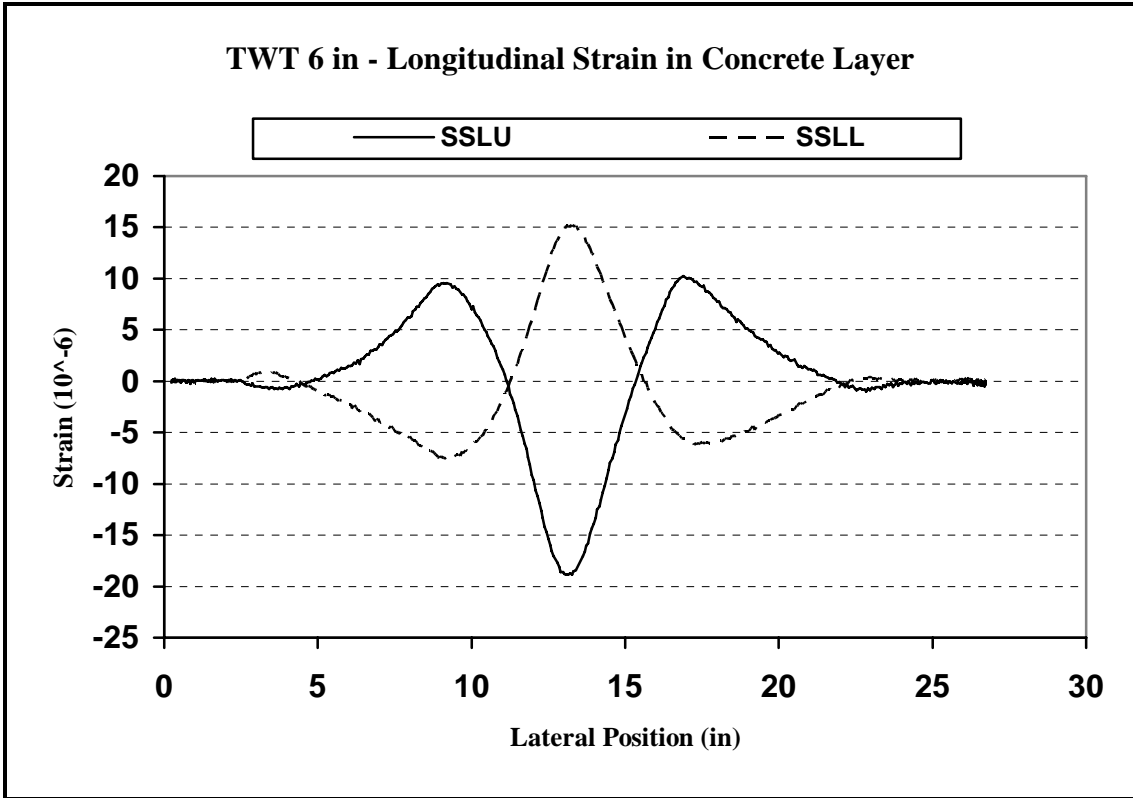


Figure 3.8: Typical Shape of Measured Longitudinal Strain

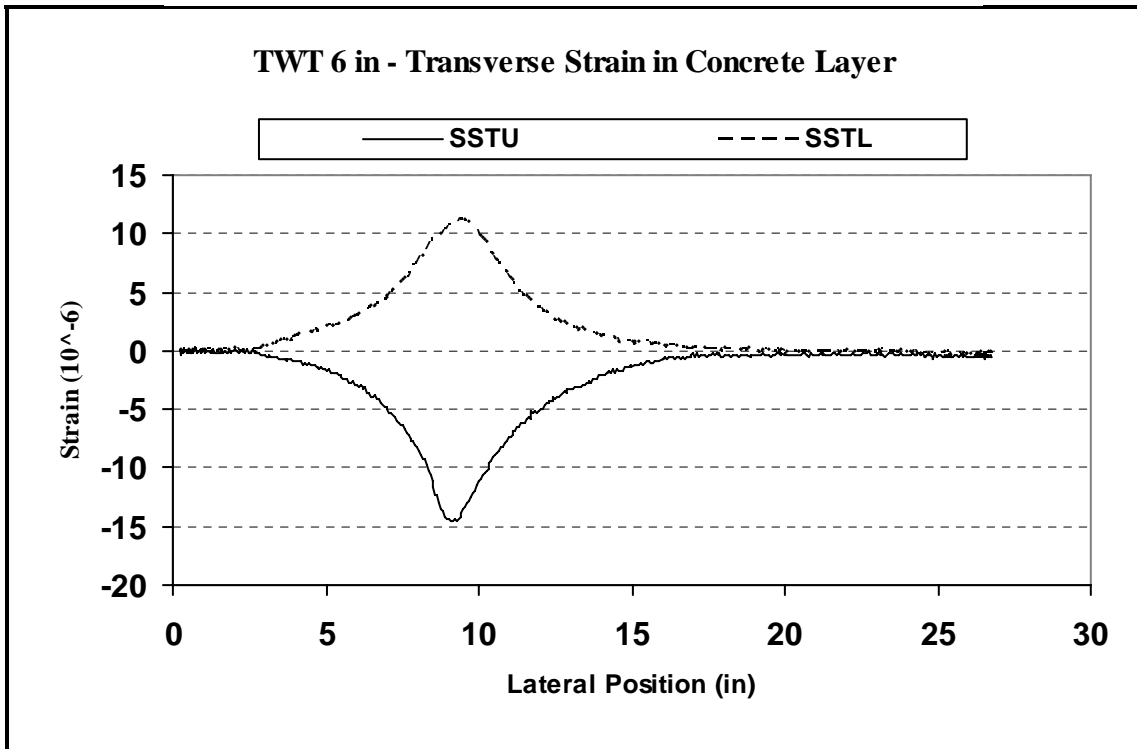


Figure 3.9: Typical Shape of Measured Transverse Strain

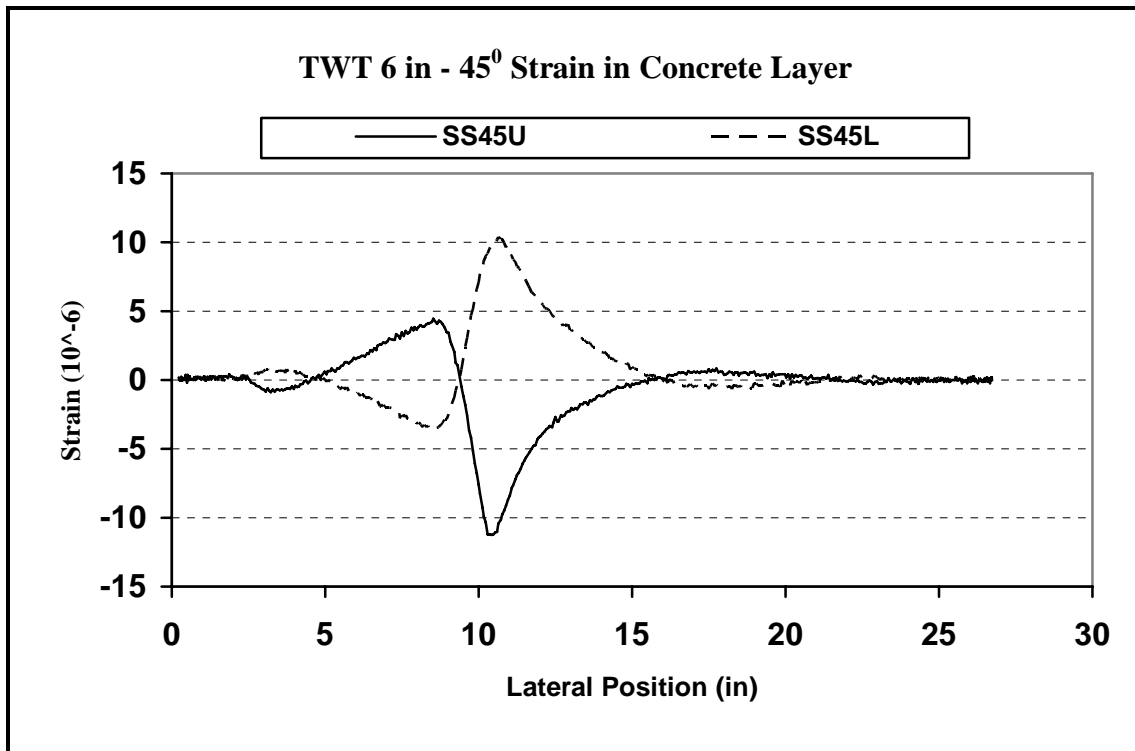


Figure 3.10: Typical Shape of Measured 45° Corner Strain

Table 3.5: Maximum and Minimum Measured Strains: 6-inch TWT

Date	Passes x1,000	Peak	Strain Gage Location					
			SSLU	SLL	SSTU	SSTL	SS45U	SS45L
12-Apr-04	0	max	11.88	5.05	15.75	0.57	8.13	1.00
12-Apr-04	0	min	-7.02	-9.38	-0.52	-16.42	-1.09	-6.92
20-Apr-04	100	max	18.81	7.18	10.81	0.24	10.89	4.21
20-Apr-04	100	min	-9.70	-15.09	-1.26	-16.29	-4.53	-13.11
27-Apr-04	200	max	14.26	7.29	18.29	0.51	9.24	2.66
28-Apr-04	200	min	-10.33	-11.23	-0.23	-20.31	-3.04	-10.03
4-May-04	300	max	12.92	7.44	18.69	0.47	8.96	2.59
5-May-04	300	min	-11.10	-9.57	-0.34	-20.12	-2.55	-8.00
11-May-04	400	max	12.04	9.19	22.81	0.46	8.13	3.23
12-May-04	400	min	-12.37	-9.92	-0.58	-24.02	-2.99	-7.91
18-May-04	500	max	10.42	9.08	26.29	0.38	6.40	3.67
18-May-04	500	min	-12.29	-7.93	-0.56	-25.79	-3.65	-5.39
25-May-04	600	max	11.18	10.87	26.55	0.60	5.29	3.71
25-May-04	600	min	-12.68	-7.81	-0.66	-26.52	-3.95	-5.48
1-Jun-04	700	max	7.84	10.75	29.41	0.81	3.99	2.22
1-Jun-04	700	min	-12.16	-5.20	-0.60	-26.64	-2.65	-3.51
8-Jun-04	800	max	7.68	9.96	27.60	0.96	4.12	2.40
8-Jun-04	800	min	-11.76	-5.11	-0.68	-24.22	-2.68	-3.18
15-Jun-04	900	max	7.82	9.97	27.16	0.93	3.63	1.98
15-Jun-04	900	min	-12.65	-5.20	-0.82	-24.66	-2.49	-3.12
24-Jun-04	1000	max	5.50	7.73	27.68	1.06	1.82	1.36
24-Jun-04	1000	min	-10.43	-3.82	-0.96	-28.61	-1.65	-1.96
1-Jul-04	1100	max	4.42	6.56	16.99	1.18	2.02	1.79
1-Jul-04	1100	min	-7.77	-2.85	-0.94	-15.68	-1.95	-1.83
8-Jul-04	1200	max	4.33	6.61	17.10	0.75	1.82	1.49
8-Jul-04	1200	min	-8.05	-2.48	-0.49	-15.88	-1.73	-1.30
15-Jul-04	1300	max	6.57	9.25	26.01	1.03	2.26	1.28
15-Jul-04	1300	min	-13.90	-4.43	-1.39	-32.59	-2.63	-3.22
22-Jul-04	1400	max	6.58	9.89	27.05	1.78	1.74	1.99
22-Jul-04	1400	min	-13.95	-3.95	-1.42	-39.23	-3.33	-3.17
29-Jul-04	1500	max	5.96	9.15	26.54	1.41	2.10	1.85
29-Jul-04	1500	min	-13.40	-3.50	-1.34	-40.29	-2.65	-2.23
6-Aug-04	1600	max	7.97	9.83	23.90	1.34	3.53	4.69
7-Aug-04	1600	min	-14.82	-4.85	-1.47	-44.19	-6.04	-3.69
13-Aug-04	1700	max	4.53	8.05	24.06	1.47	1.94	1.62
13-Aug-04	1700	min	-13.85	-6.99	-1.71	-32.71	-4.07	-3.13
20-Aug-04	1800	max	7.07	8.43	23.84	0.95	2.53	1.45
20-Aug-04	1800	min	-12.48	-7.71	-2.44	-32.39	-3.59	-3.76
30-Aug-04	1900	max	6.42	9.42	25.29	0.73	2.30	1.64
30-Aug-04	1900	min	-14.48	-6.50	-2.78	-33.58	-4.03	-4.08
15-Sep-04	2000	max	9.90	7.28	25.02	1.33	1.92	2.54
16-Sep-04	2000	min	-12.63	-10.04	-2.92	-31.26	-5.82	-3.50

Table 3.6: Maximum and Minimum Measured Strains: 4-inch TWT

Date	Passes x1,000	Peak	Strain Gage Location					
			SNLU	SNLL	SNTU	SNTL	SN45U	SN45L
12-Apr-04	0	max	11.28	3.50	22.64	0.52	16.17	2.97
12-Apr-04	0	min	-4.98	-3.42	-0.63	-21.28	-3.92	-6.32
20-Apr-04	100	max	7.86	3.44	24.48	0.31	9.93	2.33
20-Apr-04	100	min	-5.98	-5.25	-2.17	-35.03	-5.38	-6.10
27-Apr-04	200	max	8.29	7.59	29.42	0.86	8.87	5.03
28-Apr-04	200	min	-8.46	-3.90	-2.40	-40.85	-12.62	-5.66
4-May-04	300	max	8.47	8.11	27.63	1.01	7.96	2.45
5-May-04	300	min	-10.75	-3.49	-0.45	-32.05	-5.14	-4.30
11-May-04	400	max	9.88	7.92	25.24	0.66	7.49	2.71
12-May-04	400	min	-10.04	-4.46	-0.43	-30.75	-6.30	-4.51
18-May-04	500	max	3.62	11.00	19.32	0.78	16.52	3.47
18-May-04	500	min	-2.46	-2.29	-1.00	-19.09	-7.65	-6.92
25-May-04	600	max	3.38	11.23	20.57	1.15	18.67	4.13
25-May-04	600	min	-2.67	-2.52	-1.34	-19.33	-9.77	-8.24
1-Jun-04	700	max	4.79	13.01	21.54	1.00	22.37	4.68
1-Jun-04	700	min	-4.23	-2.78	-1.03	-16.12	-8.20	-10.21
8-Jun-04	800	max	5.60	11.19	22.28	1.15	24.03	5.34
8-Jun-04	800	min	-4.16	-3.65	-0.65	-15.28	-8.81	-11.11
15-Jun-04	900	max	4.64	11.61	23.13	0.70	24.93	5.61
15-Jun-04	900	min	-4.73	-4.00	-1.10	-16.10	-10.51	-12.04
24-Jun-04	1000	max	5.55	7.01	19.89	0.82	31.38	3.68
24-Jun-04	1000	min	-6.44	-5.22	-0.90	-16.58	-7.42	-16.01
1-Jul-04	1100	max	3.62	4.57	14.51	1.34	13.55	3.88
1-Jul-04	1100	min	-2.84	-1.94	-0.75	-8.06	-5.76	-6.57
8-Jul-04	1200	max	2.78	4.14	14.81	0.64	13.93	4.54
8-Jul-04	1200	min	-2.91	-1.68	-0.34	-8.12	-6.24	-6.22
15-Jul-04	1300	max	3.68	5.82	22.53	0.35	24.37	6.51
15-Jul-04	1300	min	-5.15	-4.25	-1.40	-14.45	-11.02	-11.81
22-Jul-04	1400	max	4.01	5.77	21.95	0.54	21.30	6.32
22-Jul-04	1400	min	-4.74	-3.19	-1.13	-12.84	-10.27	-10.64
29-Jul-04	1500	max	3.66	6.44	21.46	0.61	22.68	5.72
29-Jul-04	1500	min	-4.66	-2.60	-1.66	-11.00	-10.44	-10.40
6-Aug-04	1600	max	3.34	19.92	21.62	0.99	17.83	6.18
7-Aug-04	1600	min	-3.60	-4.46	-0.73	-15.14	-10.61	-7.60
13-Aug-04	1700	max	1.23		23.02	0.74	23.03	5.57
13-Aug-04	1700	min	-5.71		-1.86	-12.32	-12.17	-10.70
20-Aug-04	1800	max	1.82		22.55	0.62	20.39	5.97
20-Aug-04	1800	min	-6.84		-2.31	-9.68	-12.90	-9.06
30-Aug-04	1900	max	3.56		22.48	3.42	24.46	12.13
30-Aug-04	1900	min	-8.31		-2.04	-13.19	-10.89	-11.67
15-Sep-04	2000	max	2.17		22.30	0.98	20.62	5.75
16-Sep-04	2000	min	-6.34		-1.10	-14.48	-16.67	-9.30

3.6 TWT PAVEMENT MODELING

For the finite element modeling (FEM) of the two TWT sections, commercially available software program ANSYS was used to estimate the theoretical response of the test sections. This software has powerful capabilities of modeling structures. However, the employed version limits the user to create a mesh with up to 32,000 nodes.

3.6.1 Geometry Definition

The 3-Dimensional (3-D) FEM model was built for the two TWT sections separately. Each model was developed as a three layer pavement system, corresponding to the three layers of the pavements: concrete, asphalt and subgrade soil. Because the geometry and loading were symmetric, the model was developed for only one half of the structure. Thus, a finer mesh could be used. To model the joints in concrete layer an equivalent interlayer was used. The cracks in the asphalt layer were also taken in consideration in the asphalt layer geometry.

Two transverse gages, located at the top and bottom of the concrete layer, were placed above the saw cut of the asphalt layer, as shown in Figure 3.11. Figures 3.12 and 3.13 indicate that the strain values recorded by these two gages before loading was applied have the same absolute value. This indicates that the subgrade layer has no contribution to the horizontal equilibrium of this vertical section. This indicates that no significant bonding or friction developed between the asphalt layer and the subgrade soil. In order to include this finding in the FEM model of the pavement structures, a thin interlayer was used to model the behavior of the interface between the asphalt layer and the subgrade soil layer.

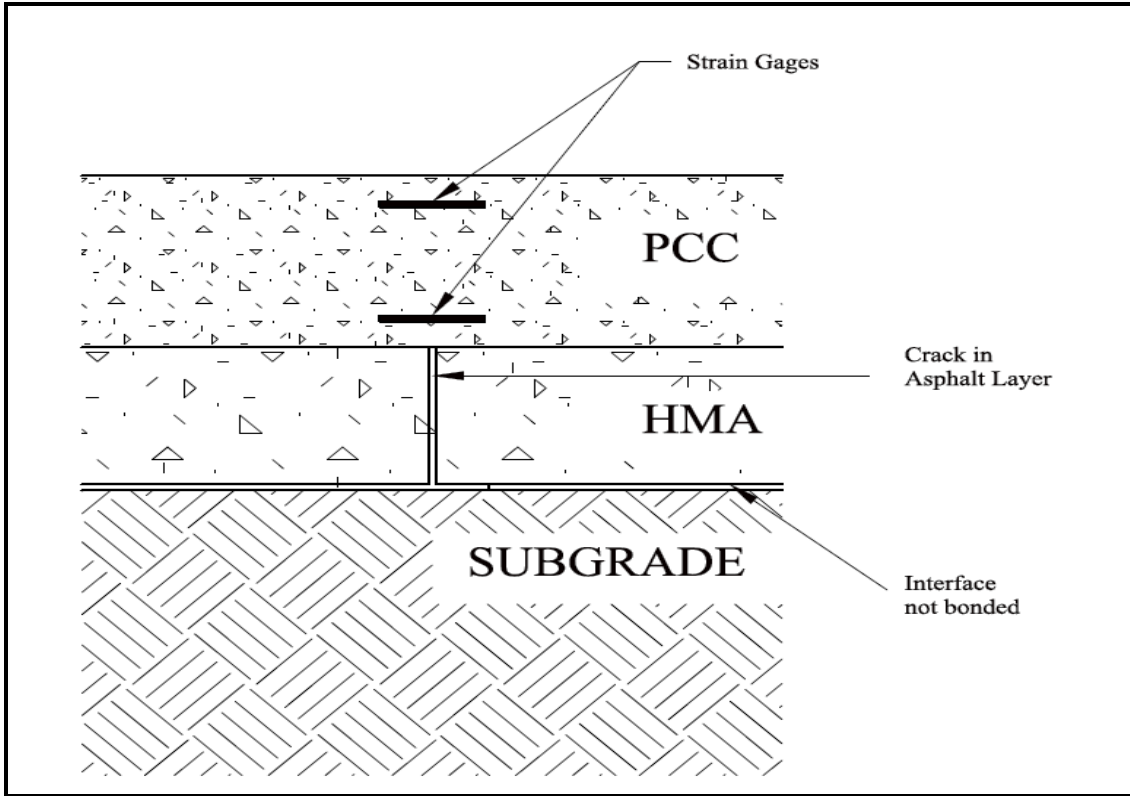


Figure 3.11: Location of Transverse Strain Gages

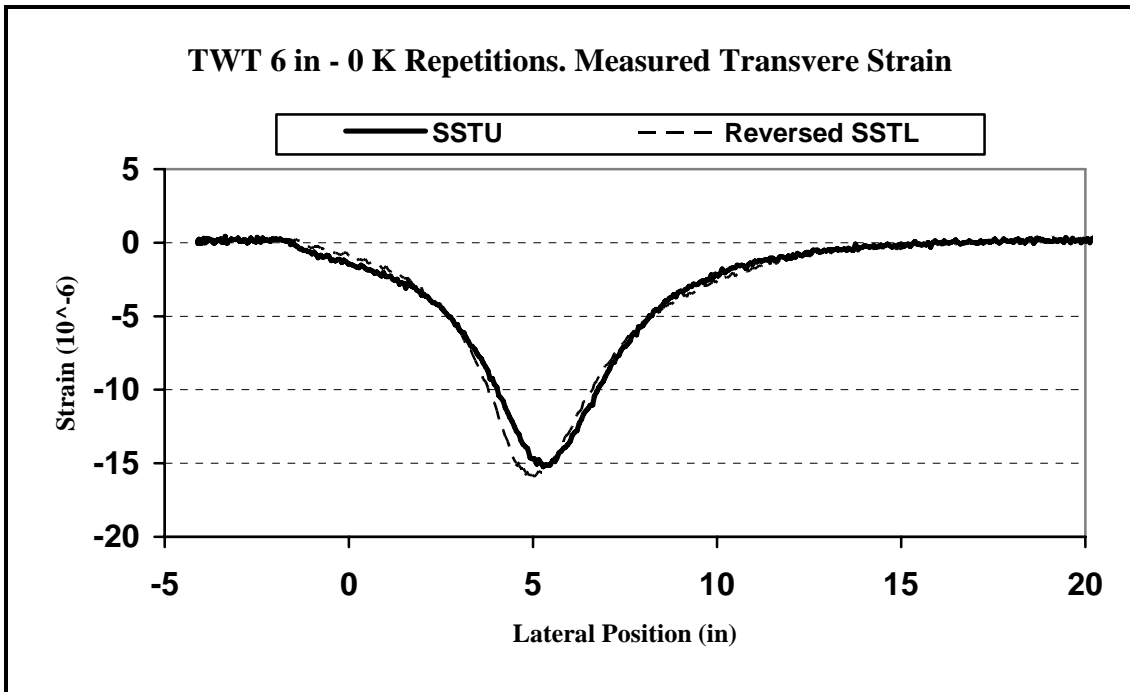


Figure 3.12: Transverse Strain above the Saw Cut in the HMA: 6-inch TWT at 0K

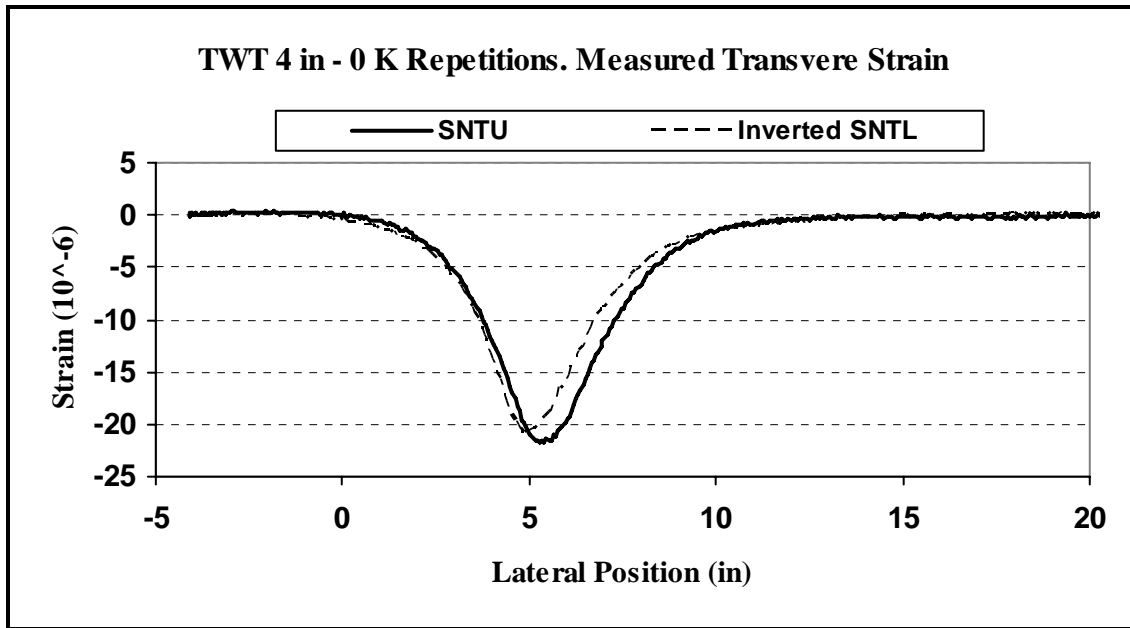


Figure 3.13: Transverse Strain above the Saw Cut in the HMA: 4-inch TWT at 0K

3.6.2 Material Properties

The analysis of the two TWT sections was performed considering all materials (concrete, asphalt and subgrade soil) as linear elastic materials. Thus, the only parameters needed for material description were modulus of elasticity and Poisson's ratio.

For the concrete layer, the modulus of elasticity was estimated from the value of compressive strength using the Equation 3-1 proposed by the American Concrete Institute (ACI). Poisson's ratio for concrete is usually between 0.1 and 0.2, and an average value of 0.15 was used.

$$E=57,000\sqrt{f'_c}\gg 4,000,000\text{psi} \qquad \text{Equation 3-1}$$

In this particular case of loading conditions, the asphalt layer also can be considered as a linear elastic material. The measurements showed an insignificant hysteretic behavior under loading-unloading cycle of the pavements; this proves that

visco-elastic behavior of asphalt layer did not affect the response of the pavement structure.

The dynamic modulus of the asphalt mix varies significantly as a function of the temperature and the frequency of loading. In addition, the dynamic modulus of asphalt is measured in compression, and gives a value of the modulus up to two times greater than the modulus measured in tension; in TWT pavements, the maximum value of the stress in asphalt layer is a tensile stress. For these reasons, the modulus of asphalt was estimated from the equilibrium of the forces in the composite asphalt-concrete section. The computations are based on the measured longitudinal strains. Figure 3.14 shows the change of estimated modulus of asphalt layer during the experiment.

For the estimation of the asphalt modulus, the equilibrium of a segment of the section of the composite section having a finite width “t” was analyzed (Figure 3.15). Because of the quasi perfect slipping between composite slab and subgrade soil, the exterior forces loading the slab are vertical; therefore the strains in the slab are caused only by the bending moments M_x and M_y (coordinates as shown in Figure 3.16). Because in our case, the section plane is parallel to the ZY plane the stresses are caused only by the M_y moment.

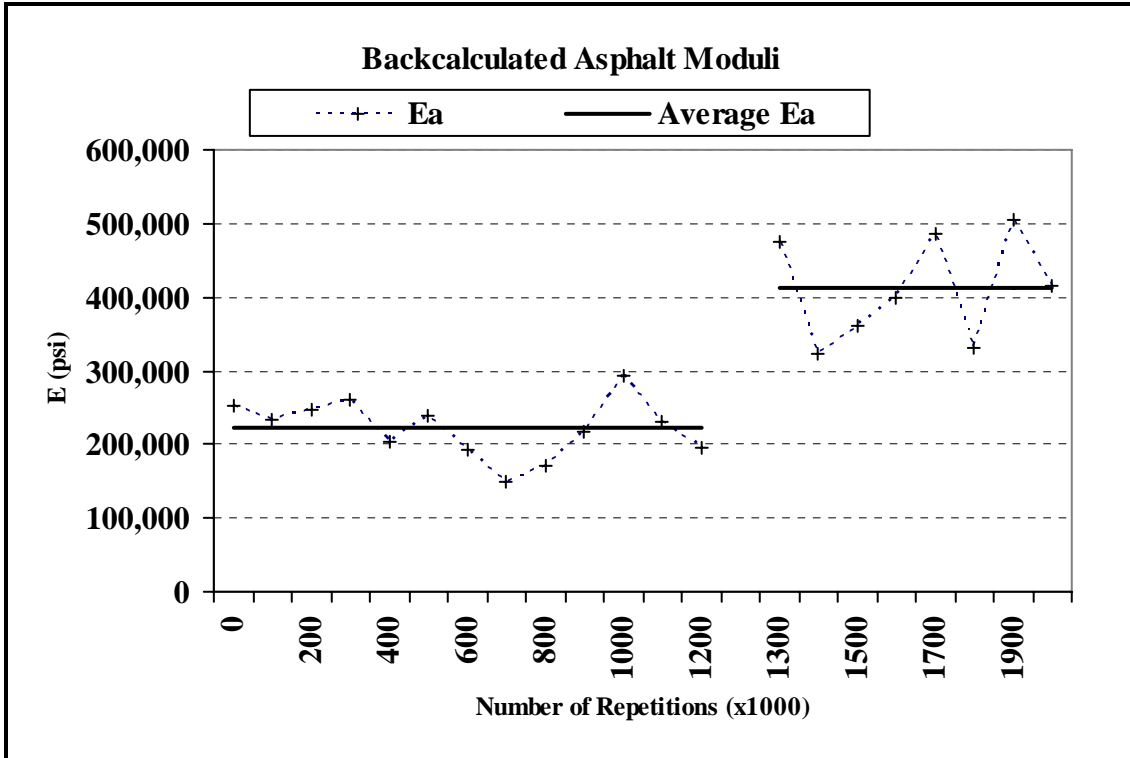


Figure 3.14: Back-Estimated Modulus of the Asphalt Layer

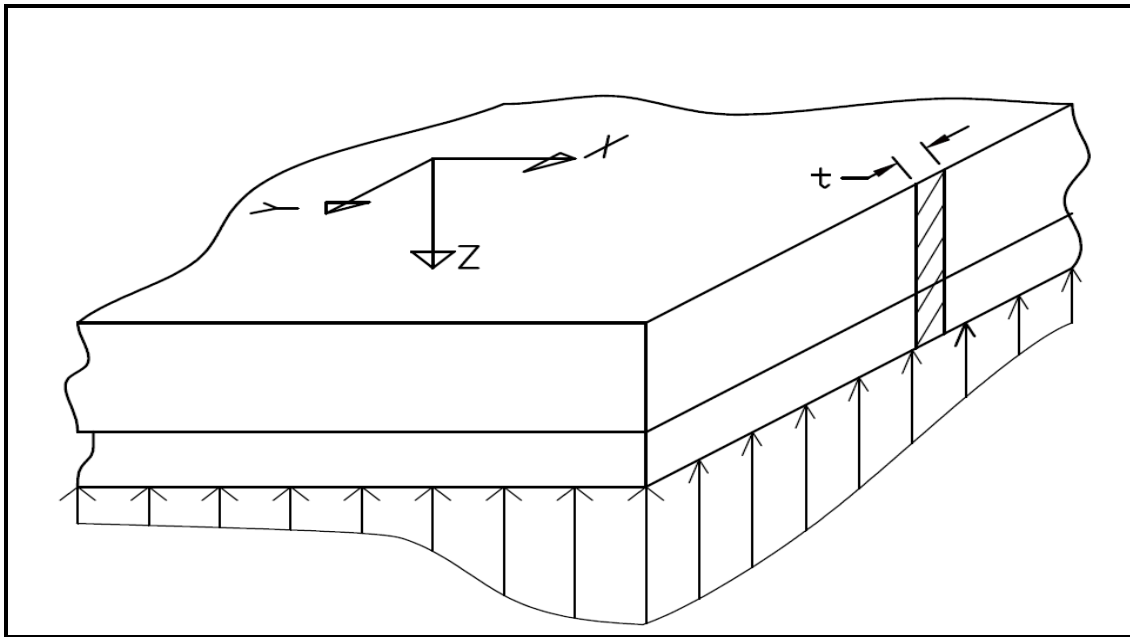


Figure 3.15: Segment Used For Asphalt Modulus Estimation

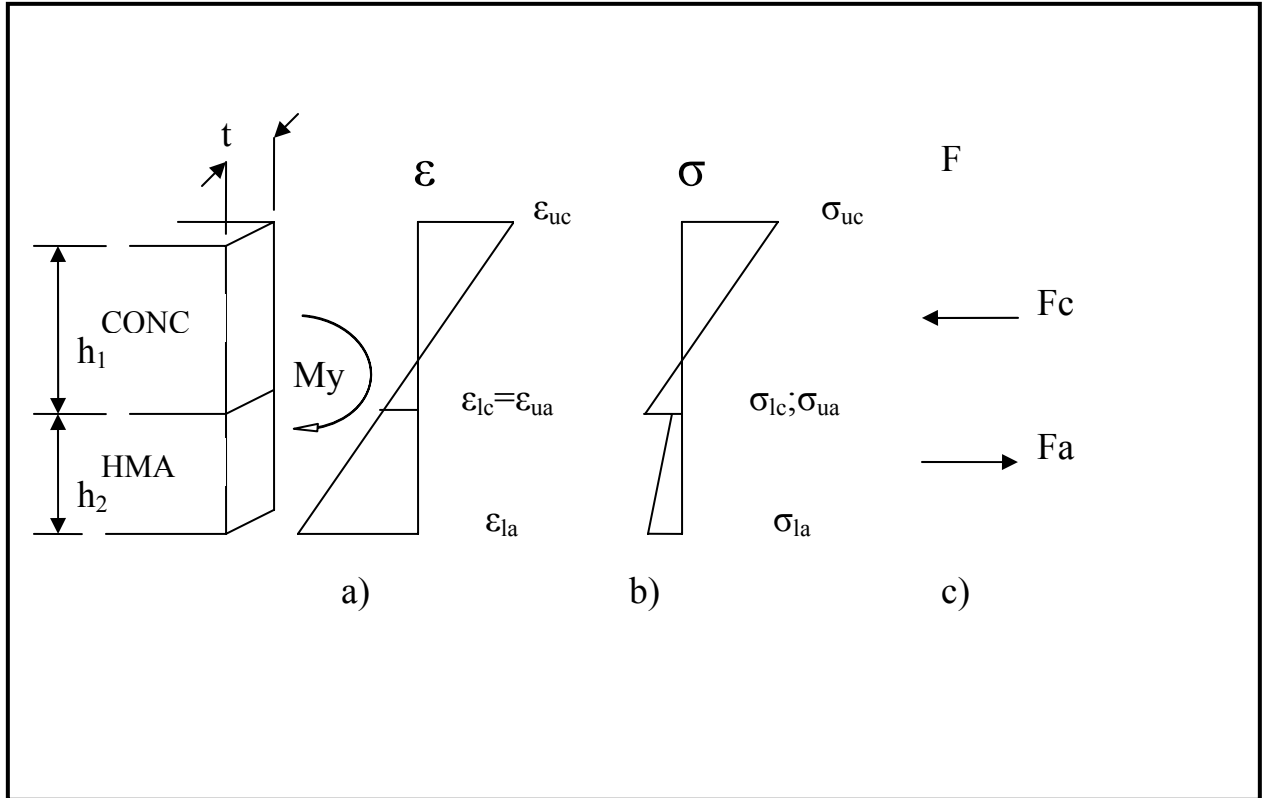


Figure 3.16: Strain and Stress Distribution in Composite Section

It was assumed that the plain sections remain plain after bending, so the strain distribution is linear in the vertical direction. Figure 3.16 shows the strain distribution, stress distribution and resultant forces for concrete and asphalt layers for a section parallel to the ZY plane. These resultants are computed as follows:

$$F_c = \frac{(\sigma_{uc} + \sigma_{lc})}{2} * h_1 * t = \frac{E_c (\epsilon_{uc} + \epsilon_{lc})}{2} * h_1 * t \quad \text{Equation 3-2}$$

$$F_a = \frac{(\sigma_{ua} + \sigma_{la})}{2} * h_2 * t = \frac{E_a (\epsilon_{ua} + \epsilon_{la})}{2} * h_2 * t \quad \text{Equation 3-3}$$

Where:

- F_c -resultant force of the concrete layer
- F_a -resultant force of the asphalt layer
- σ_{uc} -normal stress at the top of the concrete layer

- σ_{lc} -normal stress at the bottom of the concrete layer
- σ_{ua} -normal stress at the top of the asphalt layer
- ϵ_{la} -normal strain at the bottom of the asphalt layer
- ϵ_{uc} -normal strain at the top of the concrete layer
- ϵ_{lc} -normal strain at the bottom of the concrete layer
- ϵ_{ua} -normal strain at the top of the asphalt layer
- ϵ_{la} - normal strain at the bottom of the asphalt layer
- h_1 -thickness of the concrete layer
- h_2 - thickness of the asphalt layer
- E_c -concrete modulus
- E_a -asphalt modulus
- t -width of the analyzed segment

The backcalculation formula (Eq. 3.5) is computed from Equations 3-2 and 3-3, and equilibrium equation 3-4.

$$F_c = F_a \quad \text{Equation 3-4}$$

$$E_a = E_c \frac{(\epsilon_{uc} + \epsilon_{lc}) * h_2}{(\epsilon_{ua} + \epsilon_{la}) h_1} \quad \text{Equation 3-5}$$

The subgrade soil modulus was assumed based on results of the triaxial resilient modulus test performed in the laboratory ($E \approx 20,000$ psi). The Poisson's ratio was considered to be 0.45. An orthotropic interlayer having no stiffness in horizontal directions and the same modulus of elasticity and Poisson's ratio for the vertical direction as those of the subgrade soil was used to model the ideal slip between the asphalt layer and the subgrade layer. The use of the contact elements instead of the

interlayer for modeling of this interface was also considered, but computational problems were encountered.

3.6.3 Model Mesh Generation

Mesh generation is important in finite element modeling because of its influence on the accuracy of computation. In most cases, a finer mesh produces better results, but requires larger computational resources. Usually, the mesh definition is limited by the software capacity. The ANSYS software version used in this research was limited to 32,000 nodes and 32,000 finite elements. Because of the limitation of the available software, a rational balance between mesh size and the particularities of the model had to be taken in consideration during the FEM model development.

The concrete layer was manually meshed using a 3-D brick element with 20 nodes SOLID186 (Figure 3.17). Because the stress change is much larger in horizontal direction, the size of the finite element was 4 x 4 inch in horizontal plane, and 1 inch thickness. The aspect ratio of 4:1 gives accurate results for this type of finite element. Because the larger changes of the stress, the mesh was refined around the discontinuities created by joints. Also, the mesh was refined about the measuring points.

The asphalt layer was also meshed manually, using a 3-D brick element SOLID186 as concrete layer. The size of the finite element was 4 x 4-inch in the horizontal direction, and 2.5-inch in the vertical direction.

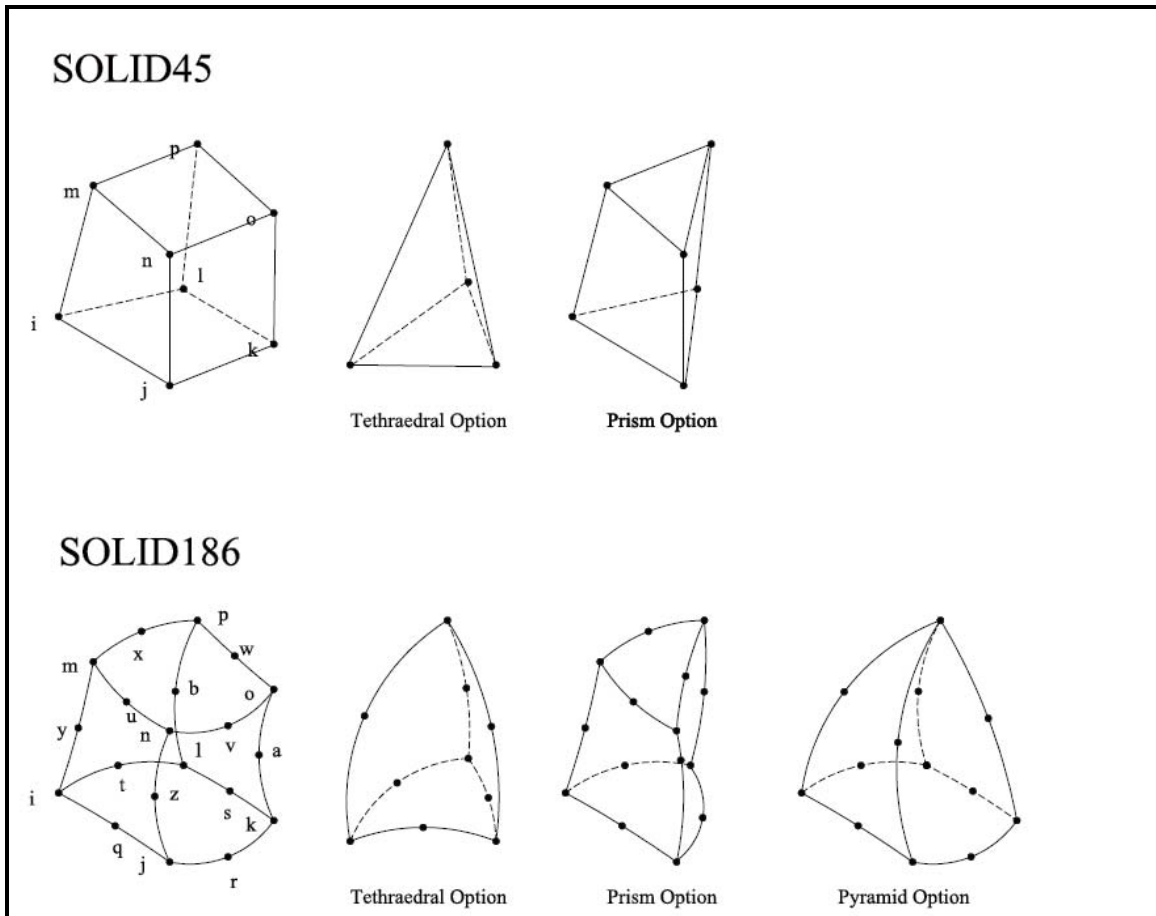


Figure 3.17: SOLID186 and SOLID45 Geometry

Because the strains are smaller as the depth in the pavement structure increases, a coarser mesh was used for the subgrade layer. The finite element used was a 3-D brick with 8 nodes SOLID45 (Figure 3.17). The mesh for this layer was generated automatically, from 4-inch mesh size at the top of the layer, to 30-inch at the bottom of the layer.

A thin interlayer was used to model the slippage between the subgrade soil and the asphalt layer. The interlayer thickness was set to 0.2-inch; a thinner layer resulted in element shape distortions. The interlayer was meshed automatically using 3-D brick elements with 8 node solid element (SOLID45).

The final meshing used about 32,000 elements and 32,000 nodes. For better accuracy of the computations and interpolations of the results, the concrete slab and asphalt layer was modeled using rectangular finite elements. Figure 3.18 shows the general meshing of the model.

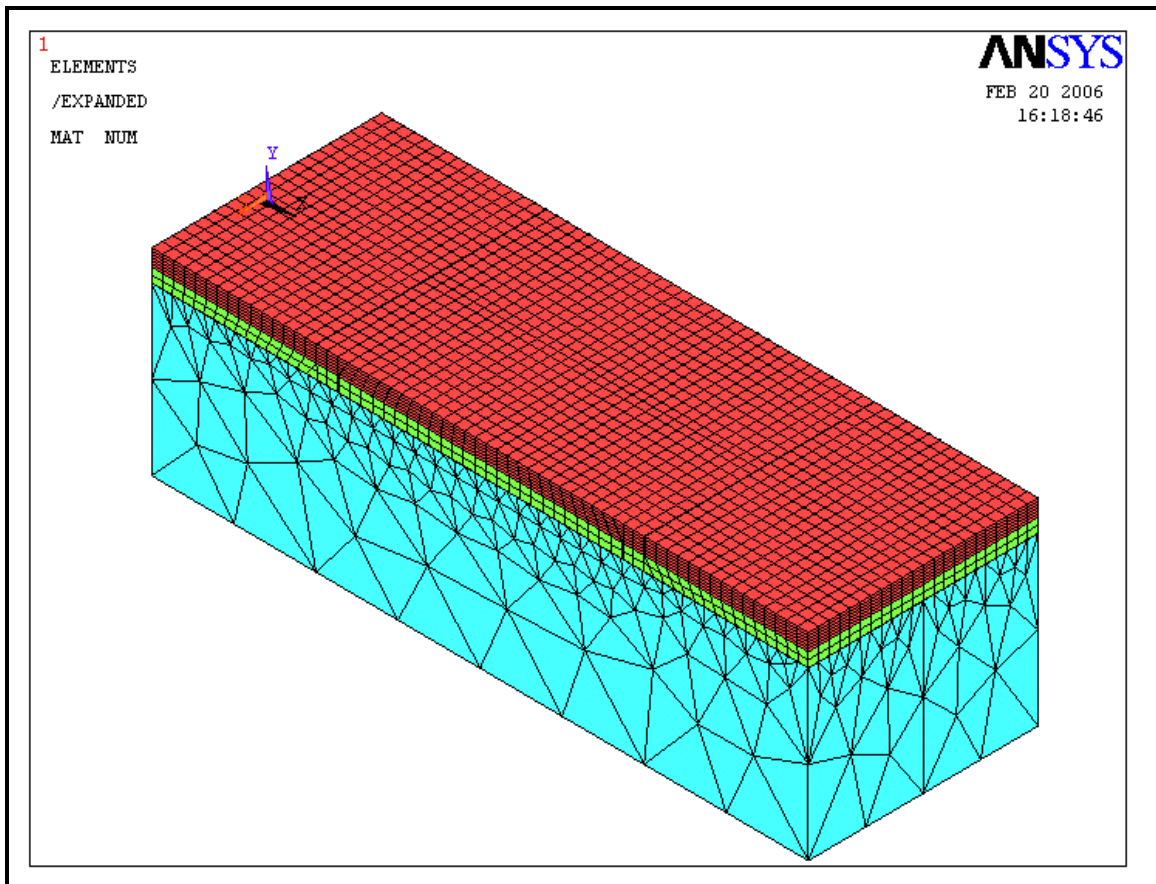


Figure 3.18: Model of the 6-inch TWT (Expanded for Symmetry)

3.6.4 Boundary Conditions and Loads

The bottom of the subgrade was assumed fixed in all directions. However, the displacements in the x, y, and z direction were restrained for all nodes. The nodes on the sides of the subgrade layer bordered by the pit were restrained in the direction of the pit walls. The nodes of the surfaces of the concrete and soil layers in the plane of

symmetry were allowed to move only in the vertical direction for a symmetrically loaded structure (M_y , M_z , and R_x restrained).

The loading was applied to the model at different positions along the wheelpath as a pressure on the element face. The longitudinal positions of the load were chosen according to the shape of the strain diagram; the spacing between loading points was shorter when the curvature of the diagram was larger. The modeled load was assumed to be rectangular, constant over the applied surface and equal to the tire inflation pressure (Figure 3.19). The length of the contact rectangle was computed from the tire width and inflation pressure as follows:

$$p = \frac{P}{S} = \frac{13,000\text{lbs}}{2 \cdot 8\text{in} \cdot L_x} = 100\text{psi} \quad \text{Equation 3-6}$$

$$L_x = \frac{13,000\text{lbs}}{2 \cdot 8\text{in} \cdot 100\text{psi}} = 8.125\text{in} \quad \text{Equation 3-7}$$

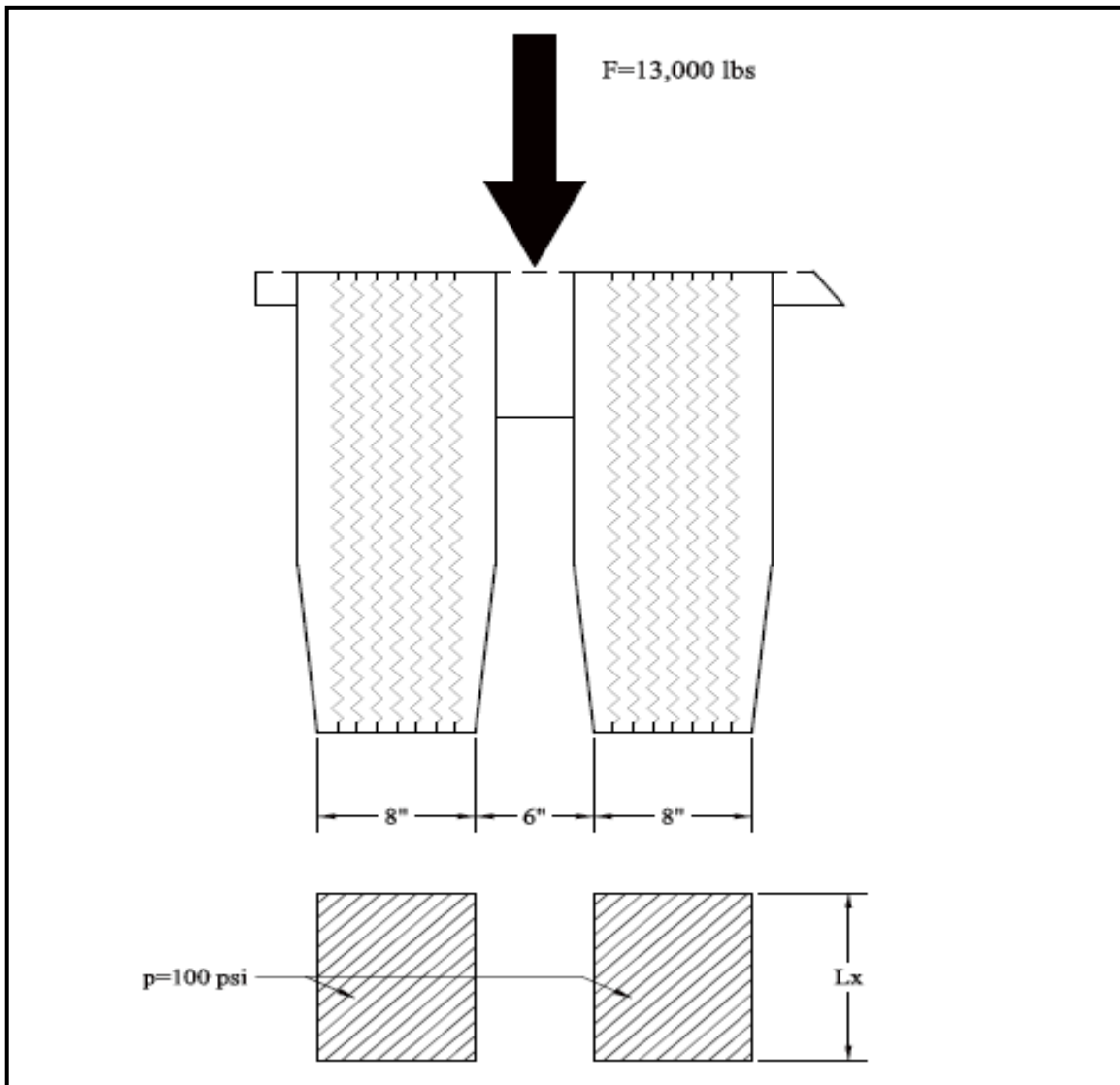


Figure 3.19: Load Model

3.7 Analysis of Response Data of Twt PAVEMENTS

The analysis of the pavements response was carried out by comparing the corresponding measured and theoretically computed strains for each pavement section. The theoretically computed strains were based on the FEM model that used the input data for material characterization presented in Table 3.7. The theoretically computed

strains used in the comparison correspond to the measuring point locations. The position of the strain gages is shown in Figure 3.4.

Table 3.7: Input Data for Material Characterization

Material	Elastic modulus (psi)	Poisson's Ratio
PCC Concrete	4,000,000	0.15
Asphalt Concrete	2,200,000	0.40
Soil	20,000	0.45
Steel	24,000,000	0.30

The initial modeling of pavement response took into consideration the known distresses of the pavements induced in the first phase of the experiment, such as saw cuts of the asphalt layer in TWT sections, and the cracking in the bottom PCC slab generated by joint faulting in TCO on PCCP sections. The coring of the central slabs of the pavements at the end of loading revealed that no de-bonding occurred in the middle slabs, so the overlays were considered fully bonded to the bottom slab. The initial loss of support achieved during joint faulting of the TCO on PCCP could not be directly measured, so the initial models did not take this distress into consideration.

The differences between measured strains and theoretically computed results were used to assess the influence of the loss of support under the joints. The model used for the initial computations considered the support provided by the subgrade soil being uniform.

3.7.1 Results of the Modeling of 4-inch TWT Pavement

As presented in Section 3.5, the FEM model was built taking into consideration the saw cuts in the asphalt layer. The subgrade was assumed to provide uniform support to the asphalt layer, and the overlay was considered fully bonded.

The theoretical response was computed based on the model previously described. The theoretical results of the strains located at the measuring points are plotted in Figures 3.20 and 3.21. The maximum values of the compressive longitudinal strains were -9.57 microstrain for the position corresponding to the SNLU strain gage, and +6.63 microstrain for the position corresponding to the SNLL strain gage. The maximum value of the theoretical transverse strain was -47.41 microstrain for the position corresponding to the SNTU strain gage, and +31.53 microstrain for the position corresponding to the SNTL strain gage.

Figure 3.22 shows the comparison of theoretical and measured strains corresponding to the SNTU strain gage. The data in the legend indicate the number of passes at which the strain measurements were recorded, in thousands. The maximum values of the measured transverse strain are close to the computed values (-47.41 microstrain computed, -43.33 microstrain measured), showing no significant influence of distresses on the strain occurred during the experiment. The evolution of the peak values of the measured strains with the number of applied passes are shown in Figure 3.23. The peak values of the measured strains are stable during the experiment; the small variation might have been caused by curling of the slab during the experiment.

Figure 3.24 shows the comparison between the theoretical longitudinal strain and measured longitudinal strain corresponding to the SNLU strain gage. The theoretical strain values (thick line with black dots) are very close to the initially (0 load repetitions) measured strain values (thick line). The evolution of the peak values of the measured longitudinal strains are plotted in Figure 3.25. These values are constant between 0 and 400,000 load repetitions, and then a significant drop can be observed. This drop may be

explained by the crack on the PCC overlay that appeared between 400,000 and 500,000 load repetitions. In addition, the graph shows an increase of the tensile peaks of the strain corresponding to a load position at the west joint of the central slab. This evolution of strain occurred between 0 and 400,000 load repetitions, and may indicate loss of support under the joint.

The FEM model was modified for different loss of support distances from the joint (0 inches, 12 inches, 24 inches) in order to compare the computed strains with the measured strains by the SNLU gage. The SNLU strain gage was chosen for comparison because in this position strains are most sensitive to the loss of support. The longitudinal strains for SNLU position corresponding to the loss of support distances were plotted in Figure 3.26. The maximum tensile values of the longitudinal strain were plotted in Figure 3.27 and the regression Equation 4-1 was obtained to relate the length of loss of support to the strain.

$$L_{LOS} = -0.7364S_{SNLU}^2 + 13.682S_{SNLU} - 39.481 \quad \text{Equation 3-8}$$

Where:

L_{LOS} -Loss of support length (in)

S_{SNLU} -Maximum computed tensile longitudinal strain at SNLU measuring point (microstrain)

Based on the regression equation (Equation 3-8), the loss of support distance was back-estimated for the period between 0 and 400,000 load repetitions, and the results are plotted in Figure 3.28. The figure shows that the loss of support increased between 0 and 200,000 load repetitions, and then stabilized to a distance of 23 inches on the West joint and 14 inches on the East joint.

The FEM model was modified and run again for loss of support lengths of 23 inches on the West joint and 14 inches on the East joint. This loss of support distances correspond to the values occurred in the whitetopping before cracking. The new computed and measured strains are compared in Figure 3.29. The figure indicates that the computed and measured strains at SNLU are very close. Thus, the assumption for the lineal extent of the loss of support is correct.

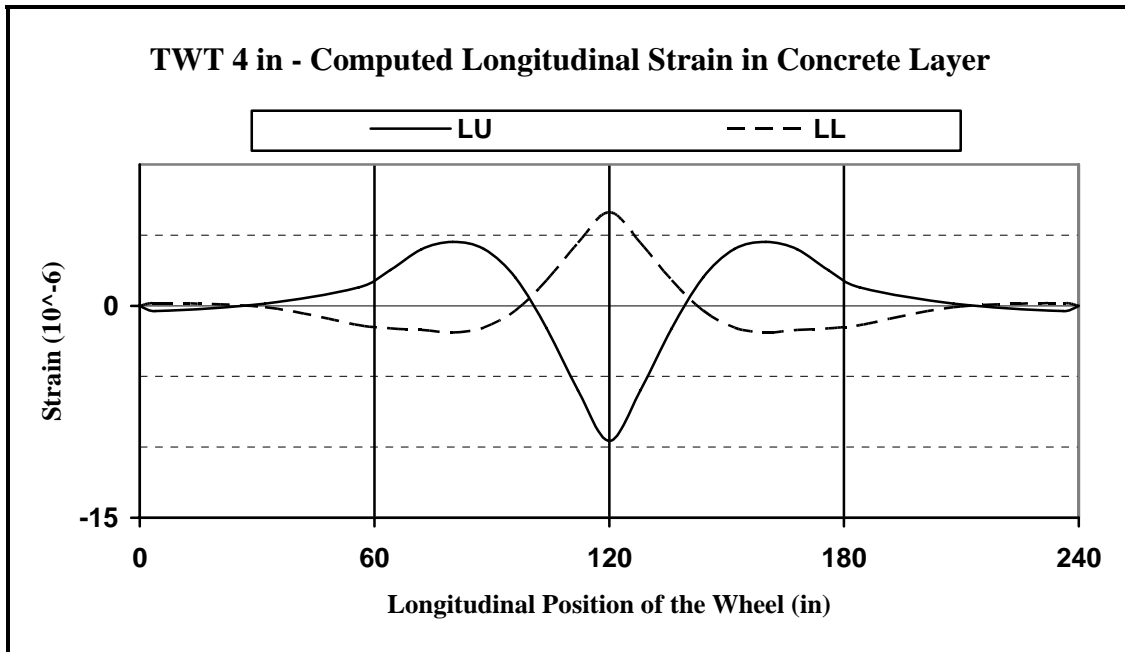


Figure 3.20: Computed Longitudinal Strains for the 4-inch TWT Pavement

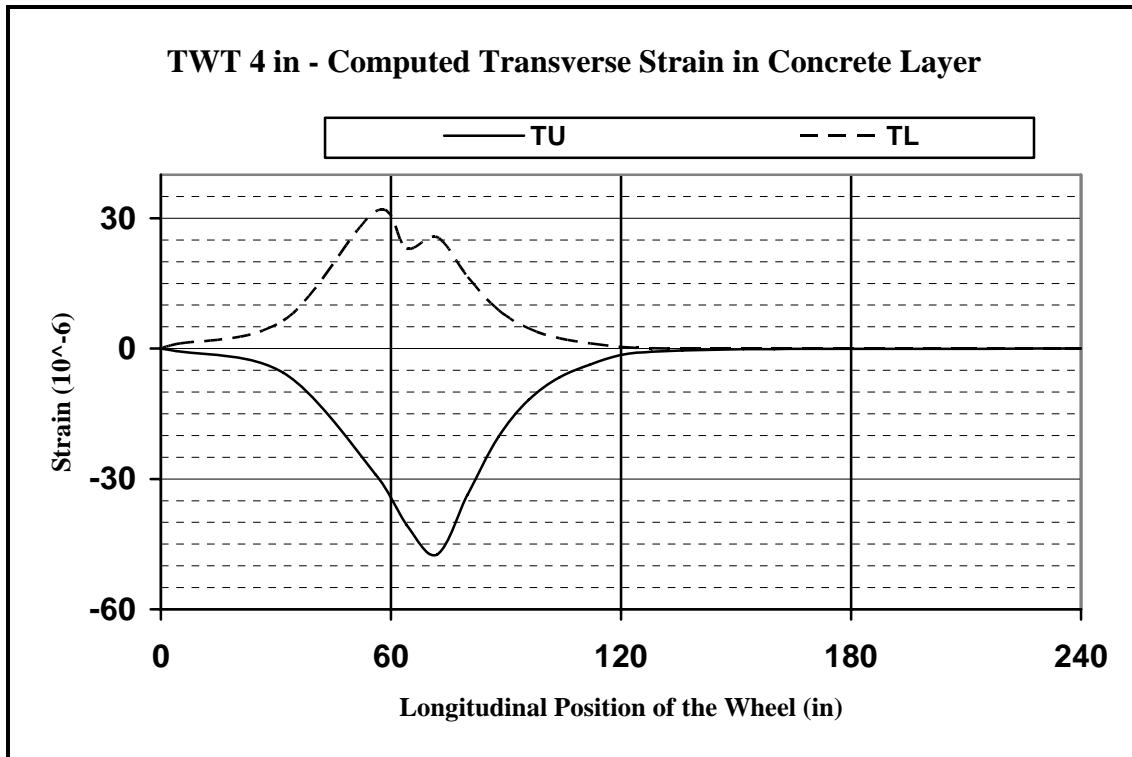


Figure 3.21: Computed Transverse Strains: 4-inch TWT Pavement

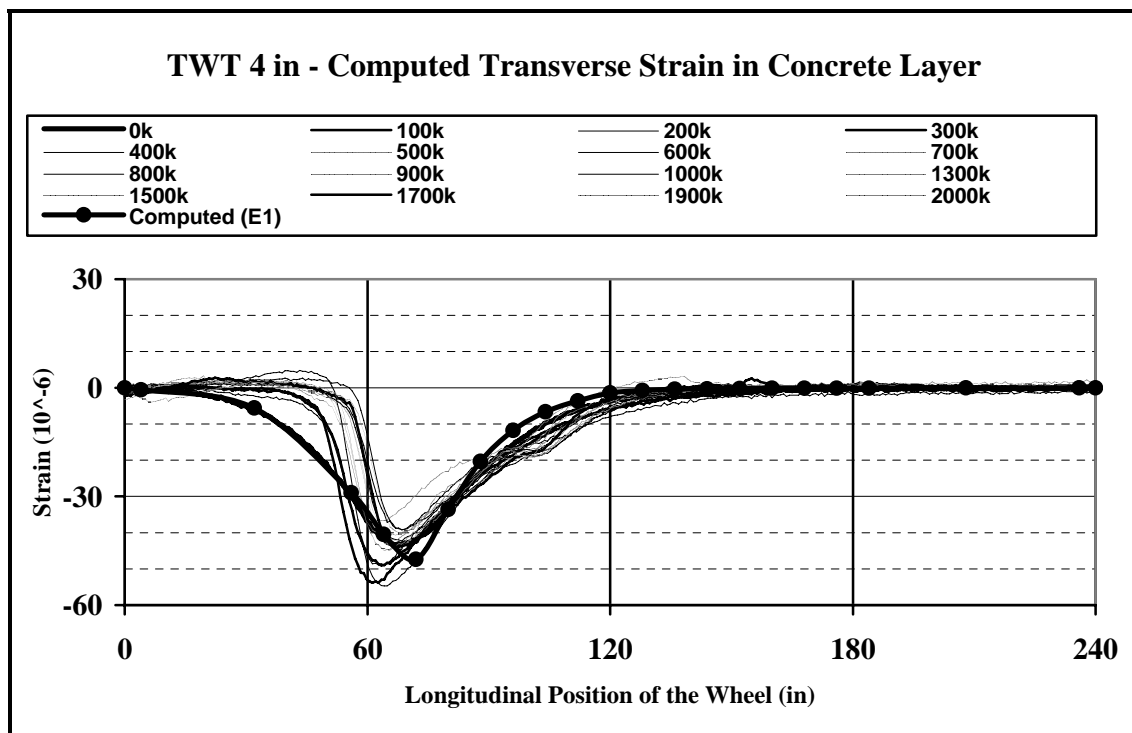


Figure 3.22: Measured vs. Computed Transverse Strains: 4-inch TWT Pavement

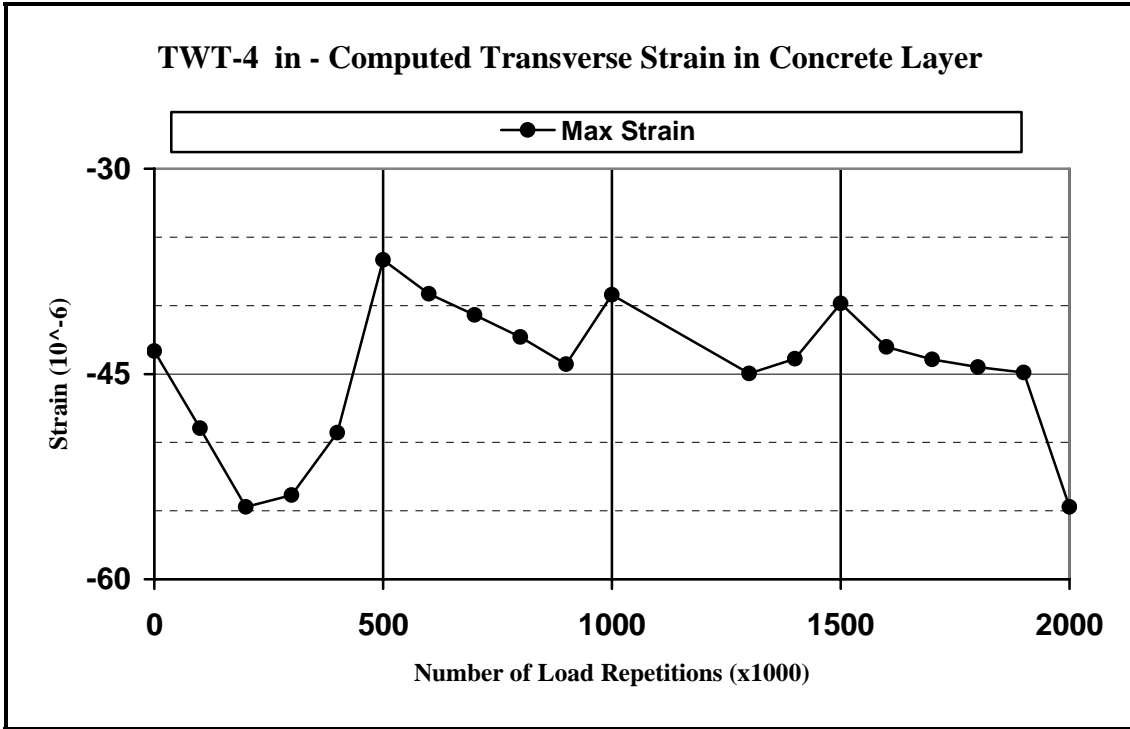


Figure 3.23: Evolution of Maximum Measured Transverse Strains: 4-inch TWT Pavement

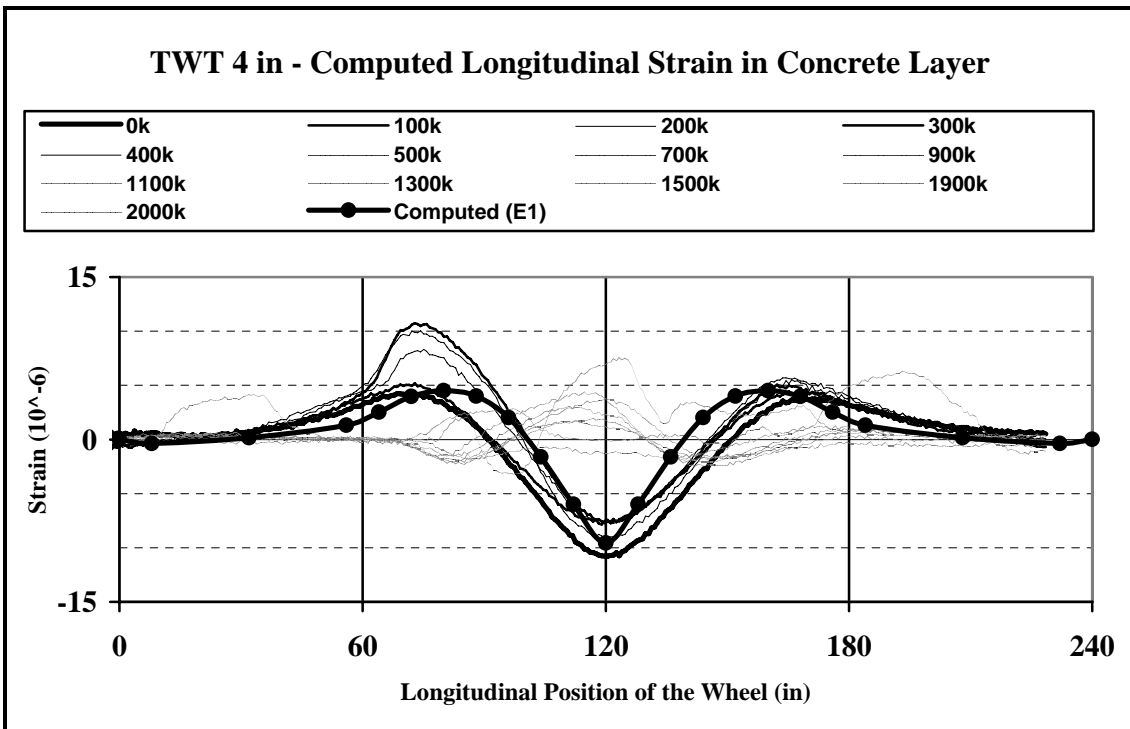


Figure 3.24: Measured vs. Computed Longitudinal Strains: 4-inch TWT Pavement

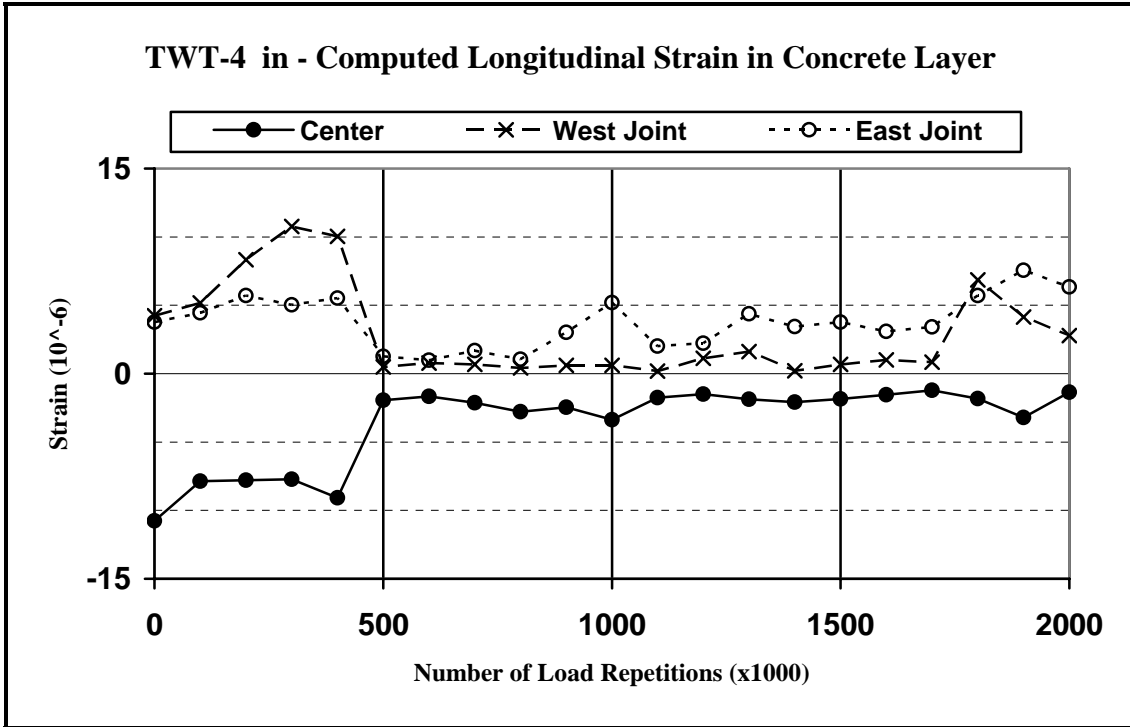


Figure 3.25: Evolution of Maximum Measured Transverse Strains: 4-inch TWT Pavement

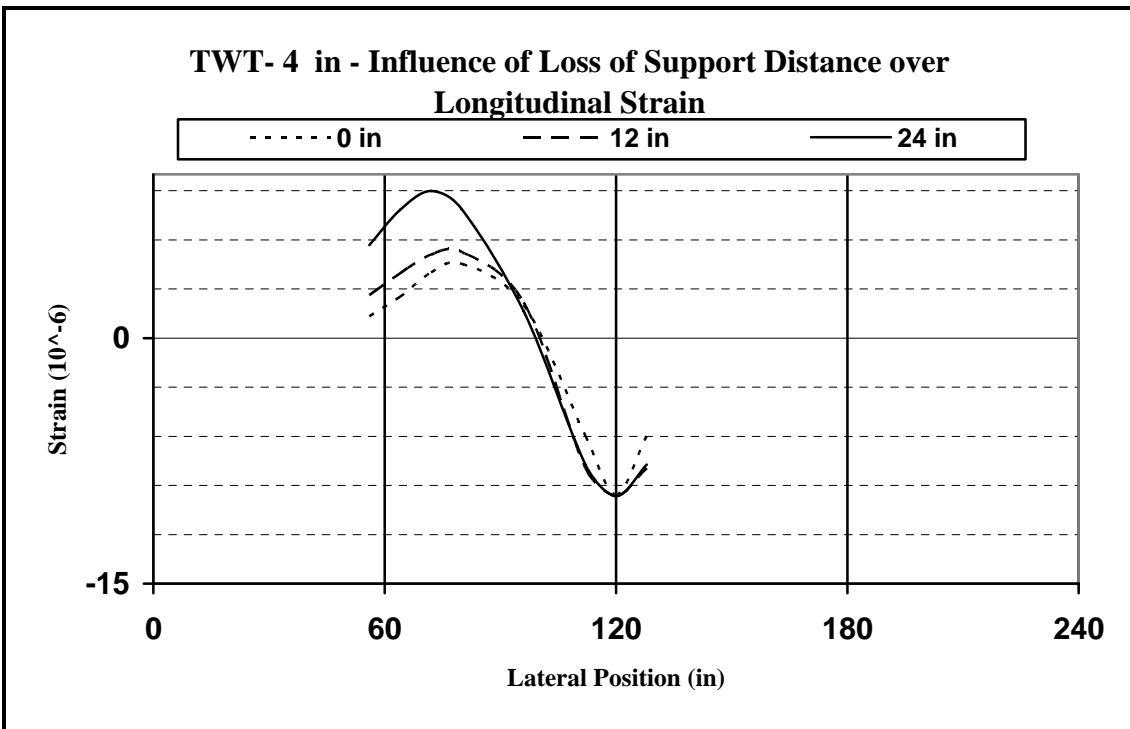


Figure 3.26: Influence of Loss of Support Distance over Longitudinal Strain: 4-inch TWT Pavement

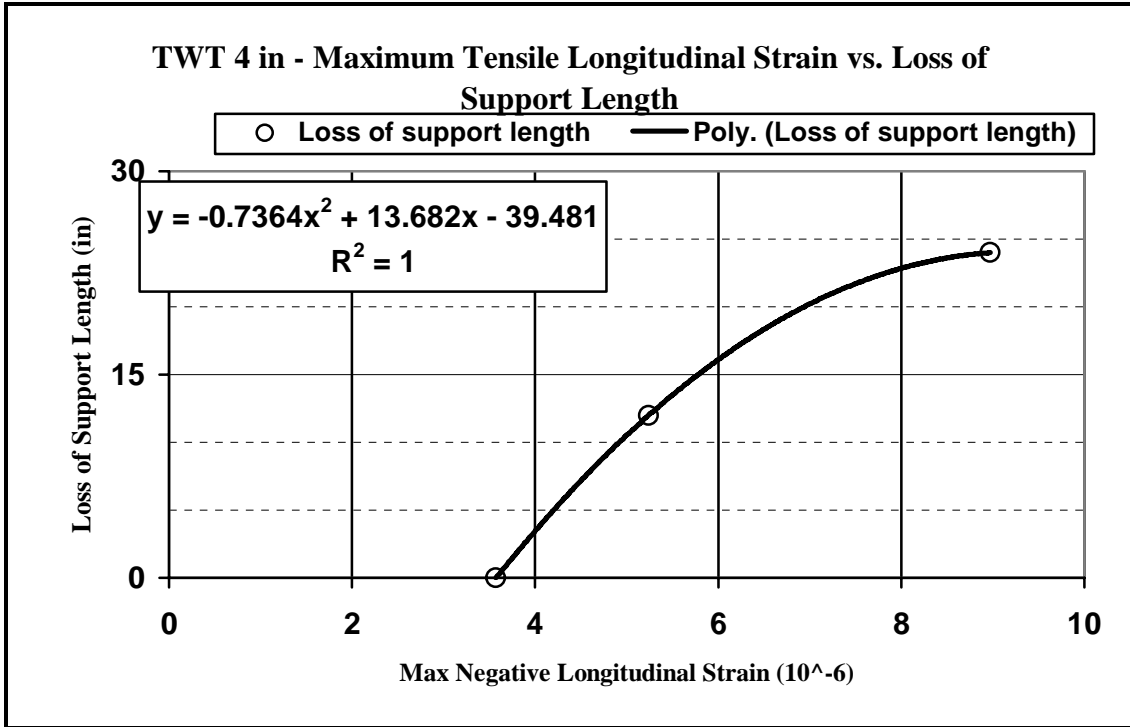


Figure 3.27: Maximum Tensile Longitudinal Strain vs. Loss of Support Length: 4-inch TWT Pavement

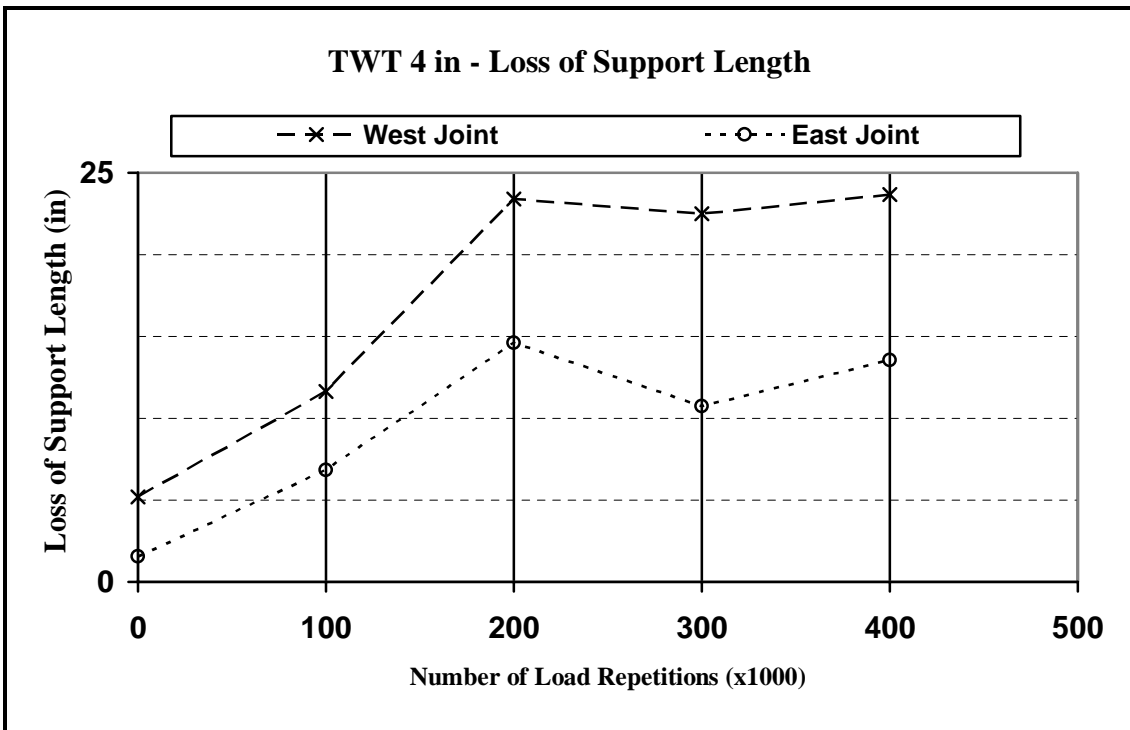


Figure 3.28: Loss of Support Length vs. Number of Load Repetitions: 4-inch TWT Pavement

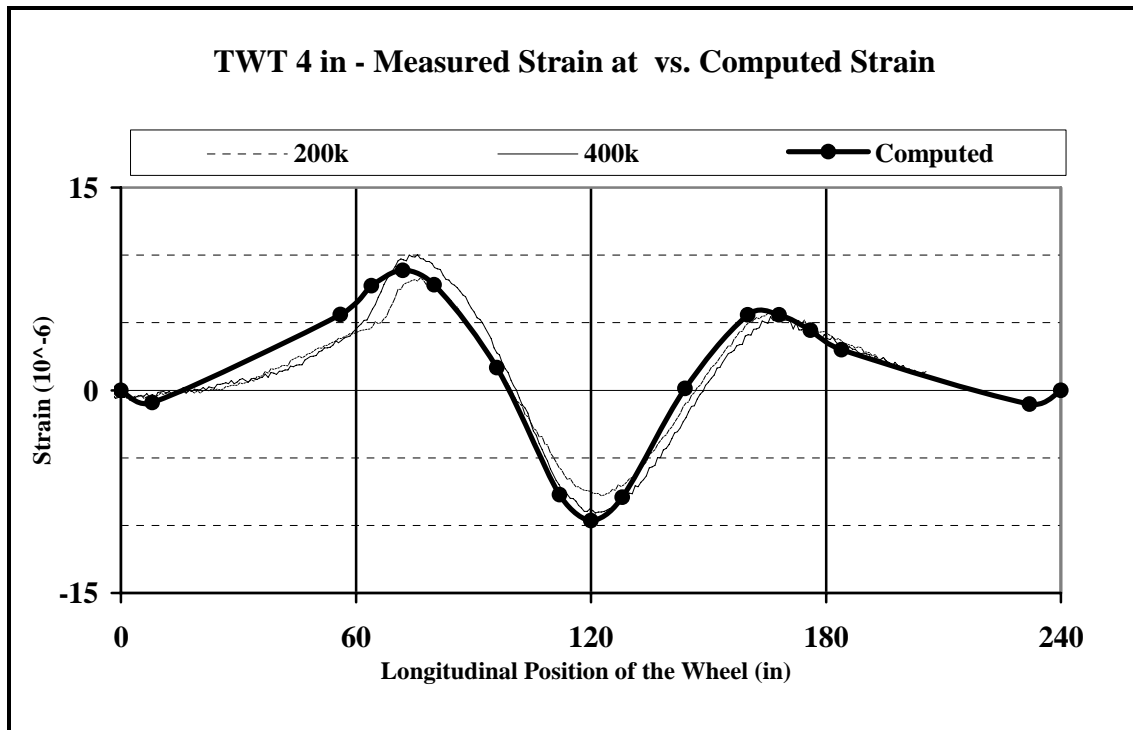


Figure 3.29: Measured vs. Computed Longitudinal Strains: 4-inch TWT Pavement

3.7.2 Results of Modeling of 6-inch TWT Pavement

The theoretically computed strains located at the measurement locations have been plotted in Figures 3.30 and 3.31. The maximum values of the longitudinal strains were 10.28 microstrain for the position corresponding to the SSLL strain gage, and -11.77 microstrain for the position corresponding to the SSLU strain gage. The maximum value of the theoretical transverse strain was -26.86 microstrain for the position corresponding to the SSTU strain gage, and +23.94 microstrain for the position corresponding to the SSTL strain gage.

Figure 3.32 shows the comparison of theoretical and measured transverse strains corresponding to the SSTU gage. The initially measured transverse strain values are much lower than the theoretically computed values (-15.23 microstrain measured, +26.86 computed). The maximum measured transverse strain increased until 500,000

load repetitions (Figure 3.33) to a value close to the theoretically computed value (-25.68 microstrain measured at 500,000 load repetitions), then had a small variation in a range between +23.30 microstrain (measured at 1,600,000 load repetitions) and -28.42 microstrain (at 700,000 load repetitions).

The comparison between theoretically computed and measured longitudinal strains at SSLU measuring location is shown in Figure 3.34. The initially measured strains (-11.11 microstrain) are very close to the theoretically computed strains measured (-11.77 microstrain). Figure 3.35 shows the evolution in time of the peaks of the measured longitudinal strain. The measured maximum tensile longitudinal strain decreased from +6.32 microstrain at 0 load repetitions to +11.55 microstrain at 500,000 load repetitions on West joint, and from +7.02 microstrain at 0 load repetitions to +11.73 microstrain at 500,000 load repetitions on East joint. After 500,000 load repetitions the values remained relatively constant. This increase of maximum tensile longitudinal strain indicates a loss of support under the concrete overlay joints.

The FEM model was modified for different loss of support distances from the joint (0 in, 12 in, 24 in). The longitudinal strains for the SSLU position corresponding to these loss of support distances were plotted in Figure 3.36. The maximum tensile values of the longitudinal strain were plotted (Figure 3.37), and a regression equation (Eq. 3-9) was determined.

$$L_{LOS} = -0.118S_{SSLU}^2 + 4.7232S_{SSLU} - 19.8 \quad \text{Equation 3-9}$$

Where:

L_{LOS} -Loss of support length (in)

S_{SSLU} -Maximum computed tensile longitudinal strain at SSLU measuring point (microstrain)

Based on the regression equation (Eq. 3-9), the loss of support distance was computed for the period between 0 and 2,000,000 load repetitions, and the results are plotted in the graph in Figure 3.38. The length of the loss of support increased between 0 and 500,000 load repetitions, and then remained constant to a distance of 15 inches on the West joint and 20 inches on the East joint.

The FEM model was modified and run again for loss of support lengths of 15 inches on the West joint and 20 inches on the East joint. The new computed strains are compared with strains measured at 400,000 load repetitions and 2,000,000 load repetitions (Figure 3.29). The comparison shows no significant differences between measured and computed strains, proving that the length of loss of support was correct.

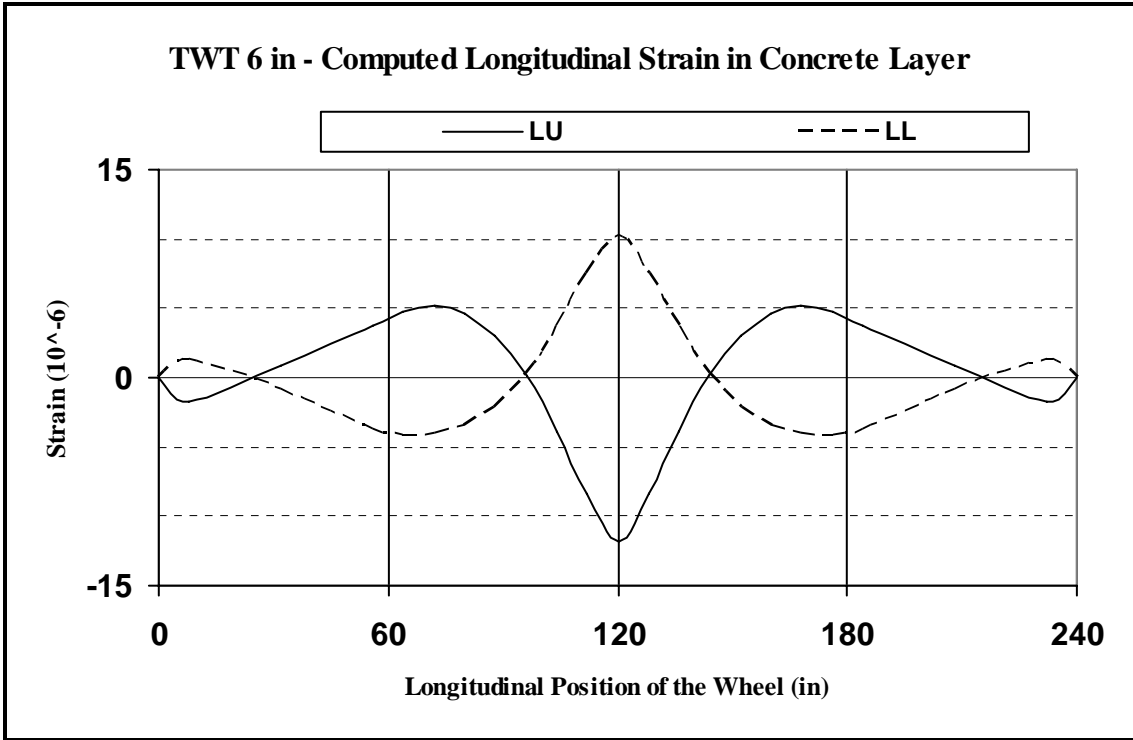


Figure 3.30: Computed Longitudinal Strains: 6-inch TWT Pavement

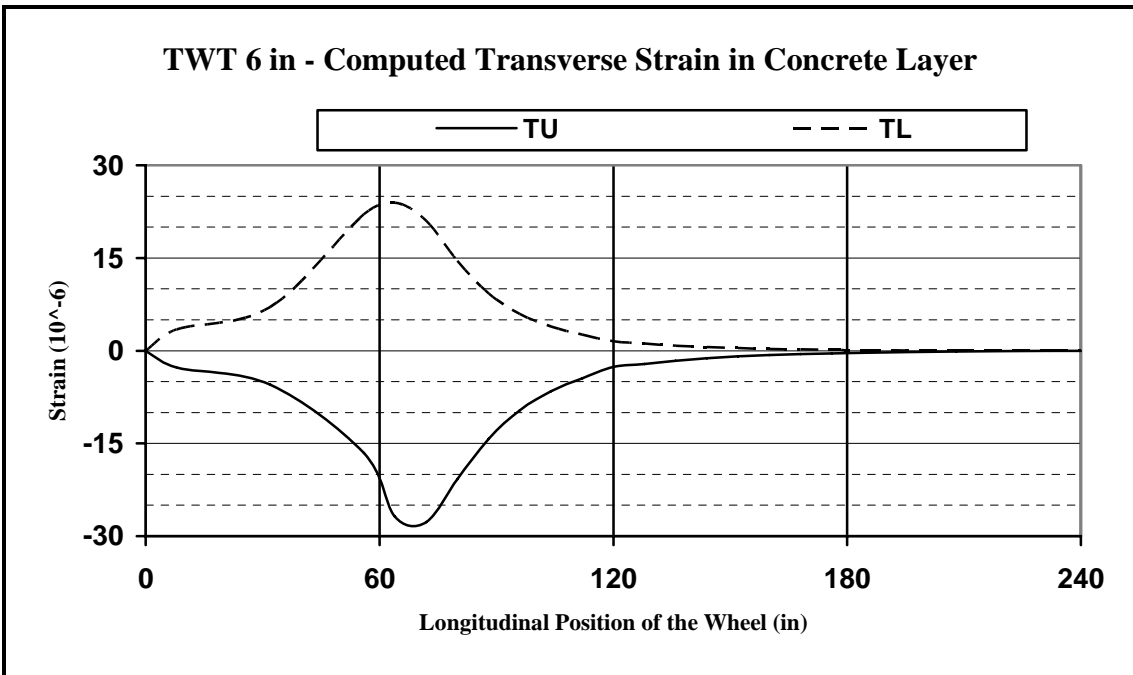


Figure 3.31: Computed Transverse Strains: 6-inch TWT Pavement

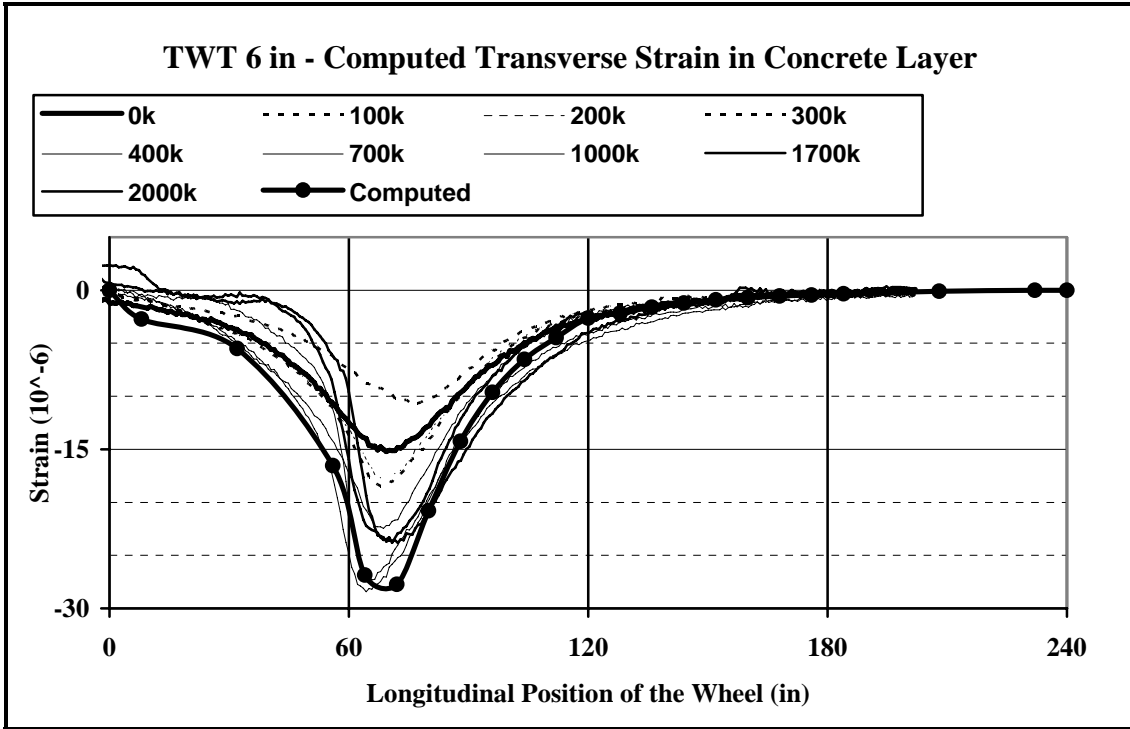


Figure 3.32: Measured vs. Computed Transverse Strains: 6-inch TWT Pavement

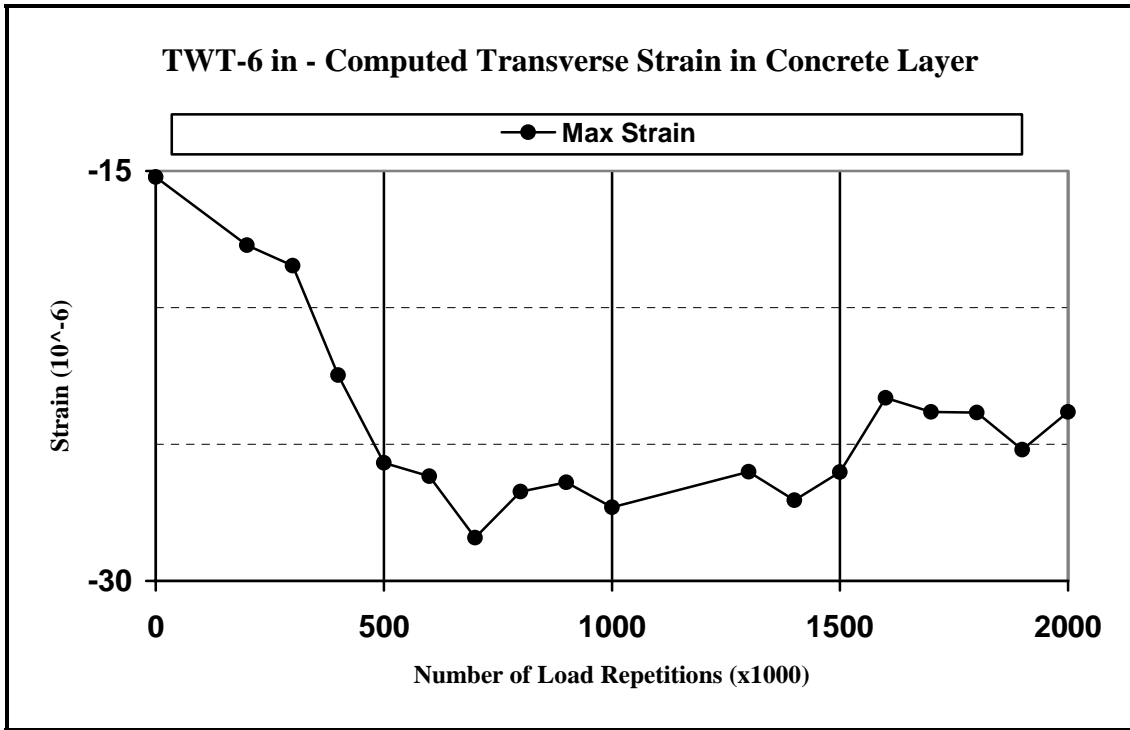


Figure 3.33: Evolution of Maximum Measured Transverse Strains: 6-inch TWT Pavement

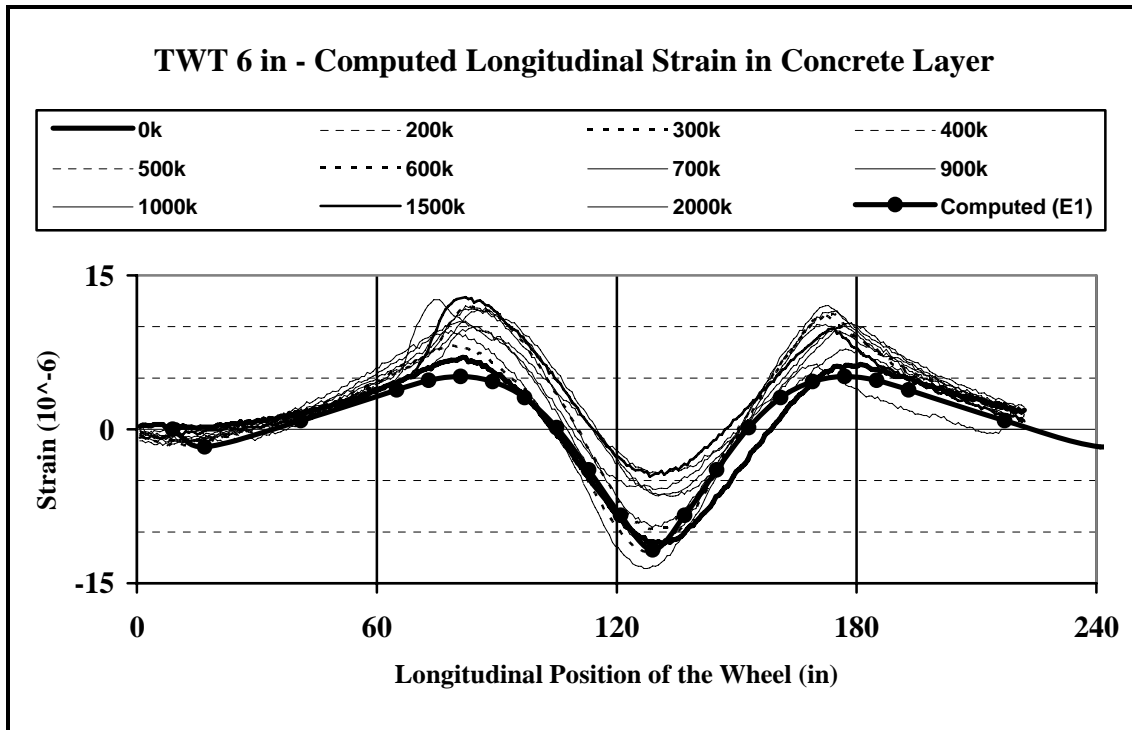


Figure 3.34: Measured vs. Computed Longitudinal Strains: 6-inch TWT Pavement

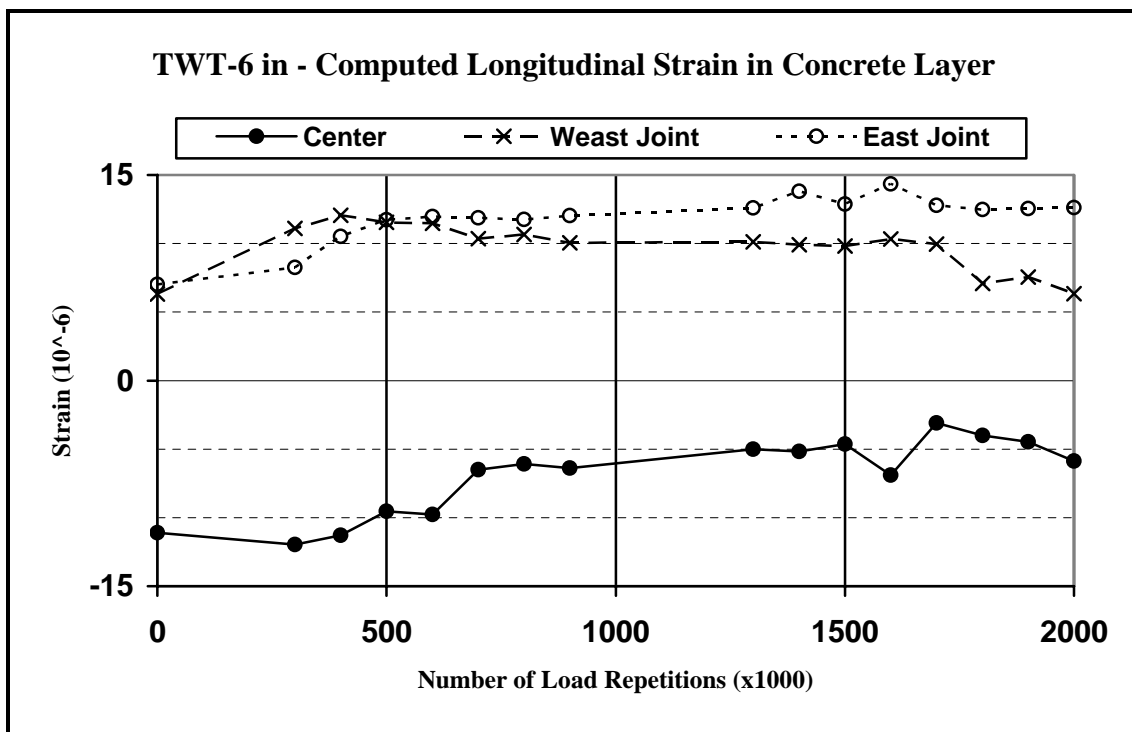


Figure 3.35: Evolution of Maximum Measured Transverse Strains: 6-inch TWT Pavement

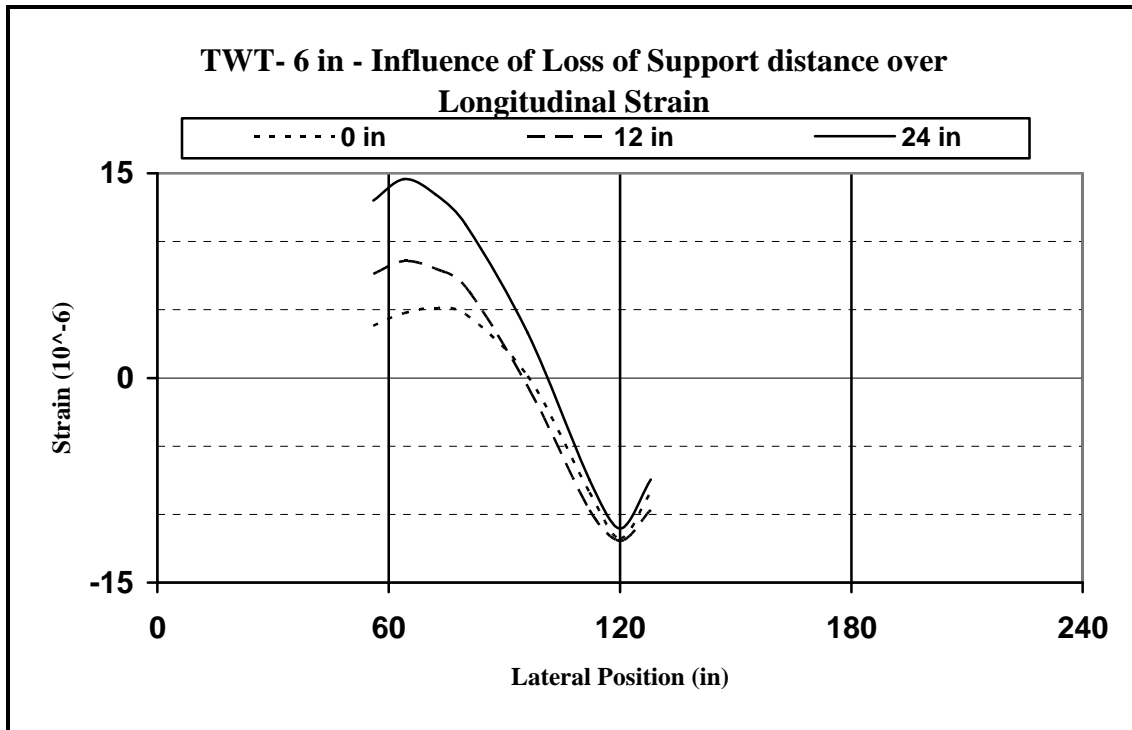


Figure 3.36: Influence of Loss of Support Length over Longitudinal Strain: 6-inch TWT Pavement

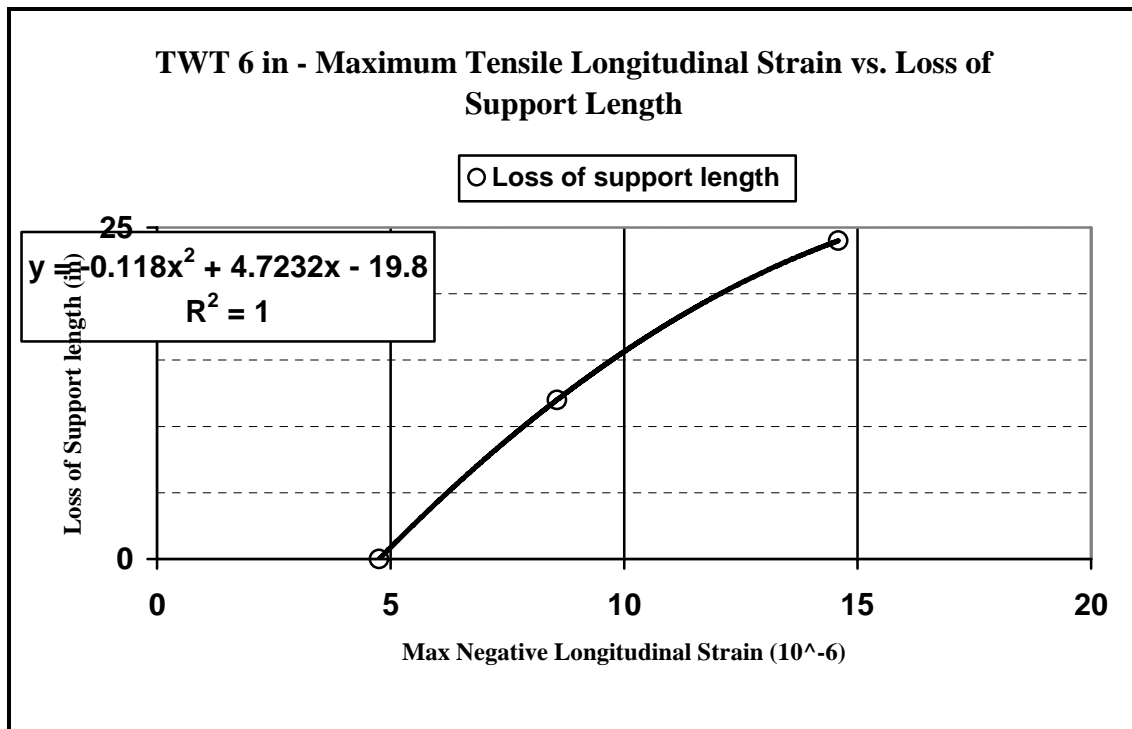


Figure 3.37: Maximum Tensile Longitudinal Strain vs. Loss of Support Length: 6-inch TWT Pavement

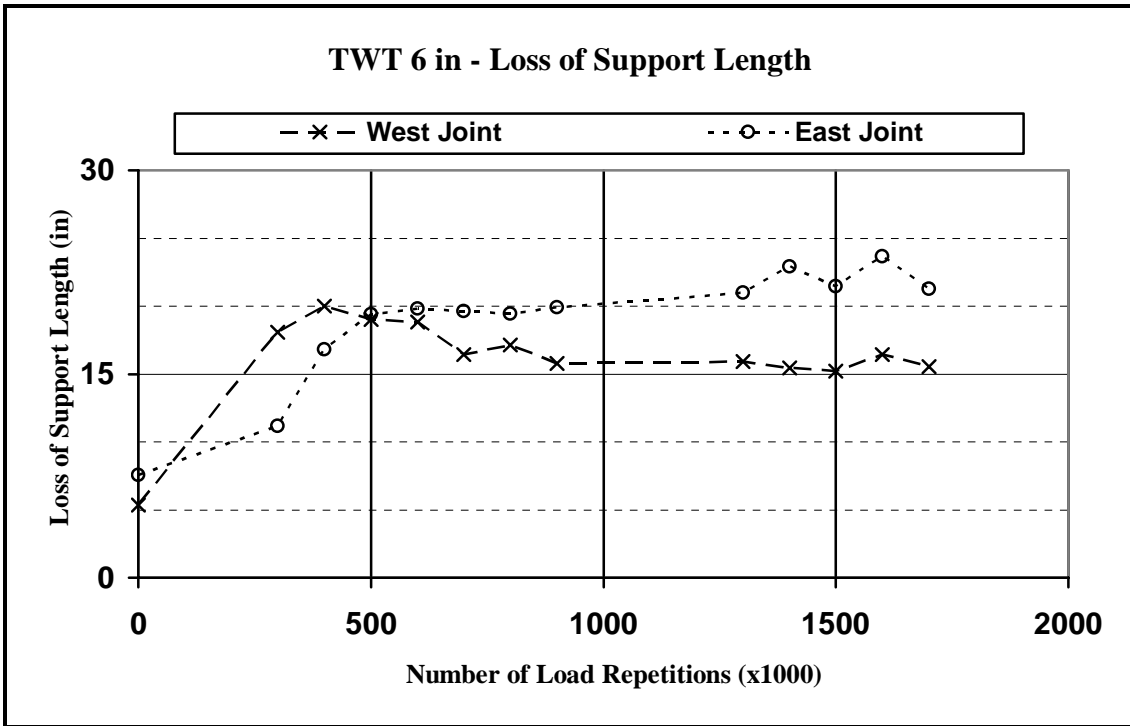


Figure 3.38: Loss of Support Length vs. Number of Load Repetitions: 6-inch TWT Pavement

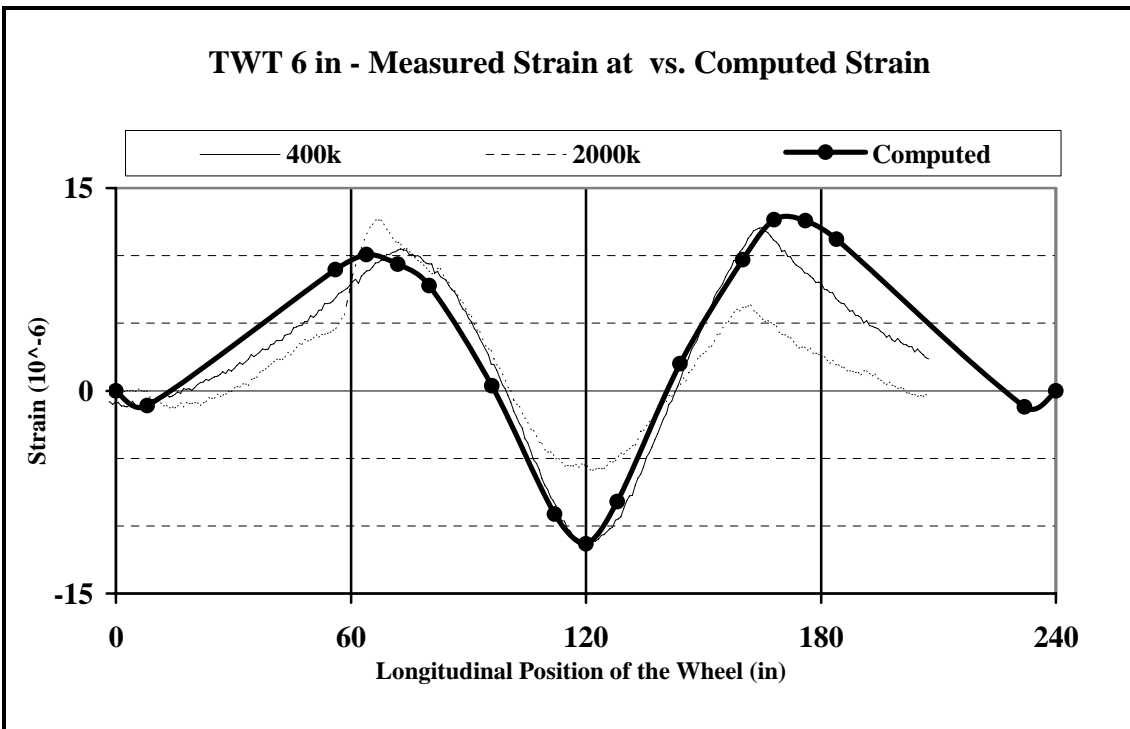


Figure 3.39: Measured vs. Computed Longitudinal Strains: 6-inch TWT Pavement

CHAPTER 4 - CONSTRUCTION, TESTING AND EVALUATION OF TCO PAVEMENTS

4.1 CONSTRUCTION of TCO ON PCC PAVEMENTS

The TCO on the PCC pavement sections were constructed in the north pit (NN and NS lanes). The construction was done in two stages:

1. Concrete slabs were built over the compacted subgrade;
2. Overlay was constructed after the concrete slabs were distressed through dynamic loading (significant cracking and/or joint movement).

Both pavements are 20 feet long and 6 feet wide. As shown in Figure 4.1, each of the TCO on PCC pavement sections consists of three layers as follows:

- NN lane: subgrade soil, 5 inches of concrete slab and 4 inches overlay;
- NS lane: subgrade, 5 inches of concrete slab and 6 inches overlay.

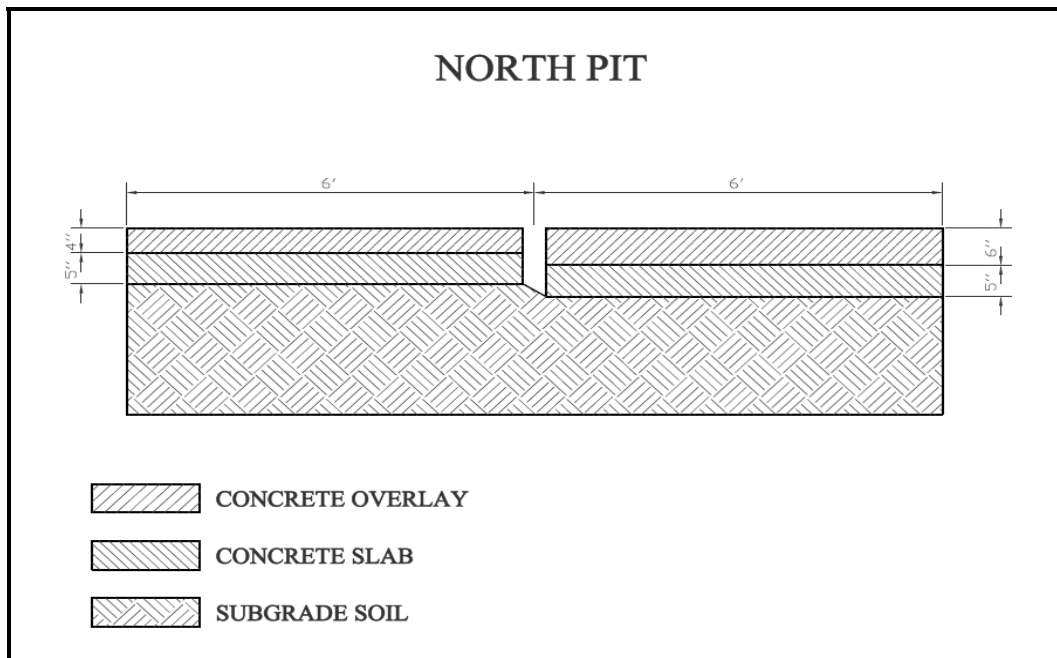



Figure 4.1: Configuration of the TCO Pavement Structures

The subgrade soil was A-7-6, a common soil in Kansas. The compaction of the soil was done in 6-inch lifts with a jumping jack compactor. The subgrade layer was built one inch above the desired level, and trimmed out to the final level. After finishing the construction of the subgrade, the level of compaction was verified at six locations (three on each pavement) with a Nuclear Density Meter. The results are presented in Table 4.1.

Table 4.1: Nuclear Density Measurements on North Pit

 <p style="text-align: center;">North Pit</p>		<p style="text-align: center;">Date:</p>			<p style="text-align: center;">7/23/2004</p>	
		<p style="text-align: center;">Time:</p>			<p style="text-align: center;">1440</p>	
		<p style="text-align: center;">Depth</p>			<p style="text-align: center;">12"</p>	
		<p style="text-align: center;">Optimum Density</p>			<p style="text-align: center;">1582</p>	
		<p style="text-align: center;">Optimum Moisture</p>			<p style="text-align: center;">21.3</p>	
		<p style="text-align: center;">Density Standard</p>			<p style="text-align: center;">682</p>	
		<p style="text-align: center;">Moisture Standard</p>			<p style="text-align: center;">2919</p>	
	% Proctor	Wet Density (kg/m ³)	Dry Density (kg/m ³)	Moisture	% Moisture	
Station #1						
A	99.1	1568	1947	378.9	24.2	
B	99.6	1575	1964	388.9	24.7	
C	98.7	1561	1958	397.4	25.5	
Average	99.1	1568.0	1956.3	388.4	24.8	
Station #2						
A	99.1	1568	1947	378.9	24.2	
B	99.6	1575	1964	388.9	24.7	
C	98.7	1561	1958	397.4	25.5	
Average	99.1	1568.0	1956.3	388.4	24.8	
Station #3						
A	99.7	1577	1931	354.7	22.5	
B	99.1	1567	1930	363.2	23.2	
C	99.7	1578	1936	357.5	22.7	
Average	99.5	1574.0	1932.3	358.5	22.8	
Station #4						
A	100.6	1591	1971	380.3	23.9	
B	99.7	1577	1968	391.7	24.8	
C	101.8	1611	1980	368.9	22.9	
Average	100.7	1593.0	1973.0	380.3	23.9	
Station #5						
A	98.1	1552	1925	373.2	24.1	
B	98.0	1551	1917	366.1	23.6	
C	98.0	1550	1916	368.1	23.6	
Average	98.0	1551.0	1919.3	369.1	23.8	
Station #6						
A	101.2	1601	1950	349.0	21.8	
B	101.5	1606	1949	343.3	21.4	
C	102.0	1614	1957	343.3	21.3	
Average	101.6	1607.0	1952	345.2	21.5	
<i>A,B,C- replicate tests in the same position</i>						

After preparation of the subgrade was finished, two soaker hoses were placed under the concrete joint location; a moisture transducer was placed under the pavement midway between the joints. Five 1-inch diameter dowel bars were set in a wire basket at 12-inch intervals on the prepared subgrade.

When the concrete slabs were poured, a 4-inch gap was kept between them to ensure the structural separation between pavements. The pit walls were sprayed with release agent to prevent adhesion to the slabs. The concrete was compacted with a small vibratory compactor, and finished with a vibratory screed. The final finishing was done manually, and then the pavements were textured by brooming. The joints were cut with a saw to one third of the slab depth; the final dimensions of the slabs being 10 x 6 feet for the central slabs, and 5 x 6 feet for the marginal slabs (Figure 4.2). For 28 days, the concrete was periodically sprayed with water and covered with plastic sheeting to ensure a proper curing. The concrete mix was designed for 4±1% entrained air and a 28 day compressive strength of 4,000 psi. The mix design is given in Table 4.2.

Table 4.2: Concrete Mix Design for the TCO Pavements

North Pit-South Lane (6 inch TCO Overlay)	
Material	Design Quantity (per cu. yd)
Sand	2019 lb
CA-6	849 lb
Type I/II cement	611 lb
A/E	3.00 oz
Water	35.1 gal
North Pit-North Lane (4 inch TCO Overlay)	
Sand	2097 lb
BCSCA-6	587 lb
KPCA-6	294 lb
Type I/II cement	550 lb
DARA65	22.00 oz
A/E	3.00 oz

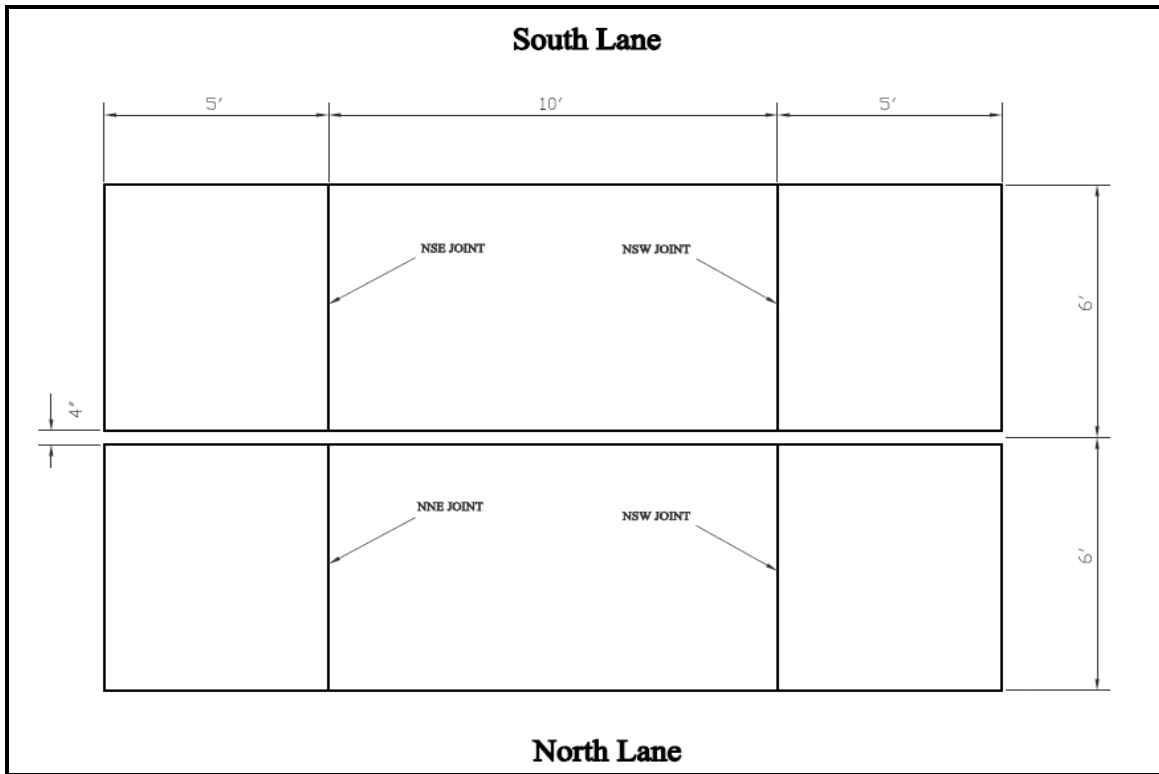


Figure 4.2: TCO on PCCP Joint Location

To induce distresses in the slabs, dynamic loads were applied on the sides of the joints using the steady state pulse equipment. The loads were sinusoidal, the phase angle of the load being computed to simulate a moving load of 30 mph. The loading process was monitored by two programmable logic controllers, connected in closed loop with the hydraulic actuators, through a load cell and a servo-valve. The controllers monitored and maintained the magnitude and shape of the sine load. The displacements of the joint edges were monitored by two LVDT's.

At the beginning, the east joints of the two pavements were loaded with the maximum force set to 20 kip, divided equally to both slabs (10 kips on each pavement). The load was later increased to 26 kips (13 kips on each pavement). After 13 million loading cycles pumping was observed on the east joint of the NN lane (NNE joint).

Because the distress of the pavements developed slowly, the load was increased to 20 kips and applied on a single lane. All joints experienced pumping; central slabs experienced cracks parallel to the joints (Figure 4.3). East joint of the NN lane (NNE joint) failed after 5.7 million cycles, west joint of the NS lane failed after 4.2 million cycles, and west joint of the NN lane failed after 4.8 million cycles. Table 4.3 gives the activity log for the loading of the TCO pavements.

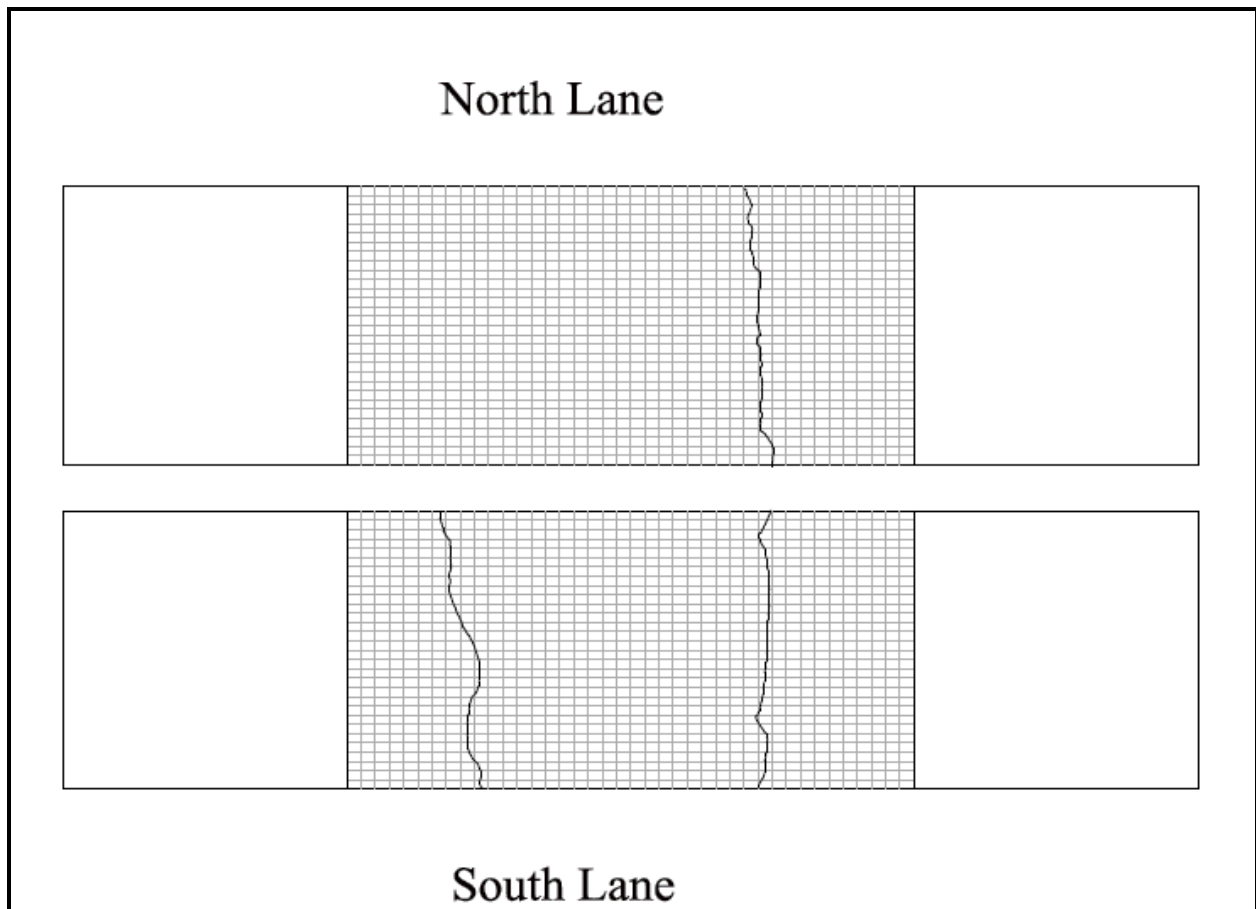


Figure 4.3: TCO on PCCP Slab Crack Mapping

The overlay performance depends on the bond development between the existing pavement and the overlay. Therefore, before pouring the overlay, the concrete slabs was prepared by shot blasting to ensure a good texture and then air blasted to

remove the dust. Based on common practices, the surface was wetted before the concrete overlay was poured.

The concrete overlays have the same horizontal dimensions as the initial concrete slabs. The pit walls were sprayed with a releasing agent to prevent adhesion to the concrete overlay. The concrete was vibrated with a small vibratory compactor, and finished with a vibratory screed. The final finishing was done manually, and then the pavements were textured by brooming. The joints in the overlays were cut to one third of the depth; the location of the cuts matched the joints of the initial slabs. Curing of concrete was done by water spraying and plastic sheeting.

Table 4.3: Activity Log for the Distressing and APT Loading of the TCO Pavements

Date	Load	Comments
Pulse Loading on the Existing PCC Pavements		
10/20/04		Started pulse loading on North pit, South end
11/1/04		Started loading 24/7
12/2/04		Increased load from 20 to 26 Kip
12/17/04		Cycle 12,913,274 Pumping observed North lane
1/14/05		Cycle 16,990,703 Stopped loading and refit for single
1/19/05		Started loading south lane east end with surface drip
2/4/05		Cycle 5,783,246 Stop loading NSE joint, pumping and cracking observed
2/9/05		Start loading NSW Joint
2/25/05		Cycle 4,212,175 stop loading NSW, Pumping and crack
3/2/05		Start loading NNW Joint
3/18/05		Cycle 4,794,801 Stop loading NNW Joint Pumping and cracking observed
APT Loading on TCO Pavements		
06/17/05	Initial	Start Wheel Loading
06/27/05	100k	Take Data and Restart
07/05/05	200k	Take Data and Restart
07/12/05	300k	Take Data and Restart
07/19/05	400k	Take Data and Restart
08/01/05	500k	Take Data and Restart
08/08/05	600k	Repair broken wheel studs
09/12/05	700k	Take Data and Restart
09/19/05	800k	Take Data and Restart
09/26/05	900k	Take Data and Restart
10/04/05	1M	Stop to install environmental chamber
11/22/05	1.1M	Take Data and Restart
11/29/05	1.2M	Take Data and Restart
12/06/05	1.3M	Take Data and Restart
12/13/05	1.4M	Stop for vacation
01/03/06	1.5M	Take Data and Restart
01/10/06	1.6M	Take Data and Restart
01/17/06	1.7M	Take Data and Restart
01/24/06	1.8M	Take Data and Restart
01/31/06	1.9M	Take Data and Restart
02/07/06	2M	Final Data

4.2 INSTRUMENTATION INSTALLED IN THE TCO PAVEMENTS

To evaluate the behavior of the TCO on PCC and to measure the response of the pavement under real wheel loads was compared with the results from the theoretical model of the pavement. The pavements were equipped with instrumentation to measure strains at the critical locations of the overlay, and to assess the response of the pavement under transient loads. Strain gages and thermocouples were embedded in the pavement to monitor the response of the pavement. The instrumentation was used only on the central slabs of the pavement sections, the marginal slabs were used to complete the real behavior of the pavement.

Similar gages as on the TWT sections were used. The position of the gages (Figure 4.4) is the same for both TCO on PCCP sections, and corresponds to the critical strain position, at the center of the joints, and at the corner of the slab. The placement was done before construction of the overlay, the gages being set in wire fixtures (Figure 3.5); one strain gage was set one inch from the top and one gage one inch from the bottom of the overlay. The strain gages were installed in the overlay as follows:

- In the middle of the wheel path and parallel to the western tied joint (between central slab and marginal slab), two inches offset from the joint. The gages are parallel to the joint. During construction, the lower strain gage on the southern lane was damaged.
- In the middle of the untied joint, two inches from the joint. The gages were parallel to the joint and the wheelpath.
- Twelve inches from the tied joint and twelve inch from the untied joint. The gages were inclined 45° to the joint and the wheelpath.

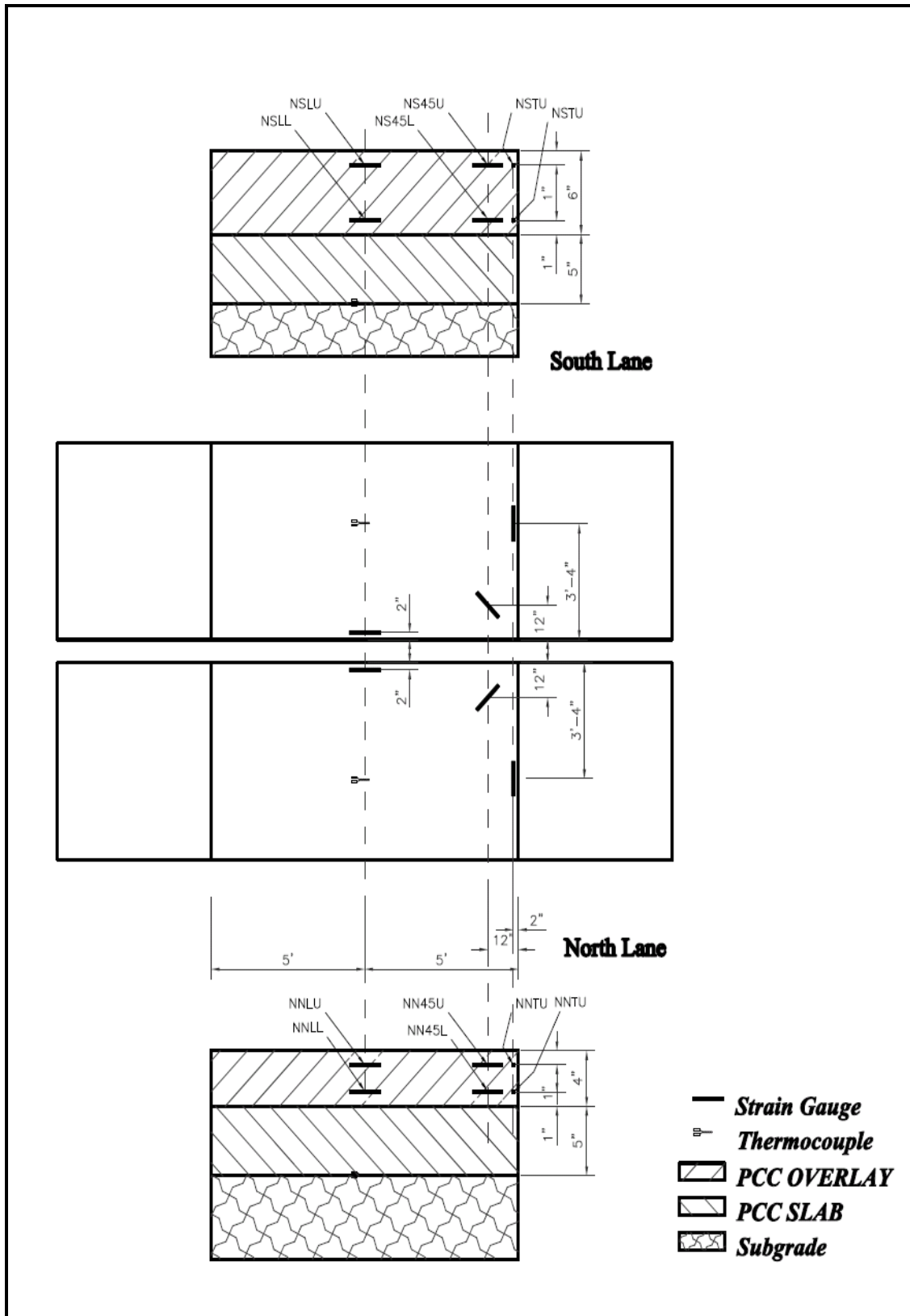


Figure 4.4: TCO on PCC- Pavement Instrumentation

4.3 APT Testing OF THE TCO ON PCCP

The test was conducted under following conditions:

- The lateral wander applied in this experiment followed the same truncated normal distribution used for the loading of the TWT pavements (Figure 3.6)
- The applied load was about 26 kips, equally distributed between the two pavements (13 kips on each pavement). The wheel load was monitored with load cells installed on each wheel;
- The first 1,000,000 load cycles were applied at the normal ambient temperature (room temperature)
- Next 1,000,000 load cycles were applied under controlled temperature.

Table 4.3 gives the activity log for the loading of the TCO pavements.

4.4 PERFORMANCE OF TCO PAVEMENTS

The TCO pavement sections also performed well under the loading by the APT machine. Since APT loading was applied at ambient temperature and that no water was added to the pavements during the APT loading of the two pavement structures, no substantial daily or seasonal changes in temperature in the upper layers or significant changes in the moisture content in the subgrade soil occurred.

The TCO pavement section exhibited cracking. One transverse crack developed in the central slabs of both pavement sections, at about 1/3 in length for the West joint, at 1.1 million passes of the APT machine in the 4-inch TCO pavement section and 1.7 million passes in the 6-inch TCO pavement section. Several other cracks developed after that only in the 4-inch TCO pavement section; no other cracks

developed in the 6-inch TCO pavement section. No significant joint faulting was recorded.

At the end of the loading phase of the experiment (after 2,000,000 load cycles), the cracks of the overlay were mapped (Figure 4.5), and 4-inch diameter cores were extracted from the central slabs of TCO on PCCP pavements. The examination of the cores showed good bond between the concrete layers. It was thus assumed, and then confirmed by the modeling of the pavement response, that the failure of these pavement sections was due to the loss of support underneath the transverse joints. This led to the transverse cracking observed at the surface.

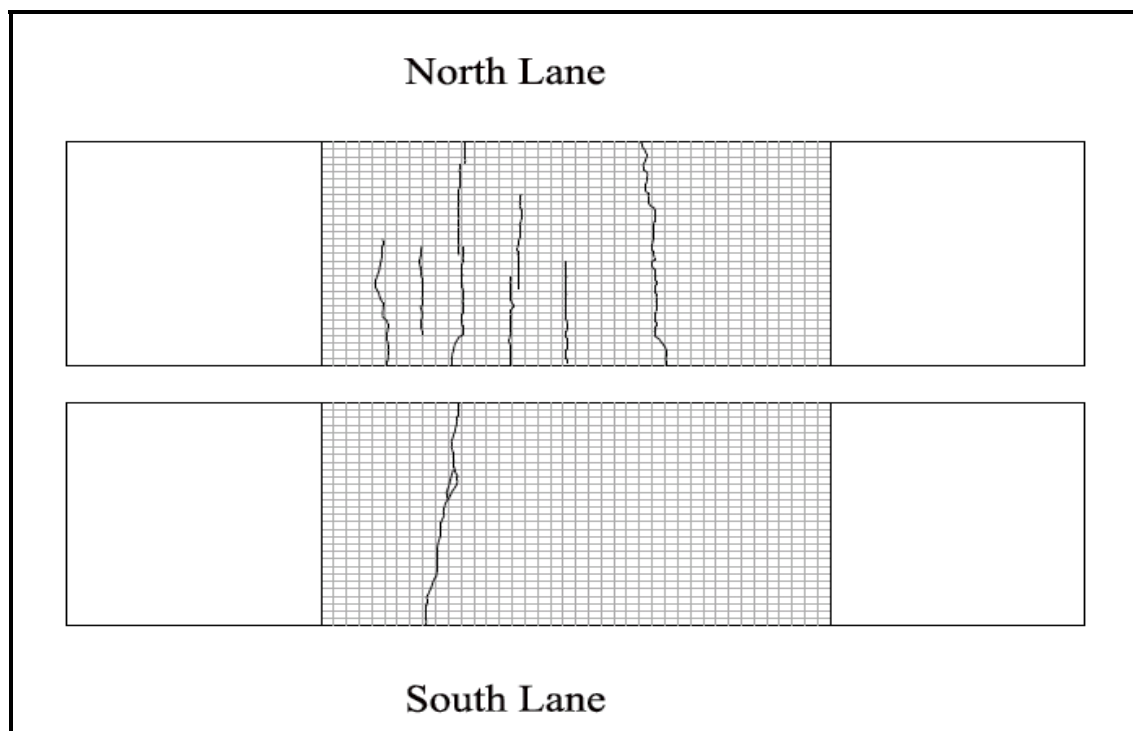


Figure 4.5: TCO - Overlay Crack Mapping

4.5 Horizontal Strains in Concrete Overlay

The strain measurements were made when the wheel assembly was in the middle of the wheel path (corresponding to “0” position of the wandering device). The

sampling rate was 100 readings per second, recorded for approximately 4 complete cycles (8 passes). The measurements were performed at an interval of 100,000 load cycles, and the data was recorded and stored in spreadsheet format together with the data for the load position and magnitude.

Because the applied load varied from the target value of 26-kip for the single axle, the measured strain values were normalized to a 26-kip single axle load. The maximum and minimum values of measured strains are tabulated in Tables 4.4 and 4.5. Figures 4.6, 4.7 and 4.8 present the typical shapes of the strain signals for the three gage locations (doweled joint, lateral joint and corner, respectively) for the 6-inch TCO on PCCP section. The strains signals had the same shape as the 4-inch TCO on PCCP section.

Table 4.4: Maximum and Minimum Strains Values: 6-inch TCO

Date	Passes x1000	Peak	Strain (microstrain)					
			NSLU	NSLL	NSTU	NSTL	NS45U	NS45L
17-Jun-05	0	max	16.05	2.95	17.38	0.00	4.72	1.04
17-Jun-05	0	min	-13.69	-2.88	-0.70	0.00	-6.36	-1.82
27-Jun-05	100	max	16.09	2.82	17.17	0.00	4.77	0.50
27-Jun-05	100	min	-18.14	-3.58	-1.73	0.00	-7.93	-1.86
12-Jul-05	300	max	19.05	2.83	16.33	0.00	4.44	0.40
12-Jul-05	300	min	-22.18	-3.38	-0.90	0.00	-8.60	-1.98
19-Jul-05	400	max	14.21	2.69	16.25	0.00	3.99	0.56
19-Jul-05	400	min	-23.90	-3.84	-1.55	0.00	-8.99	-1.60
1-Aug-05	500	max	14.37	2.43	15.18	0.00	3.42	0.79
1-Aug-05	500	min	-22.47	-3.91	-2.26	0.00	-8.88	-1.41
8-Aug-05	600	max	18.33	2.92	15.91	0.00	3.50	0.47
8-Aug-05	600	min	-20.20	-3.86	-2.28	0.00	-9.05	-1.51
12-Sep-05	700	max	16.60	2.61	16.16	0.00	3.40	0.51
12-Sep-05	700	min	-25.59	-4.39	-2.47	0.00	-8.81	-1.32
19-Sep-05	800	max	16.20	2.76	15.26	0.00	3.28	0.66
19-Sep-05	800	min	-25.81	-4.31	-1.85	0.00	-8.99	-1.17
26-Sep-05	900	max	14.32	2.60	14.05	0.00	3.36	0.65
26-Sep-05	900	min	-27.74	-4.42	-1.55	0.00	-8.92	-0.96
4-Oct-05	1,000	max	17.20	2.62	13.93	0.00	3.43	0.62
4-Oct-05	1,000	min	-28.39	-4.99	-1.34	0.00	-9.92	-1.34
22-Nov-05	1,100	max	15.15	2.82	14.19	0.00	2.90	0.54
22-Nov-05	1,100	min	-29.22	-4.67	-1.63	0.00	-8.76	-0.76
29-Nov-05	1,200	max	11.55	2.70	13.77	0.00	3.14	0.75
29-Nov-05	1,200	min	-17.73	-2.52	-1.44	0.00	-8.59	-1.06
6-Dec-05	1,300	max	12.01	1.99	13.74	0.00	3.13	0.57
6-Dec-05	1,300	min	-19.53	-2.83	-1.16	0.00	-9.06	-1.13
13-Dec-05	1,400	max	10.76	2.15	14.12	0.00	3.52	0.36
13-Dec-05	1,400	min	-20.69	-2.62	-1.48	0.00	-9.28	-1.19
3-Jan-06	1,500	max	10.25	2.24	15.57	0.00	3.29	0.33
3-Jan-06	1,500	min	-22.90	-3.51	-1.22	0.00	-9.25	-1.16
10-Jan-06	1,600	max	10.79	2.15	14.14	0.00	3.09	0.56
10-Jan-06	1,600	min	-22.33	-3.08	-1.59	0.00	-9.57	-0.92
17-Jan-06	1,700	max	11.31	2.00	14.29	0.00	3.21	0.72
17-Jan-06	1,700	min	-21.31	-3.18	-1.14	0.00	-9.51	-0.83
24-Jan-06	1,800	max	11.33	2.31	13.58	0.00	3.00	0.67
24-Jan-06	1,800	min	-20.55	-2.93	-1.36	0.00	-9.64	-0.84
31-Jan-06	1,900	max	11.09	2.27	13.68	0.00	3.06	0.45
31-Jan-06	1,900	min	-21.43	-2.95	-1.07	0.00	-9.56	-0.92
7-Feb-06	2,000	max	10.55	2.15	13.79	0.00	2.86	0.42
7-Feb-06	2,000	min	-21.86	-3.07	-1.40	0.00	-9.75	-0.84

Table 4.5: Maximum and Minimum Strains Values: 4-inch TCO

Date	Passes x1000	Peak	Strain (microstrain)					
			NNLU	NNLL	NNTU	NNTL	NN45U	NN45L
17-Jun-05	0	max	13.95	8.71	20.45	4.06	10.92	4.68
17-Jun-05	0	min	-11.48	-6.56	-3.85	-3.33	-4.34	-3.54
27-Jun-05	100	max	16.71	8.53	12.10	0.45	5.52	0.75
27-Jun-05	100	min	-18.98	-9.35	-0.44	-17.39	-8.95	-2.83
12-Jul-05	300	max	10.55	5.19	12.25	1.35	6.07	2.05
12-Jul-05	300	min	-11.29	-5.94	-1.45	-14.38	-7.84	-1.66
19-Jul-05	400	max	9.64	4.81	9.51	1.21	6.38	1.22
19-Jul-05	400	min	-13.01	-5.67	-0.41	-12.76	-7.34	-1.43
1-Aug-05	500	max	9.39	4.62	11.45	1.44	7.63	0.96
1-Aug-05	500	min	-15.95	-5.76	-1.01	-12.71	-6.35	-2.04
8-Aug-05	600	max	9.33	4.46	12.64	1.51	6.88	1.15
8-Aug-05	600	min	-14.41	-5.75	-1.05	-14.95	-7.39	-1.25
12-Sep-05	700	max	9.40	4.31	14.74	1.95	5.56	1.01
12-Sep-05	700	min	-15.01	-6.31	-0.38	-16.27	-8.01	-1.13
19-Sep-05	800	max	9.95	4.54	14.20	1.26	6.27	0.86
19-Sep-05	800	min	-14.94	-6.20	-0.39	-16.24	-7.50	-1.09
26-Sep-05	900	max	9.49	4.31	13.62	1.44	5.94	1.02
26-Sep-05	900	min	-15.17	-6.30	-0.60	-16.78	-6.95	-1.18
4-Oct-05	1,000	max	9.46	4.16	12.71	1.96	6.48	1.12
4-Oct-05	1,000	min	-16.59	-7.44	-1.02	-15.08	-6.00	-1.84
22-Nov-05	1,100	max		4.83	12.13	1.70	5.90	1.29
22-Nov-05	1,100	min		-6.23	-0.48	-15.54	-7.48	-1.06
29-Nov-05	1,200	max	10.14	4.93	9.95	1.46	5.10	1.31
29-Nov-05	1,200	min	-12.82	-6.35	-0.25	-12.81	-7.69	-0.87
6-Dec-05	1,300	max	11.04	4.97	10.63	0.94	5.88	1.42
6-Dec-05	1,300	min	-15.49	-6.88	-0.35	-13.45	-8.20	-0.69
13-Dec-05	1,400	max	10.68	4.76	11.03	0.72	6.16	1.09
13-Dec-05	1,400	min	-15.18	-6.80	-0.28	-14.38	-7.30	-1.32
3-Jan-06	1,500	max	10.00	4.82	12.45	1.12	7.36	1.56
3-Jan-06	1,500	min	-17.33	-7.46	-0.93	-16.33	-6.67	-2.78
10-Jan-06	1,600	max		5.19	13.70	1.42	6.26	1.12
10-Jan-06	1,600	min	-23.26	-6.95	-0.63	-18.22	-10.55	-0.99
17-Jan-06	1,700	max	10.55	5.34	13.67	1.32	6.87	1.26
17-Jan-06	1,700	min	-14.38	-6.73	-0.57	-18.57	-9.59	-0.86
24-Jan-06	1,800	max		1.37		4.68	2.39	0.30
24-Jan-06	1,800	min		-1.91	-3.51	-0.40	-2.02	-0.38
31-Jan-06	1,900	max	2.92	1.35		4.53	2.37	0.20
31-Jan-06	1,900	min	-4.19	-1.92	-3.42	-0.31	-2.01	-0.45
7-Feb-06	2,000	max	2.57	1.31		4.63	2.44	0.31
7-Feb-06	2,000	min	-4.64	-1.90	-3.42	-0.36	-2.17	-0.43

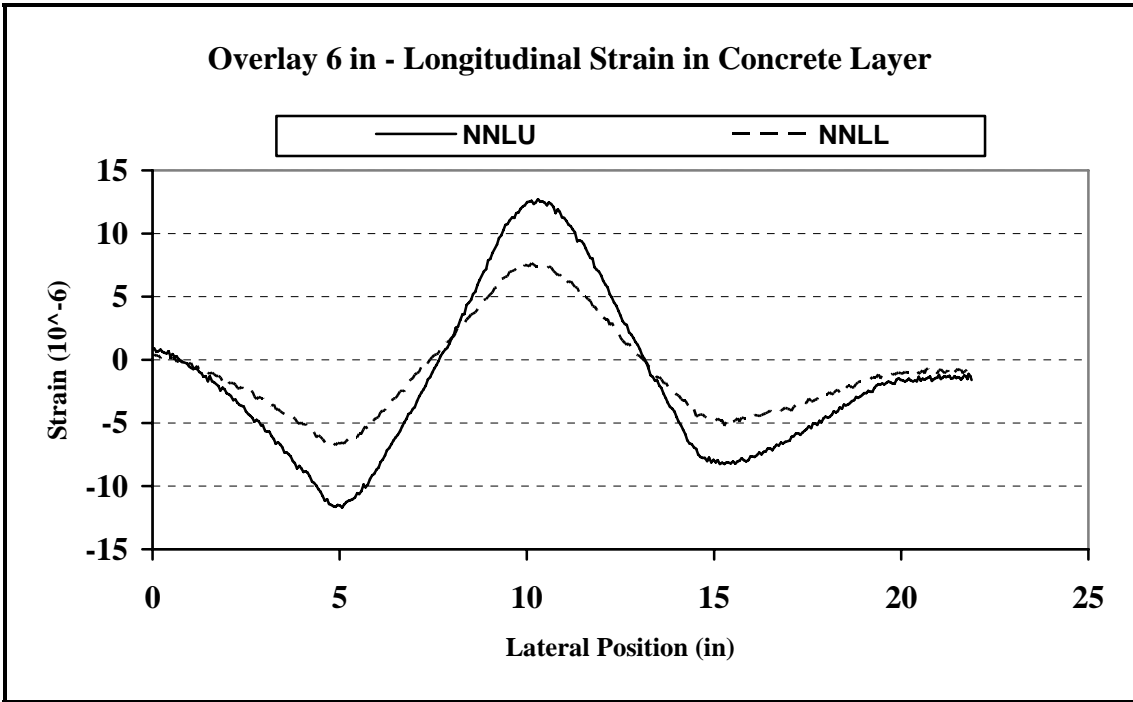


Figure 4.6: Typical Shape of Measured Longitudinal Strain

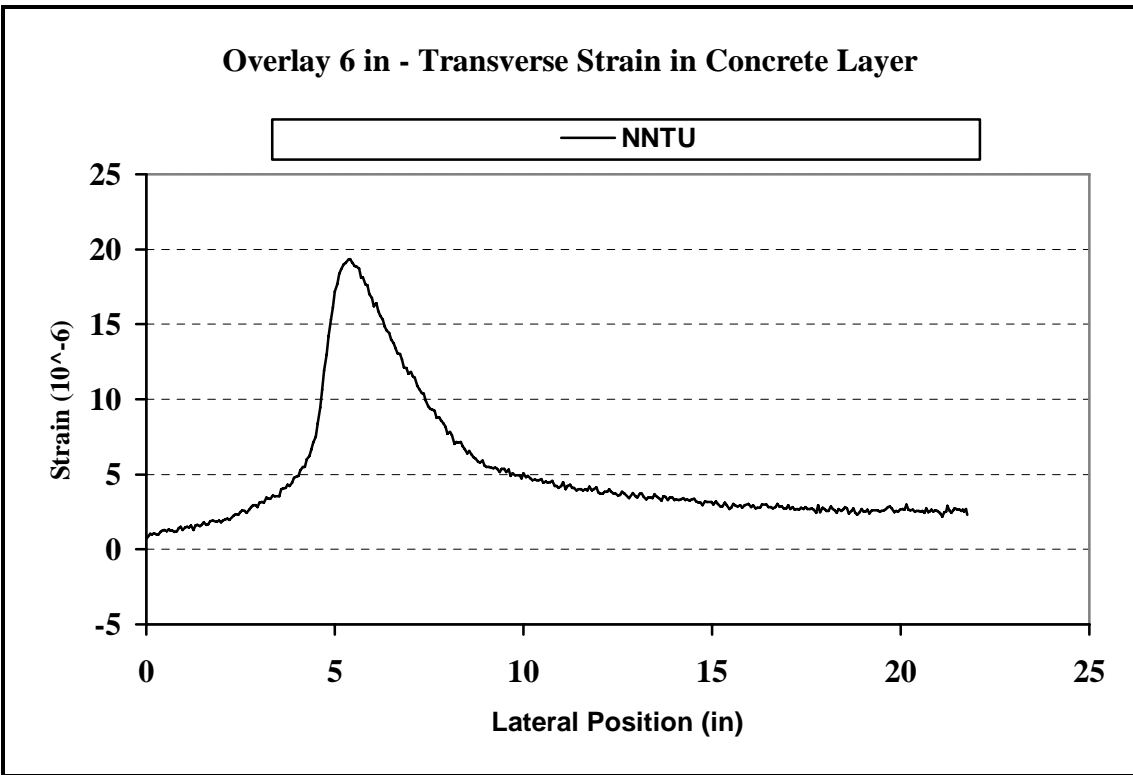


Figure 4.7: Typical Shape of Measured Transverse Strain

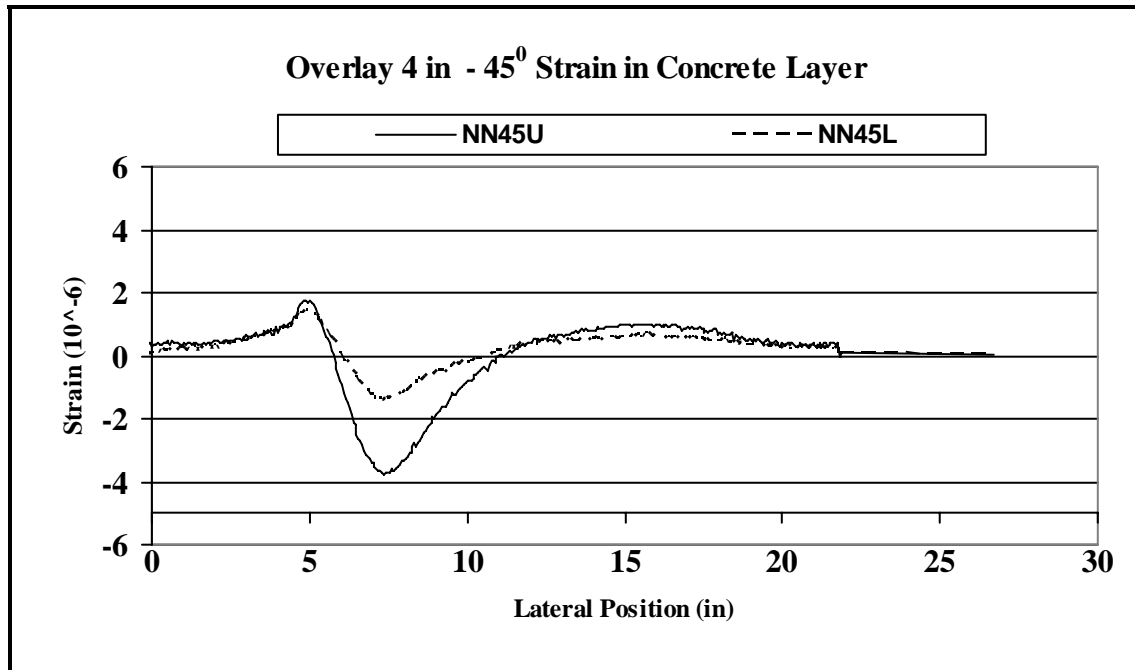


Figure 4.8: Typical Shape of Measured 45° Corner Strain

4.6 TCO PAVEMENT MODELING

The TCO pavements were modeled using the finite element software ANSYS.

Two models were developed for each pavement:

- One model for initial condition, considering the cracking in the initial concrete slab, and full support used as reference for damage estimation.
- One model considering the cracks in the concrete slab and different lengths of loss of support, in order to evaluate the loss of support.

4.6.1 Geometry Definition

Since the available software version limits the user to create a mesh of up to 32,000 nodes, the two sections were modeled separately. Because the geometry and loading were symmetric, the model was built only for the half of the structure; thus a finer mesh could be used. Pavements were modeled in 3-D as a three layer system: subgrade soil, concrete slab, and concrete overlay. The interface between the layers

was considered perfectly bonded, and the cracks in the concrete slabs were modeled using contact elements.

4.6.2 *Materials Properties*

The TCO on PCCP sections contained three different materials: concrete in PCCP, subgrade soil, and steel dowels. All materials were considered as linear elastic materials, thus the only parameters used for material description were the modulus of elasticity and the Poisson's ratio. The thermal loading was not considered.

The concrete modulus of elasticity was obtained from the empirical relationship between the compressive strength and the modulus of elasticity (Equation 3-1). An average value of 0.15 was used for Poisson's ratio.

Because the same soil was used in the TCO sections as in the TWT sections, the same values of modulus of elasticity and Poisson's ratio were assigned for the subgrade soil ($E=20,000$ psi; $\nu=0.45$)

The modulus of elasticity and Poisson's ratio of the steel dowels were taken as those provided by the dowel manufacturer ($E=24,000,000$ psi; $\nu=0.30$).

4.6.3 *Model Meshing*

Because of the limitations of the software, the mesh was done taking into consideration the balance between the geometry of structure and the finite element size. A finer mesh was used in the proximity of the material discontinuities, loading areas, and locations where the strains were measured.

The concrete overlay was manually meshed using a 3-D brick element with 20 nodes (SOLID186). Because the stress change is much larger in vertical direction than in horizontal direction, a larger size of the finite element in the horizontal plane than in

the vertical direction was used for the middle panel (4 inch x 4 inch in the horizontal plane and one inch in thickness). In addition, the mesh was refined around the measurement points. The element size for the marginal slabs was set to 4 inches. The maximum resulting aspect ratio of the solid 3-D elements of 4 to 1 lies in the range recommended by the software.

The concrete slab was also meshed using 20-node SOLID186 finite element. To fit the overlay mesh, the mesh size was set to 4 inches at the top of the slab and 6 inches at the bottom. The mesh was automatically refined at the dowel contact zone to fit the dowel mesh.

The dowel bars were meshed using 8-node SOLID45 finite elements. The mesh size was 4 inch in longitudinal direction, 0.15 inch in radial direction and 0.30 inch along the circumference. The aggregate interlock at the joints and cracks was modeled with the contact elements, assuming a coefficient of friction of 1.5 and no stiffness, when the contact is open.

The subgrade layer was modeled using 8-node SOLID45 elements. Because the stress change decreases as depth increases, a coarser mesh was used for this layer. The mesh was generated automatically, starting from a 6-inch mesh size at the top of the layer, then to a size of 30 inches at the bottom of the layer.

The final meshing used about 32,000 nodes. Most of the solid elements were rectangular, for better accuracy and interpolations of the results. Figure 4.9 shows the general mesh of the model.

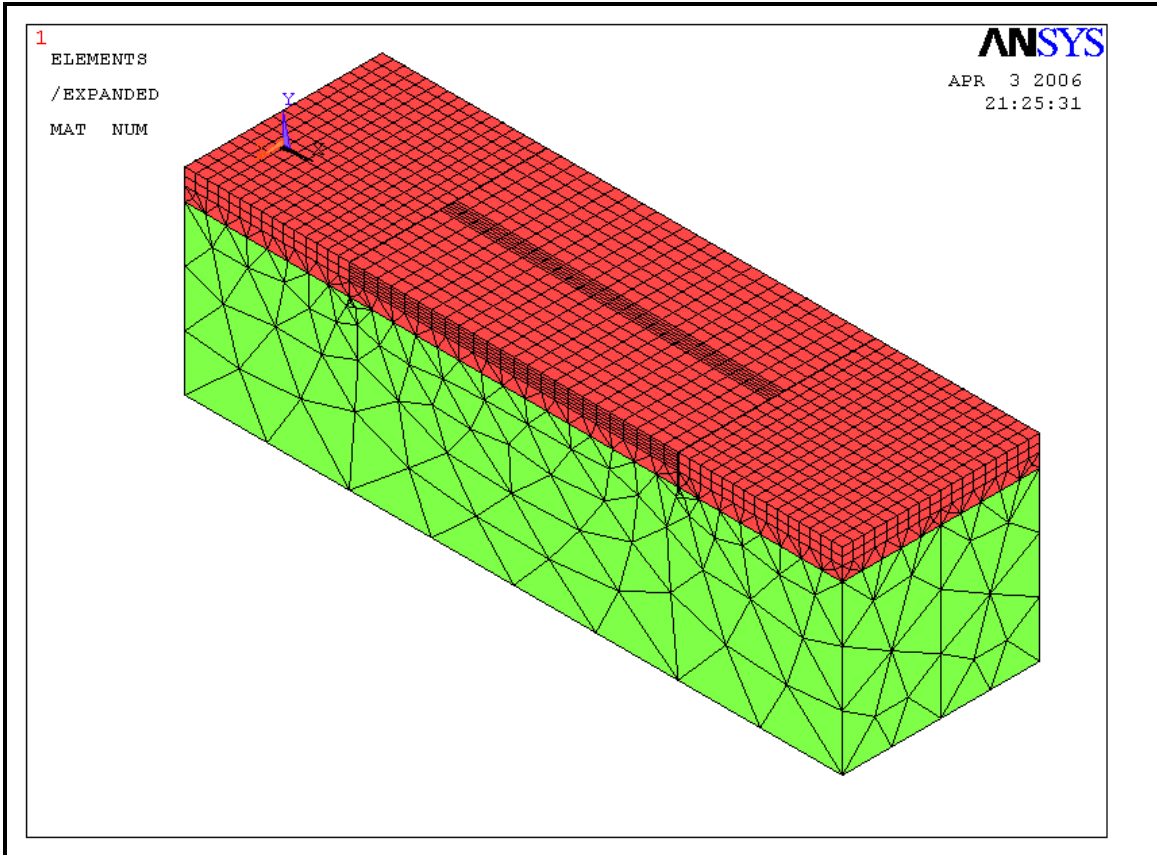


Figure 4.9: FEM Mesh of the Model Used for the 6-Inch TCO Pavement

4.6.4 Boundary Condition and Loading

The bottom of the subgrade was assumed fixed in all directions. The displacements in x, y, and z direction were restrained for all nodes. The nodes on the sides of the subgrade layer bordered by the pit were restrained in the direction of the pit walls. The nodes on the surfaces of the slab, overlay, subgrade and dowel bars were constrained in the plane of symmetry corresponding to a symmetrically loaded structure (My, Mz, Rx restrained).

The loading was applied to the model as a pressure on the element face. The modeled load was assumed to be rectangular, constant over the applied surface, and equal to the tire inflation pressure. The dimensions of the rectangular contact area were

computed from the tire width and inflation pressure in a manner similar to the TWT section.

4.7 Analysis of the Response Data of the TCO Pavements

4.7.1 Results of the Modeling of 6-inch TCO on PCCP Pavement

The results of the computed longitudinal and transversal strains at the measuring point locations are presented in Figures 4.10 and 4.11. The maximum values of the computed longitudinal strains location was -16.00 microstrain for the NSLU strain gage and -2.60 microstrain for the NSLL strain gage. The maximum values of the computed transverse strains corresponding to the NSTU strain gage was -13.00 microstrain and 4.09 microstrain for the NSTL strain gage.

The comparison between the computed and the measured transverse strains for the NSTU location (Figure 4.12) showed that values of computed strain are close to those of the measured strain. The transverse strain measured at this location before loading was slightly higher (-15.92 microstrain) than the computed strain (-13.00 microstrain).

The absolute value of the peak measured transverse strain decreased with the number of loading cycles (Figure 4.13). The maximum values occurred at the beginning of the experiment: -15.92 microstrain at zero load repetitions, and -16.22 microstrain at 100,000 load repetitions. Then the strain decreased with an approximate constant rate until about 1,100,000 load repetitions. After 1,100,000 load repetitions the maximum transverse strain stabilized to a value of about -12 microstrain. The measured and computed strains are close. This proved that, if any damage occurred in the pavement, it was not sufficient to influence the transverse strains.

The comparison between theoretical computed and measured longitudinal strains is presented in Figure 4.14. The maximum value of the longitudinal strain measured at zero load repetitions coincides with the maximum computed longitudinal strain (-15.9 microstrain measured vs. -16.00 microstrain computed). The absolute value of the minimum computed strains is smaller than the absolute values of measured strains. This difference may be caused by the initial loss of support developed at the bottom slab (the model used considered a uniform support under the PCC Slab).

The evolution of the peak values of measured longitudinal strain with the number of applied passes are presented in Figure 4.15. The values were approximately constant between 0 and 1,100,000 load repetitions (about 15 microstrain), dropped between 1,100,000 and 1,200,000 load repetitions, and then stabilized to a value of about 10 microstrain after 1,200,000 load repetitions. The maximum tensile longitudinal measured strain decreased from +12.56 microstrain at zero load repetitions to +22.755 microstrain at 1,100,000 load repetitions on West joint, and from +12.55 microstrain at zero load repetitions to +28.093 microstrain at 1,100,000 load repetitions on East joint. Between 1,100,000 load repetitions and 1,200,000 load repetitions the absolute value of the maximum tensile measured strain dropped, then the values remained somewhat constant at about a value of +10 microstrain for the West joint position, and about +20 microstrain for the East joint load position. This behavior is explained by the increasing lineal extent of the loss of support that caused an increase of the longitudinal stress in concrete, leading to the development of transverse crack in the PCC slab and overlay at 1,100,000 load repetitions.

To estimate the loss of support (lineal extent) between zero and 1,100,000 load repetitions, the FEM model was modified and run for different values of loss of support distances (12 in, 24 in, 36 in). The results are presented in Figure 4.16. The maximum tensile longitudinal strain (NNLU) being most affected by the loss of support is plotted in Figure 4.17. The regression equation [4.1] was developed to estimate the length of loss of support at both joints (Figure 4.18).

$$L_{LOS} = 0.0837S_{NSLU}^2 - 0.8411S_{NSLU} + 1.248 \quad \text{Equation 4-1}$$

Where:

L_{LOS} -Loss of support length (in)

S_{NSLU} -Maximum computed tensile longitudinal strain at SNLU
(microstrain)

The FEM model was modified and run again for the loss of support length corresponding to 1,200,000 load repetitions and computed with Equation 4-1. The computed strains were compared to the measured values (Figure 4.19). The longitudinal strain at the top of the overlay at the wheelpath was computed for the load positioned at the joint. This is the critical position for the load, since it induces the maximum longitudinal strain in the overlay. The measured and computed values of the strain at 1,200,000 load repetitions for the NNLU strain gage are very close. It was also found that the maximum longitudinal strain caused by the critical load correlates well with the position of the crack that developed in the concrete overlay (Figure 4.20), confirming the prediction of the finite element model.

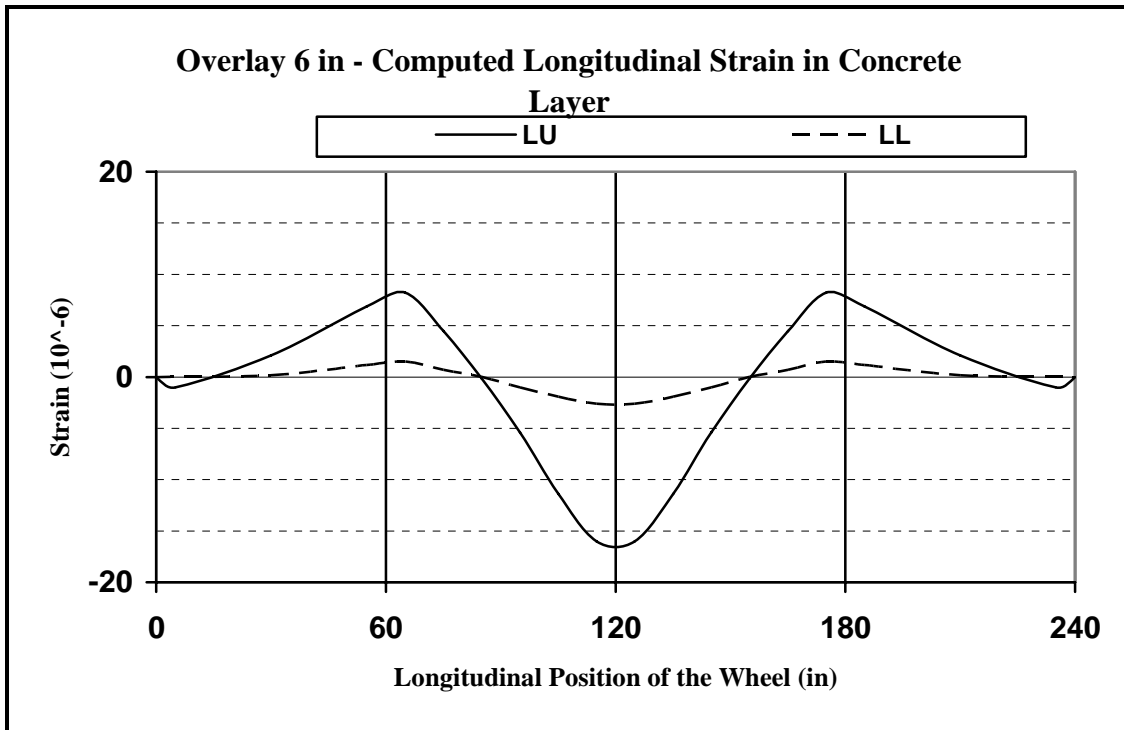


Figure 4.10: Computed Longitudinal Strains: 6-inch TCO Pavement

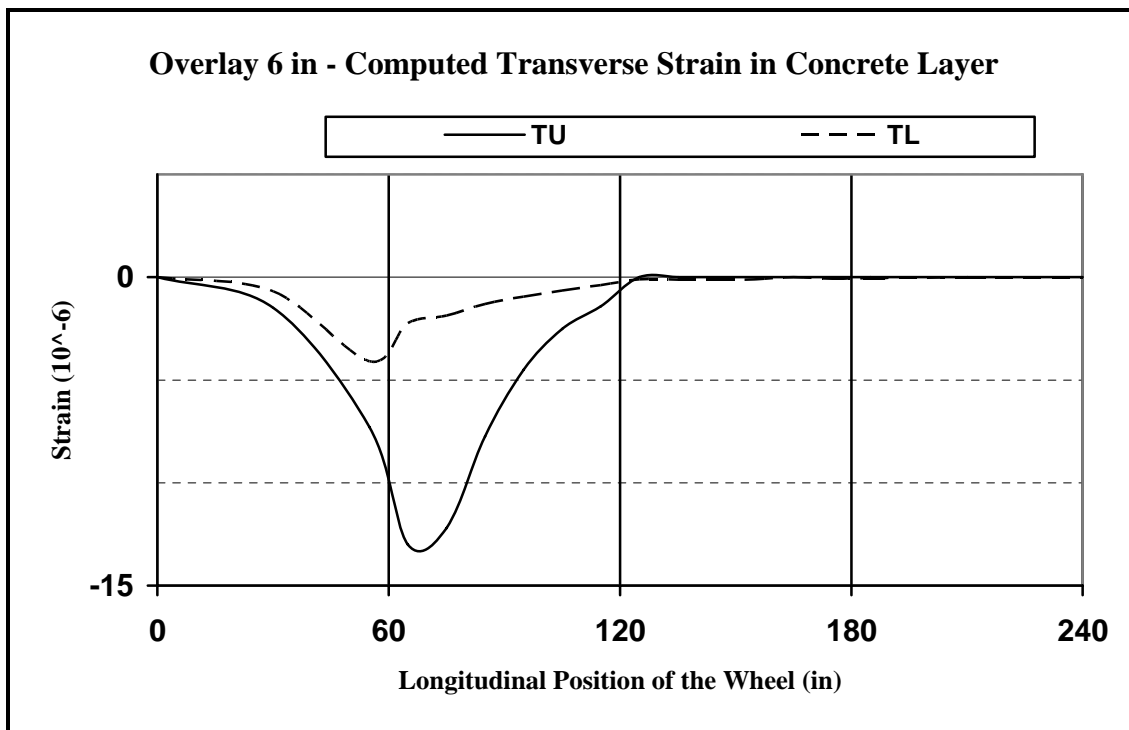


Figure 4.11: Computed Transverse Strains: 6-inch TCO pavement

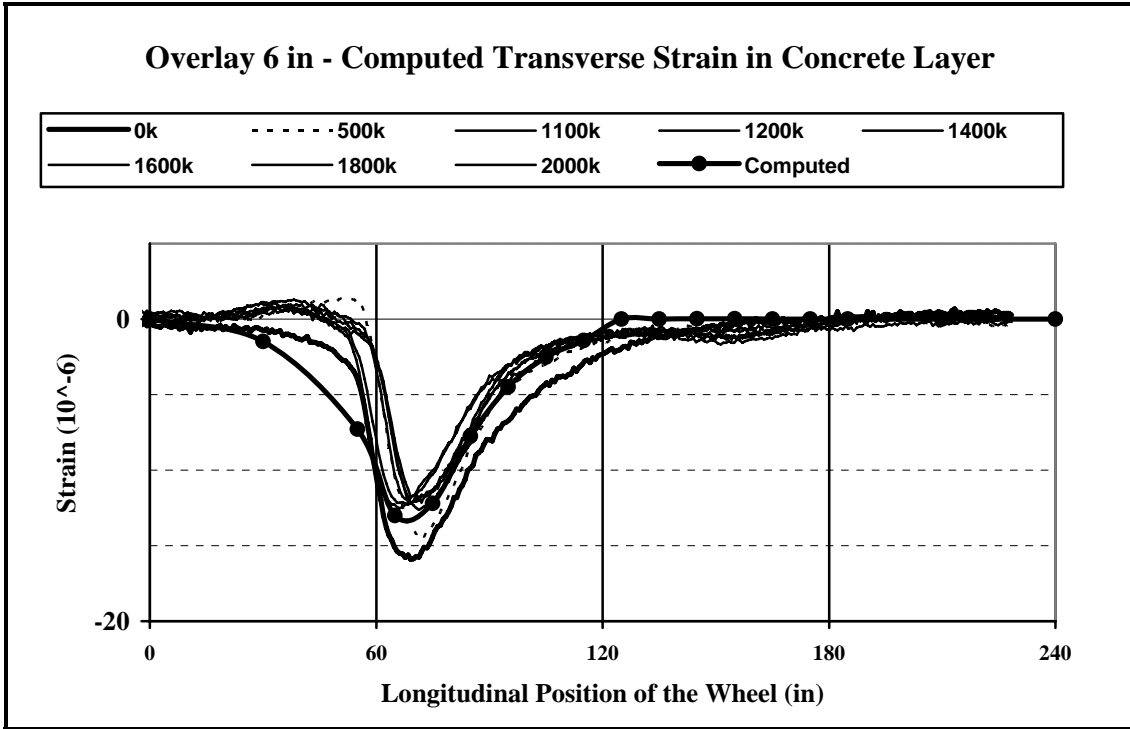


Figure 4.12: Measured vs. Computed Transverse Strains: 6-inch TCO pavement

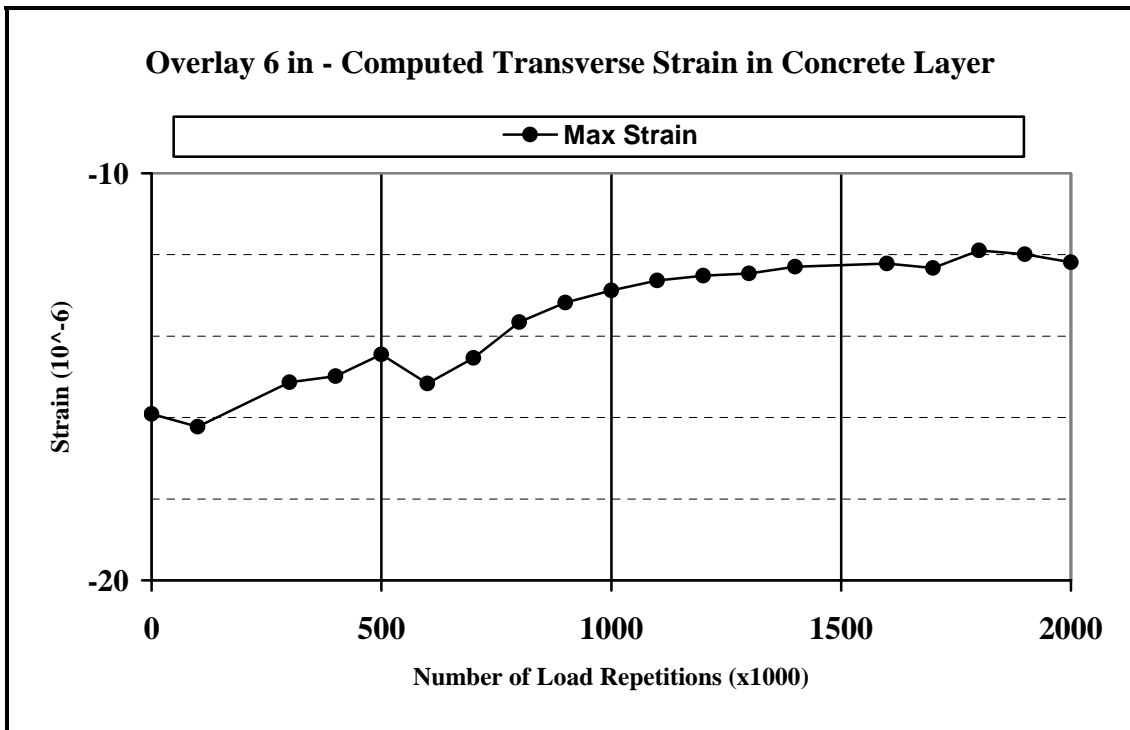


Figure 4.13: Evolution of Maximum Measured Transverse Strains: 6-inch TCO pavement

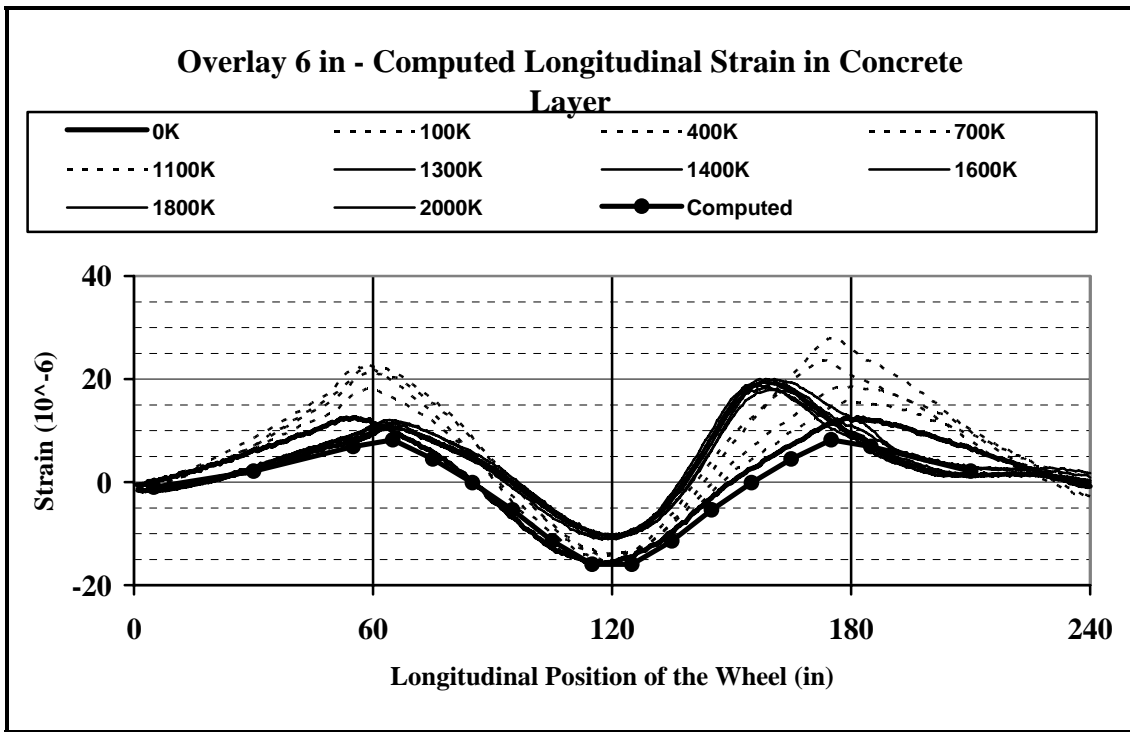


Figure 4.14: Measured vs. Computed Longitudinal Strains: 6-inch TCO pavement

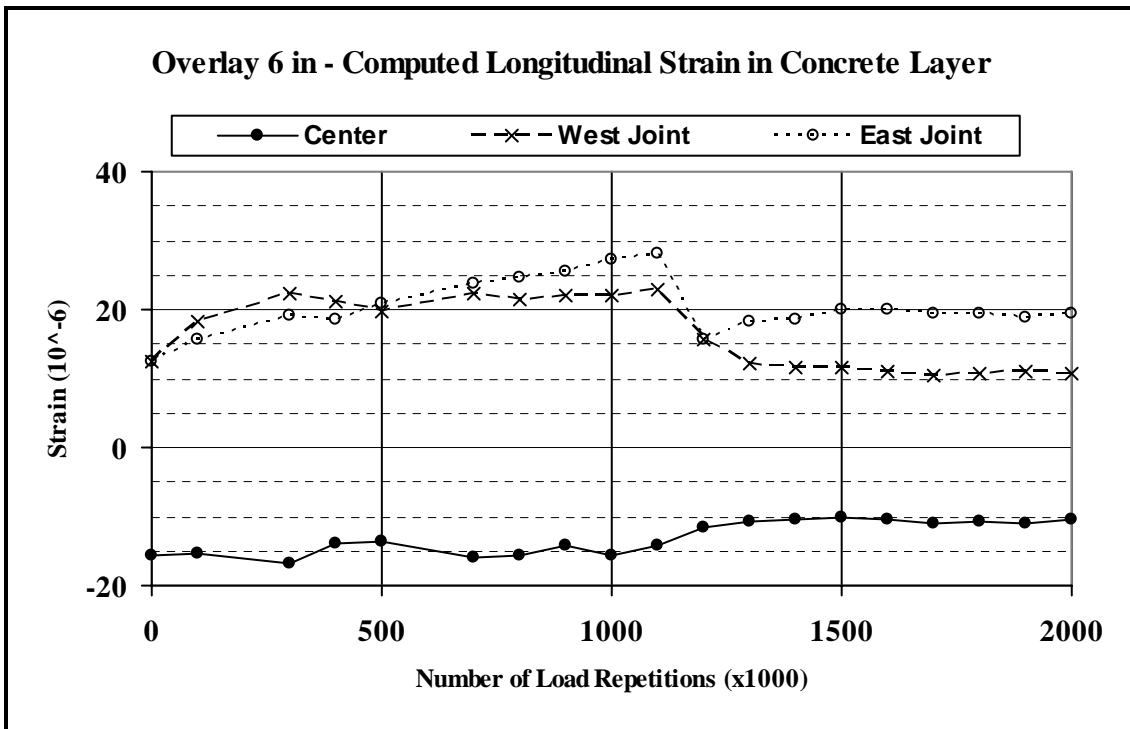


Figure 4.15: Evolution of Maximum Measured Transverse Strains: 6-inch TCO pavement

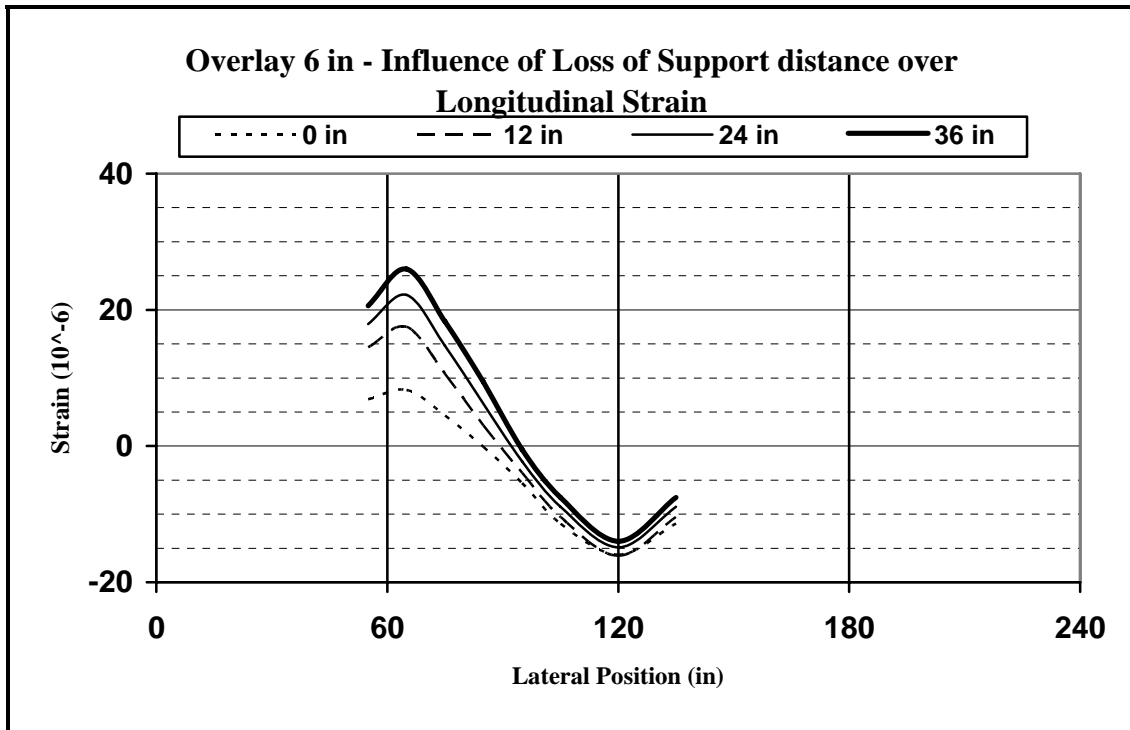


Figure 4.16: Influence of Loss of Support Length over Longitudinal Strain: 6-inch TCO pavement

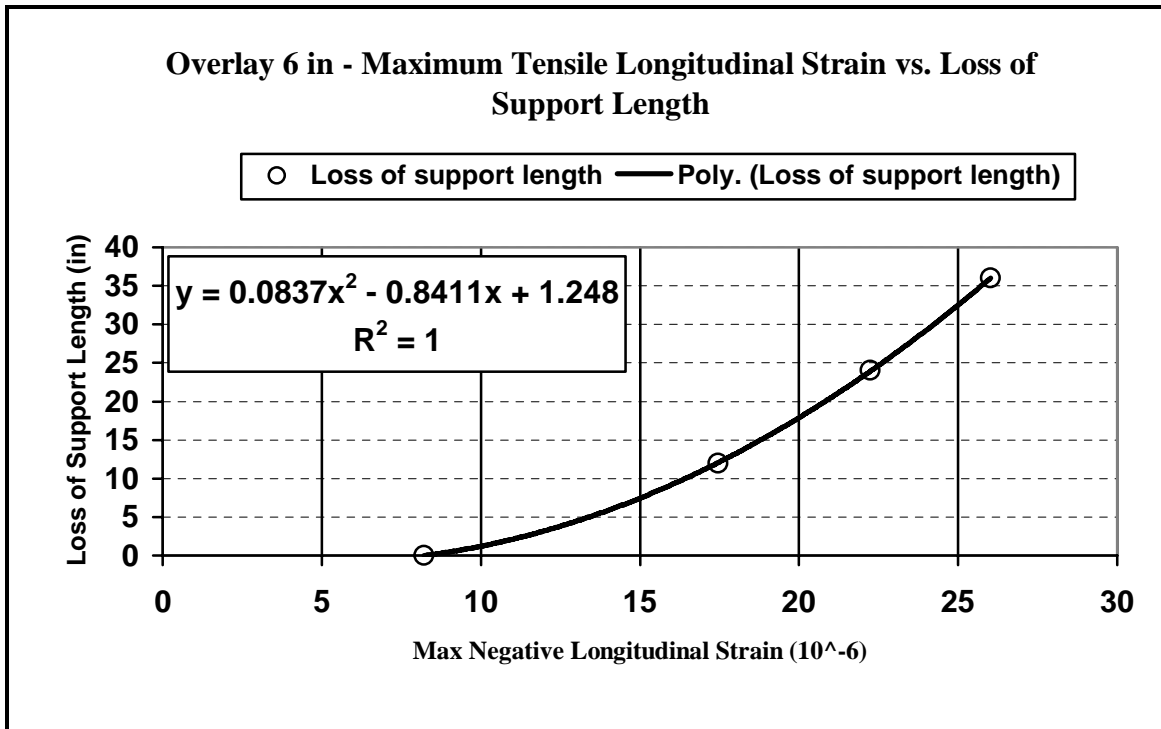


Figure 4.17: Maximum Tensile Longitudinal Strain vs. Loss of Support Length

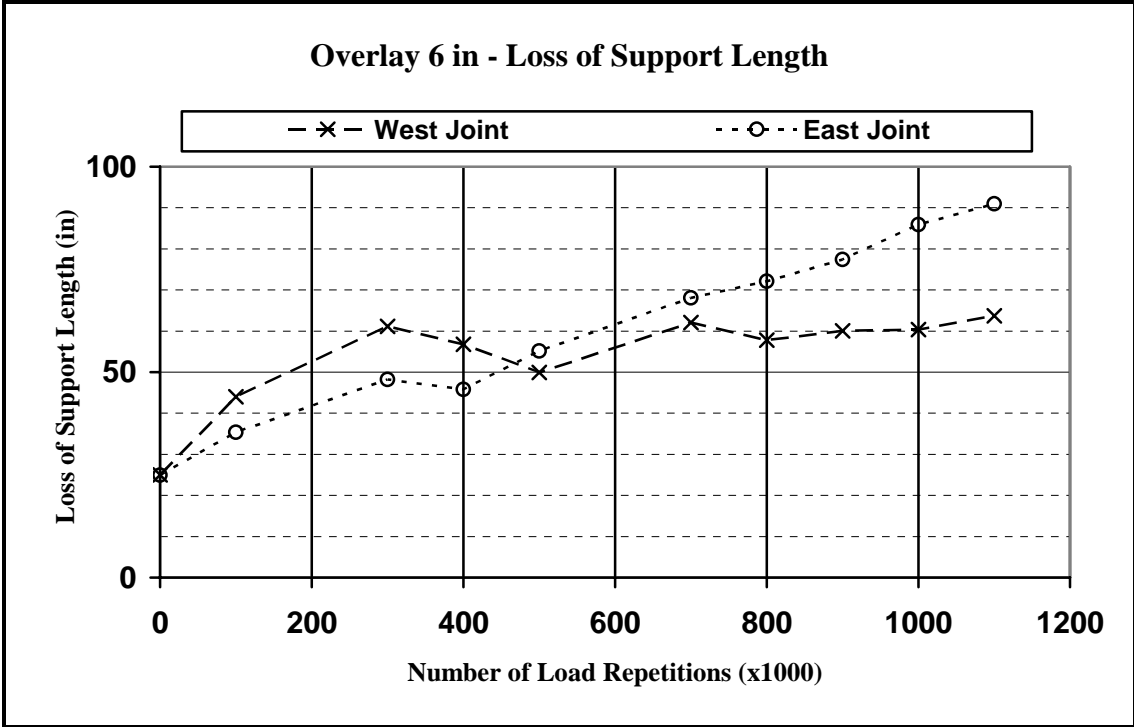


Figure 4.18: Loss of Support Length vs. Number of Load Repetitions

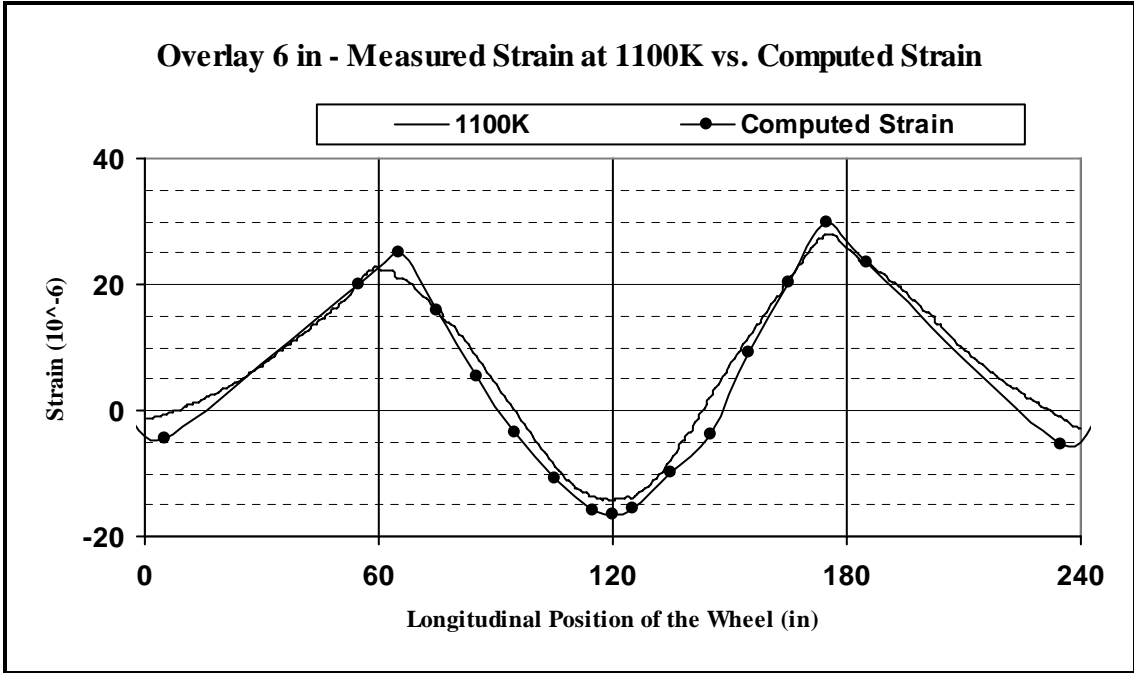


Figure 4.19: Measured vs. Computed Longitudinal Strains at 1.1M Passes

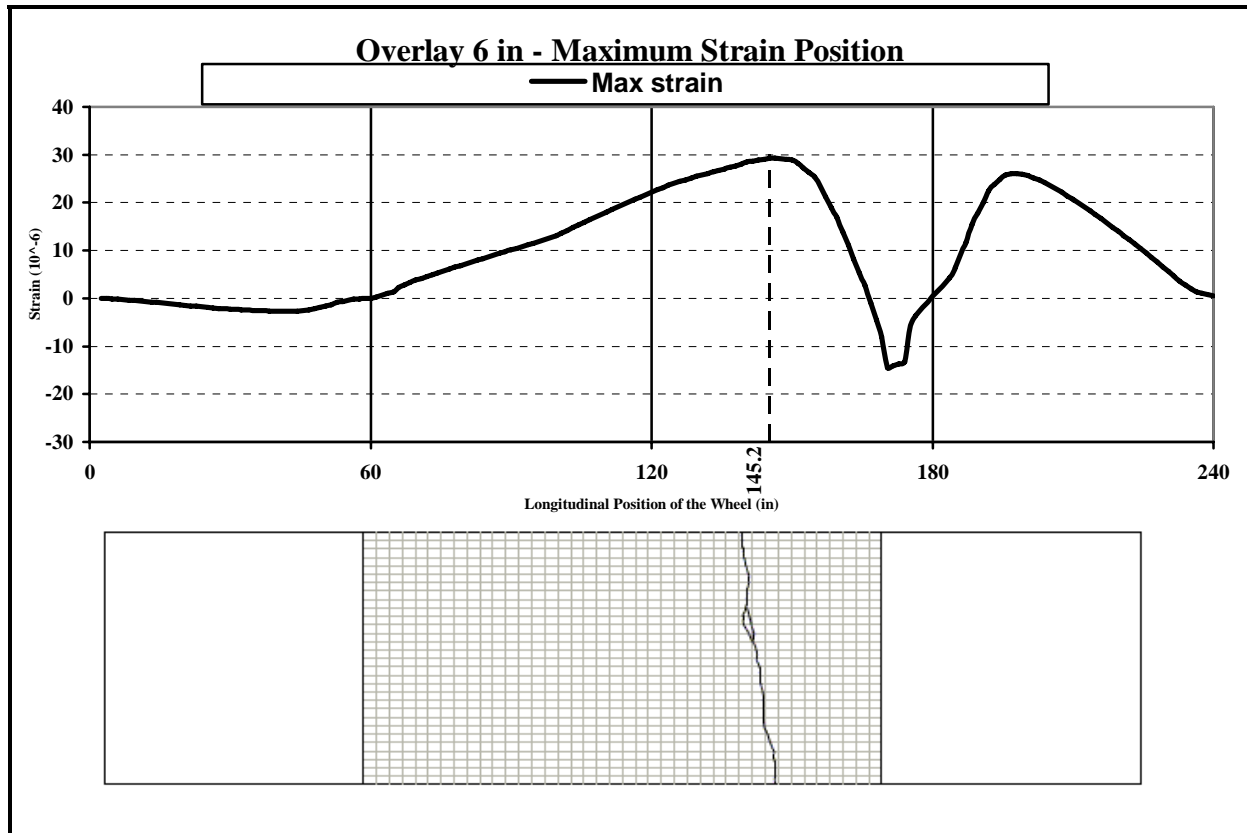


Figure 4.20: Correlation between Maximum Tensile Strain and Slab Cracking

4.7.2 Results of the Modeling of 4-inch TCO on PCCP Pavement

The results of the computed longitudinal and transversal strains at the measuring point locations are presented in Figures 4.21 and 4.22. The maximum value of the computed longitudinal strains was -12.40 microstrain for the NNLU strain gage and -5.62 microstrain for the NNLL strain gage. The maximum values of the computed transverse strains corresponding to the NNTU strain gage was -12.78 microstrain and -8.11 microstrain for the NNTL strain gage.

The comparison between the computed and the measured transverse strain for the NSTU location (Figure 4.23) shows that the measured and computed strain values were very close. The initially measured (zero repetition) transverse strain measured at this location was -12.78 microstrain, and the computed strain was -12.04 microstrain.

Between zero repetitions and 1,700,000 load repetitions, the maximum measured transverse strain had a variation of about ± 2.5 microstrain around the theoretically computed value (Figure 4.24). The variation of the maximum transverse strain in this interval has a range between -9.35 microstrain at 400,000 load repetitions and -14.20 microstrain at 800 load repetitions. After 1,700,000 load repetitions the measured values showed a significant drop, and a change of the signal shape.

Figure 4.25 shows that the maximum compressive strains computed for and measured by the NNLU gage were similar: -12.40 microstrain computed and -13.04 microstrain measured. The computed and measured tensile strains were also similar when the wheel load was near the East joint: +6.43 microstrain computed and +7.79 measured, respectively. However, for the first 300,000 load repetitions, the maximum measured longitudinal strain (tensile) when the wheel load was at the West joint was higher than the computed strain absolute value for the same wheel location (+11.48 measured, +6.43 computed). Starting from 500,000 load repetitions, the maximum tensile longitudinal strain recorded by the NNLU gage not only increased to about +15 microstrain, but also was recorded when the wheel was further away from the west joint, at about 80 inches from the west wall of the pit.

This increase in the magnitude and the change of the wheel position that caused the maximum tensile longitudinal strain measured at the NNLU gage may be explained by the development of a transverse crack in the concrete slab underneath the PCC overlay at about 12 inches east from the West joint (Figure 4.26). As shown in Figure 4.3, the West joint of the 4 inch TCO pavement (North Lane) is the only joint not

exhibiting a transverse crack after the loading with the steady state pulse equipment (Figure 2.8).

The evolution of the peak measured values of longitudinal strain during the experiment is presented in Figure 4.27. The maximum values have an approximate constant value of about -10 microstrain until 1,700,000 load repetitions, then the values decrease to a value of about -3 microstrain. The maximum tensile longitudinal strain corresponding to the location of the load at the east joint had small variation around the computed value (-5.52 microstrain) until 1,700,000 load repetitions, when the values decreased to a value of about -2.5 microstrain. The conclusion of severe cracking of the slab after 1,700,000 load repetitions can be correlated with the crack mapping and the evolution of measured transverse strains.

Since the joint was distressed, a loss of support could be expected. To evaluate the extent of the loss of lineal support between zero and 1,100,000 load repetitions, the model was modified for different values of loss of support distances (12 inches, 24 inches, 36 inches) and the results are presented in Figure 4.28. The maximum tensile longitudinal strain being most sensitive to the loss of support distance, was plotted in Figure 4.29, and a regression equation was developed (Equation 4-2). Based on this equation, the loss of support was computed for both joints (Figure 4.30), showing an insignificant loss of support under the joints corresponding to a normal seasonal variation.

$$L_{LOS} = 0.1244S_{NNLU}^2 + 1.001S_{NNLU} - 10.647 \quad \text{Equation 4-2}$$

Where:

L_{LOS} - Loss of support length

S_{NNLU} -Longitudinal strain at NNLU measuring point

The measured and computed values (Figure 4.31) are very close, showing that the model for predicting the length of the loss of support is valid.

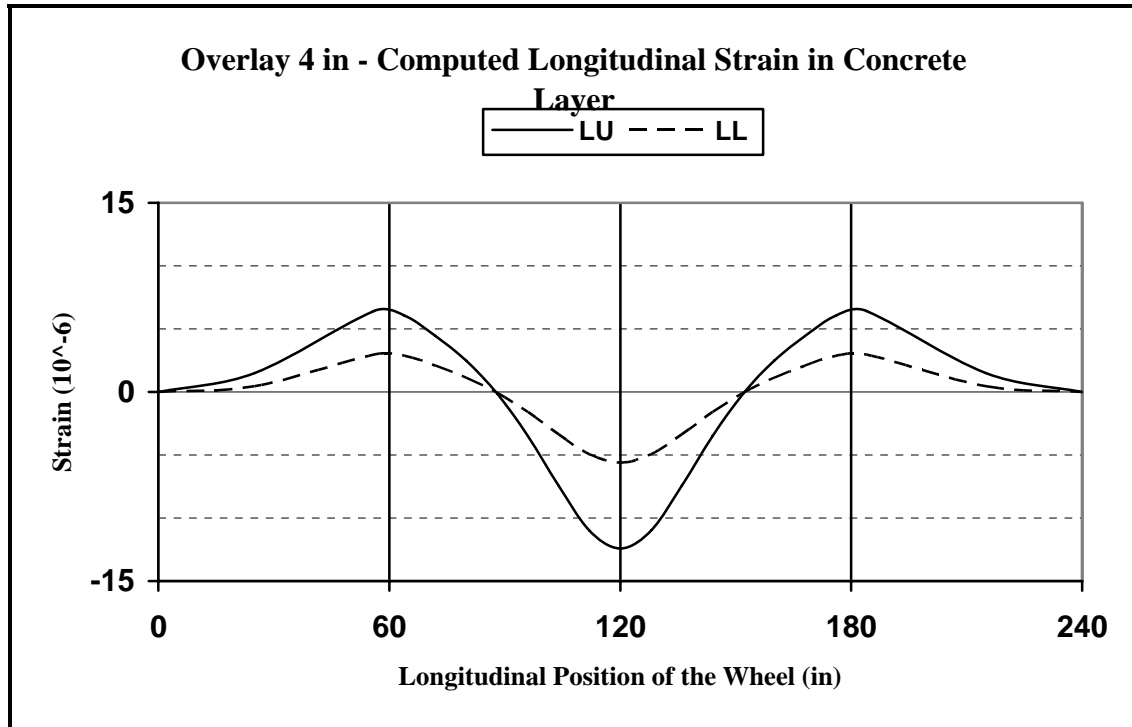


Figure 4.21: Computed Longitudinal Strains: 4-inch TCO Pavement

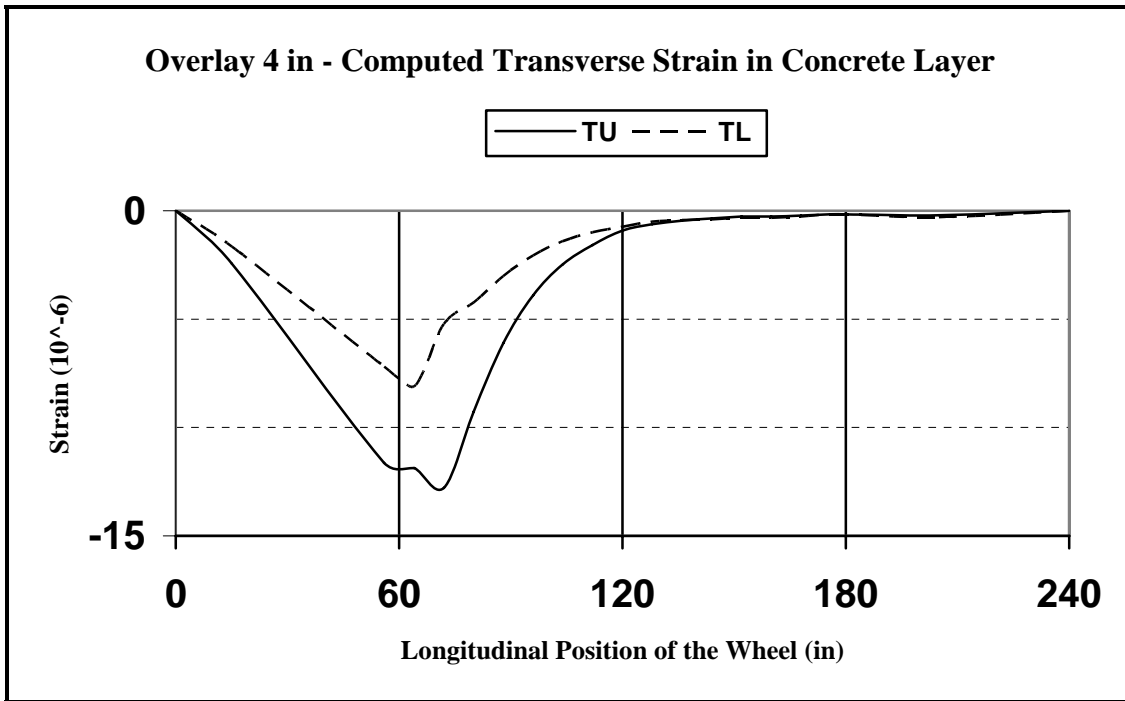


Figure 4.22: Computed Transverse Strains: 4-inch TCO Pavement

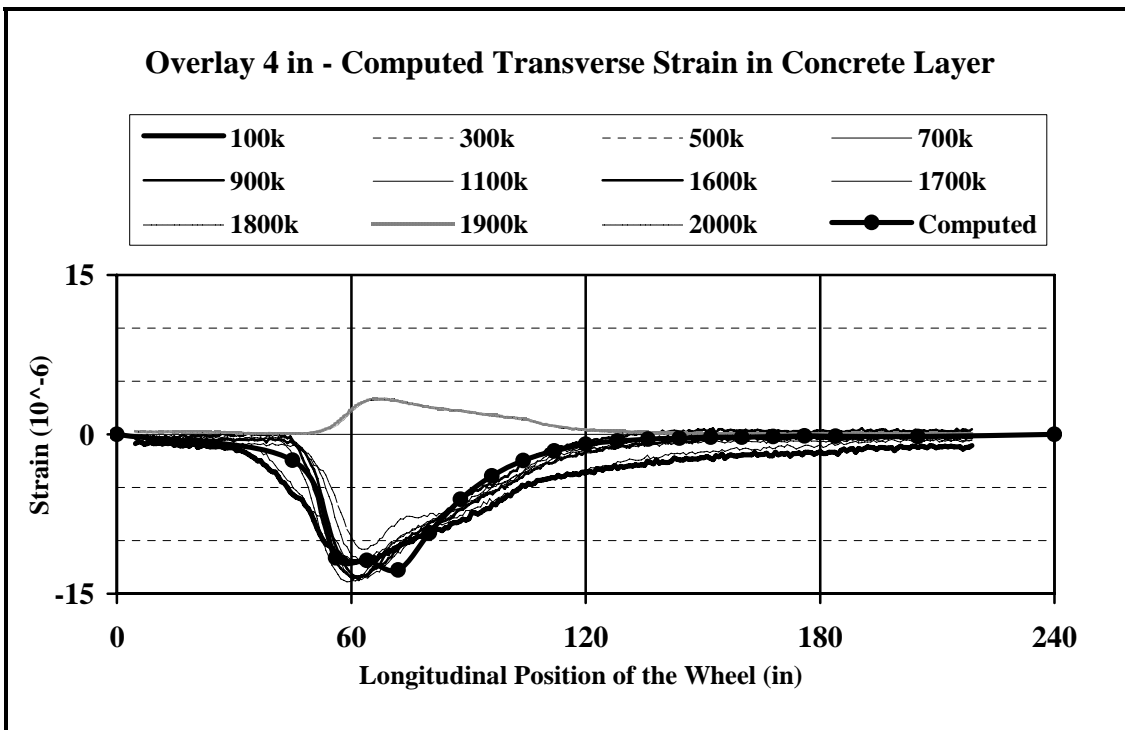


Figure 4.23: Measured vs. Computed Transverse Strains: 4-inch TCO Pavement

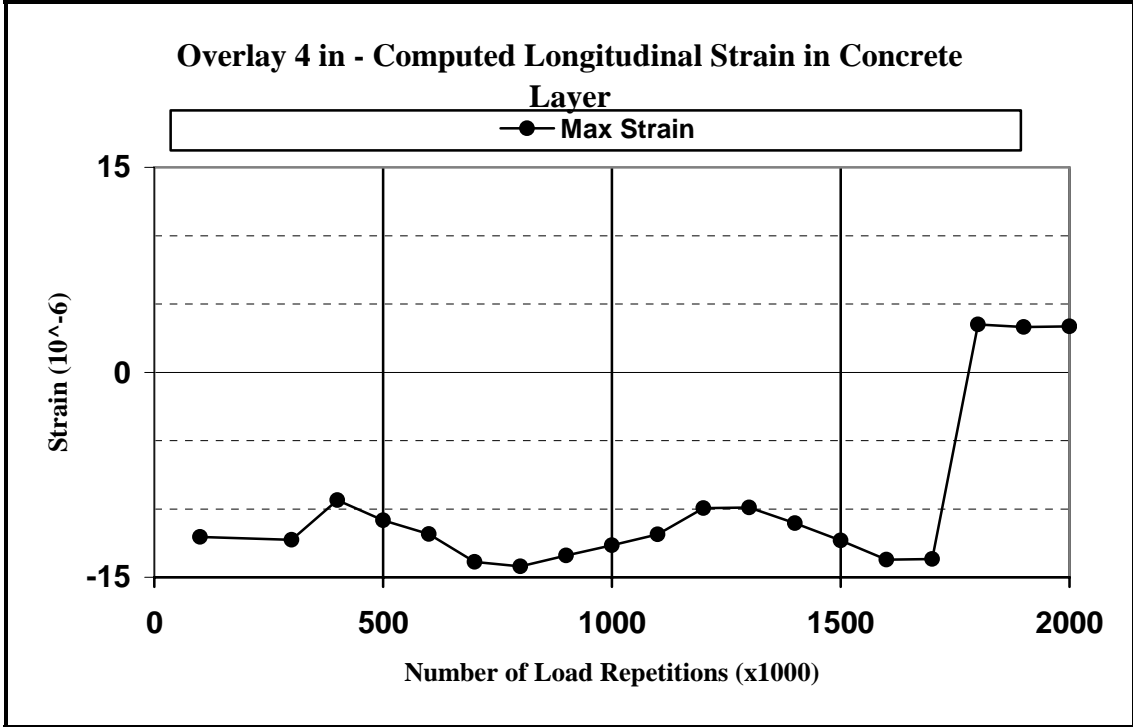


Figure 4.24: Evolution of Maximum Measured Transverse Strains: 4-inch TCO Pavement

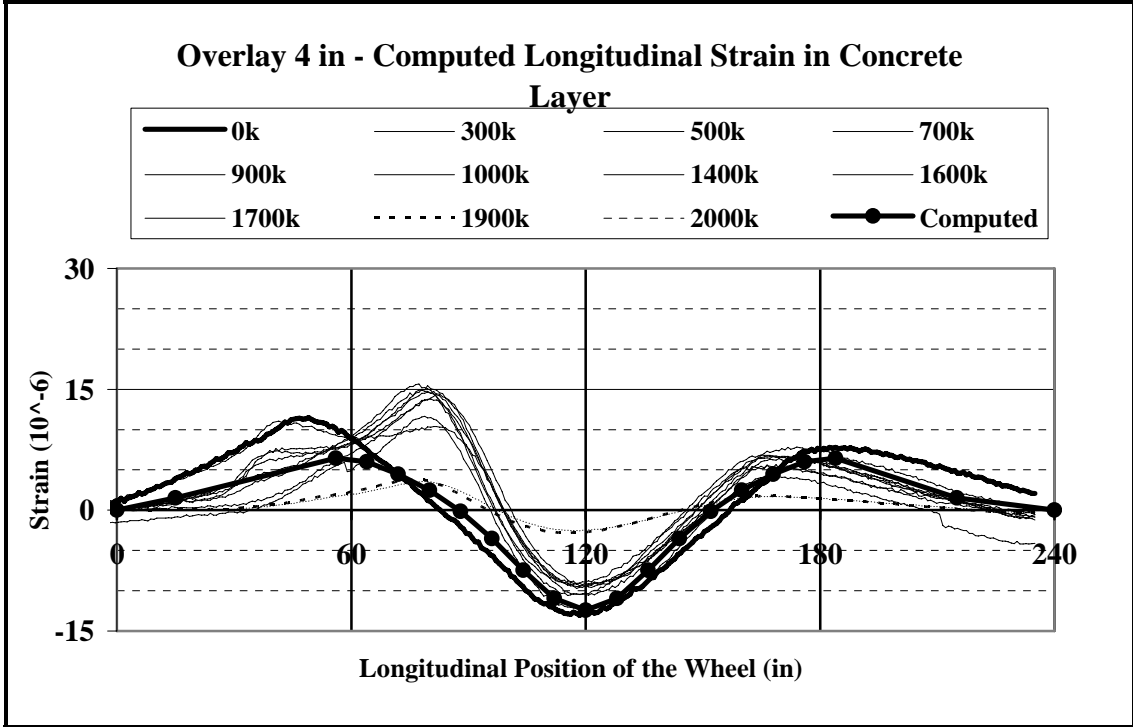


Figure 4.25: Measured vs. Computed Longitudinal Strains: 4-inch TCO Pavement

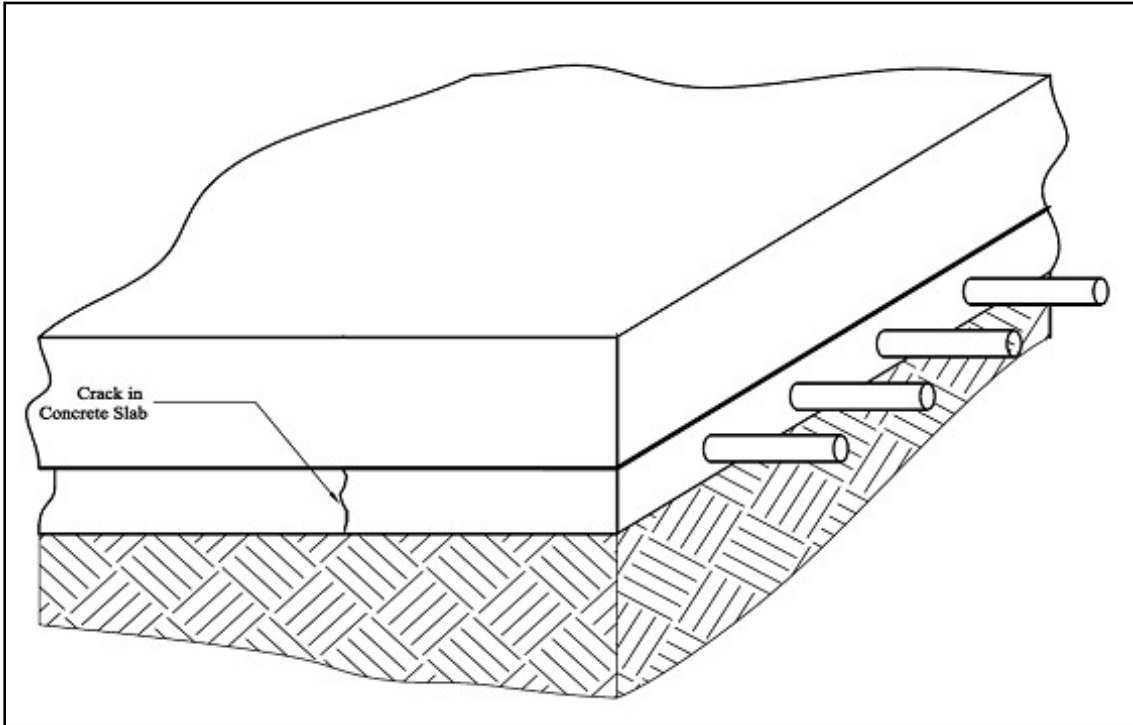


Figure 4.26: Transverse Crack in the Concrete Slab Underneath the 4-inch TCO Pavement

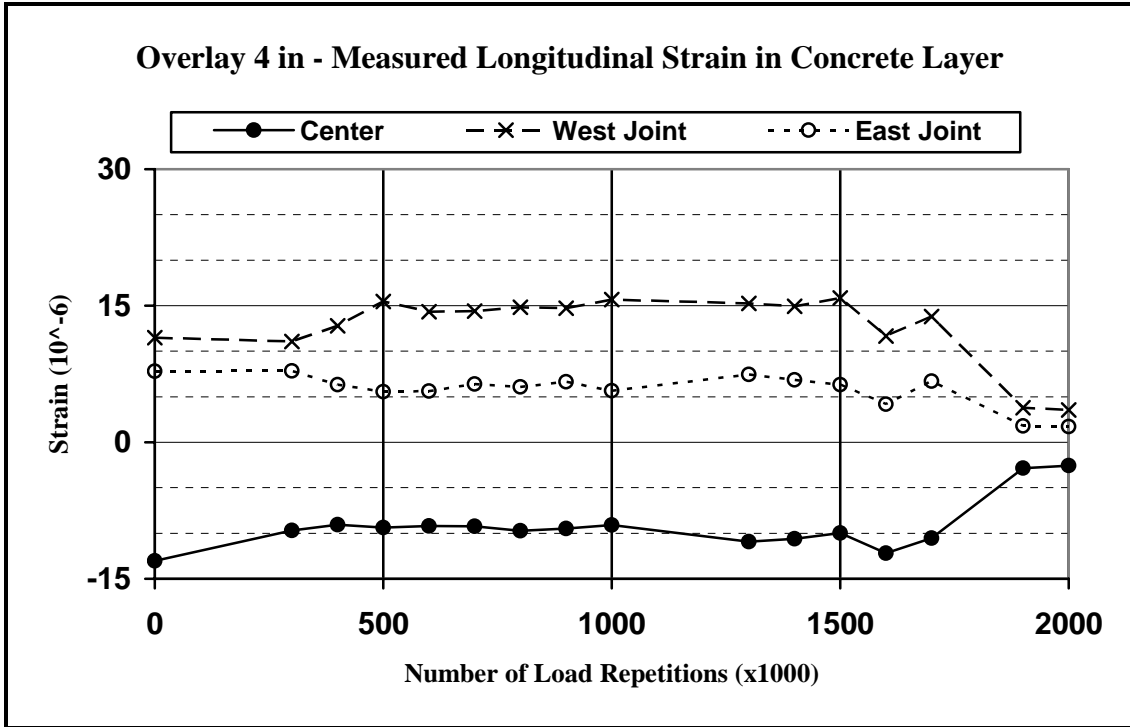


Figure 4.27: Evolution of Maximum Measured Longitudinal Strains: 4-inch TCO Pavement

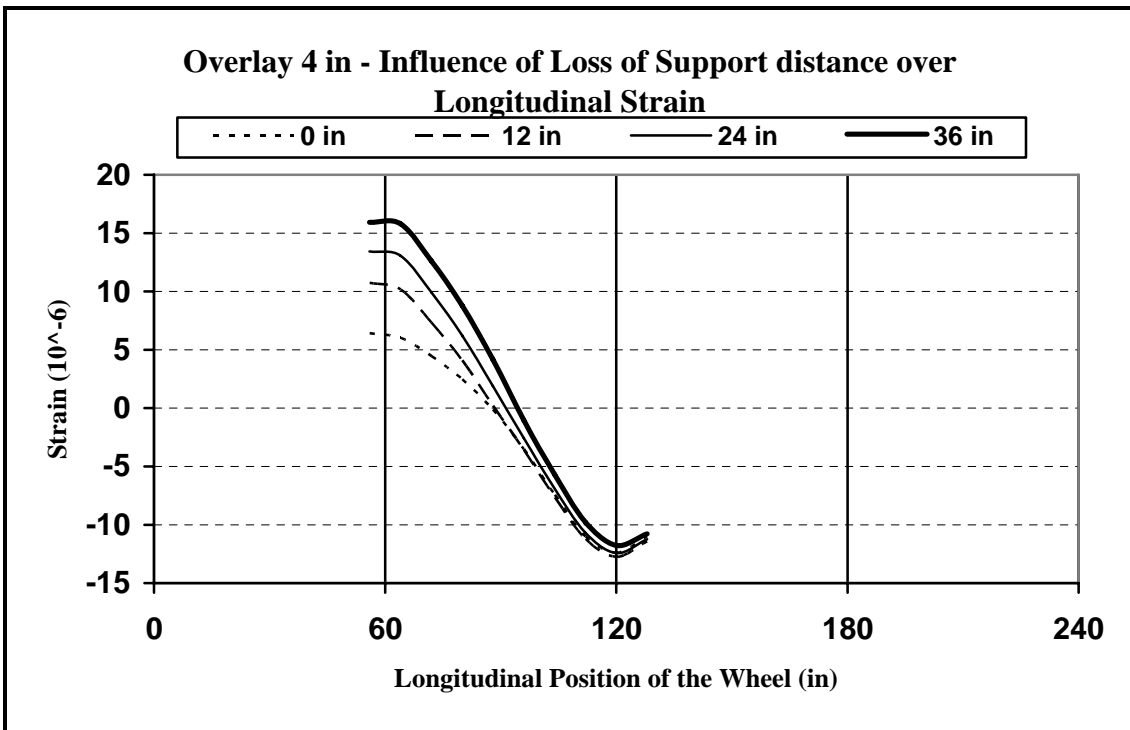


Figure 4.28: Influence of Loss of Support Length on Longitudinal Strains: 4-inch TCO Pavement

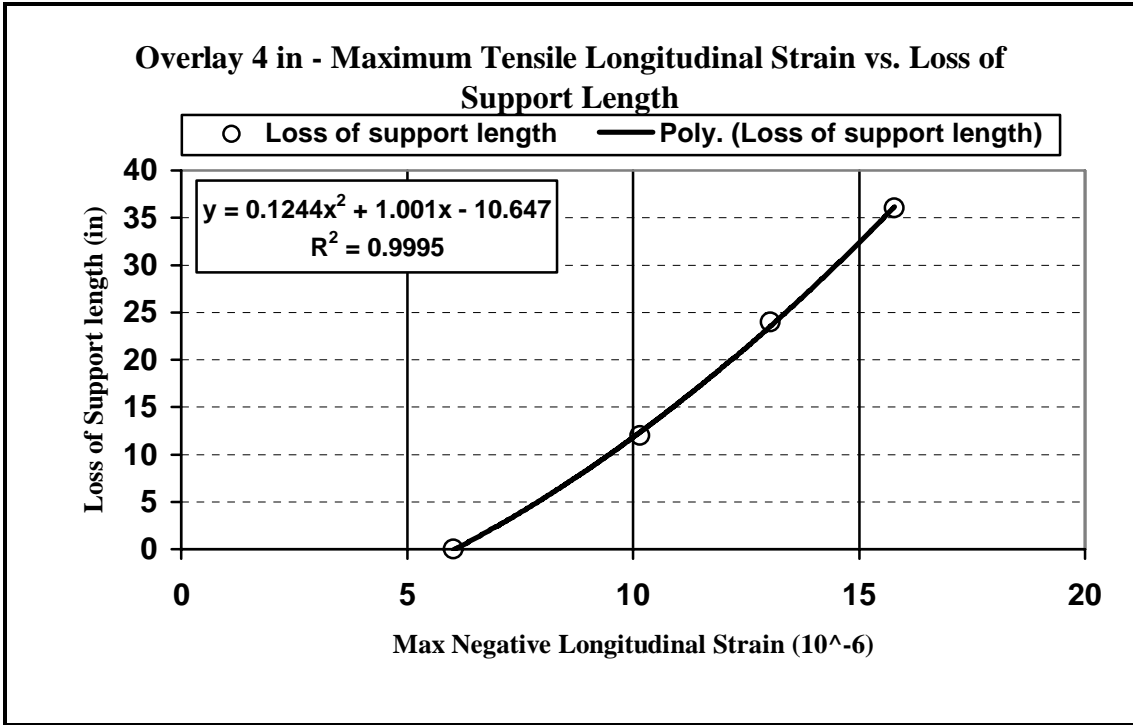


Figure 4.29: Maximum Tensile Longitudinal Strain vs. Loss of Support Length

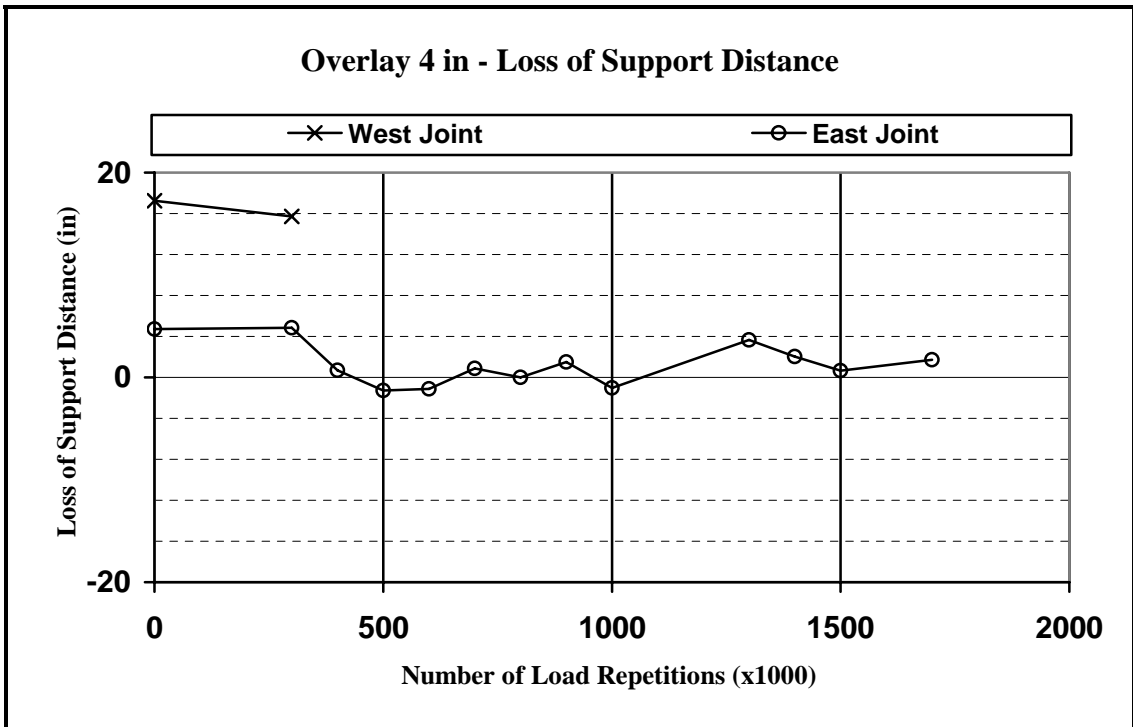


Figure 4.30: Loss of Support Length vs. Number of Load Repetitions

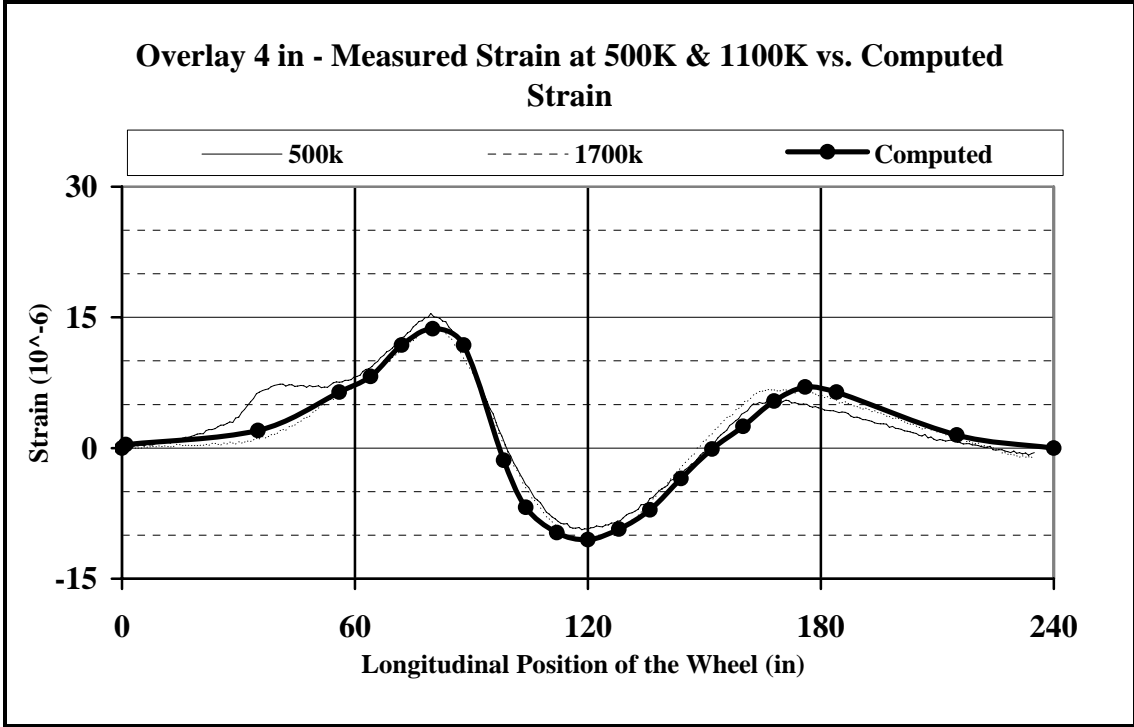


Figure 4.31: Comparison of Measured vs. Computed Longitudinal Strains

CHAPTER 5 - CONCLUSIONS AND RECOMMENDATIONS

This research study aimed to evaluate the performance of thin bonded PCC overlays on existing PCC and HMA pavements through accelerated pavement testing (APT) and to determine the failure modes of these pavement structures. The advantage of using accelerated pavement test when compared to in-situ field tests is that the results of the comparative APT study can be obtained in a few months. In in-situ field tests, the results are obtained after observing the behavior of the road test sections for a period of minimum five years. Also, on in-situ field tests, some of the environmental factors and traffic loadings cannot be controlled. However, pavement performance evaluation using APT has two major limitations: a) the effect of the environment cannot be well simulated even though temperature can be controlled and, b) APT loading may differ from the vehicle loading provided by in-service traffic, in terms of speed and frequency (headway) of loading, lateral wheel wander, load spectra. The effects of long term exposure to water and extreme temperatures (e.g. freezing and thawing, water damage) and long term changes in material properties (e.g. ageing of asphalt binders) cannot be reproduced in an APT test.

With these benefits and limitations in mind, the proposed study was conducted at the Civil Infrastructure Systems Laboratory (CISL) of Kansas State University. Four pavement sections tested in the thirteenth experiment carried out at CISL:

- Two Thin Concrete Overlay (TCO) pavements, with 4-and 6-inch overlay thicknesses, were constructed on top of a 5-inch thick PCCP pavement built without a subbase layer and with distress at the joints from cyclic loading applied by a pulse load system.

- Two Thin Whitetopping (TWT) pavements, with 4- and 6-inch overlay thicknesses, were constructed on top of a 5-inch hot-mix asphalt (HMA) layer built directly on the clayey subgrade. Longitudinal and transverse full-depth cuts were made in the HMA layer before placing the PCC overlay to simulate longitudinal and transverse cracking that would be present in a distressed flexible pavement.

Appropriate construction methods were used during construction to ensure optimum bond between the overlays and the supporting layers.

The pavements were equipped with instrumentation to measure the strains in selected locations in each PCC overlay and the parameters that affect the mechanical characteristics of the material (moisture in subgrade soil and temperature in the asphalt layer). Each of the four pavements was loaded with two million passes of the CISL APT machine. Response measurements and performance evaluations were performed at about every 100,000 passes of the CISL APT machine.

Three of the four pavements performed well during the APT test. The 4-inch TCO on PCCP pavement developed a transverse crack after 1,100,000 load repetitions. The 6-inch TCO on PCCP pavement developed a transverse crack after 1,700,000 load repetitions. The 6-inch TWT pavement experienced no cracking after 2,000,000 load cycles. The 4-inch TWT pavement exhibited the first crack after 400,000 load cycles. No significant joint faulting was recorded. Cores taken at several locations in the TCO pavements showed that no loss of bond developed between the two PCC layers.

Theoretical values for the strains developed at the locations where the strain gages had been placed were computed using a finite element model developed using

the ANSYS finite element software. The FEM considered all materials linear elastic and a perfect bond between the overlays and the supporting layers.

The transverse joints between the slabs were modeled using orthotropic elements. The steel dowel bars were modeled using 3-D brick elements; one half of each bar was allowed to slip from the surrounding concrete. No temperature or moisture gradients were modeled since the APT experiment was conducted without temperature and moisture changes. The position of the wheel load was changed along the slab to determine the changes in the values of the strain at the gage location when the wheel traveled along the pavements.

The comparison between the measured and the computed strains was done by looking at the signal of the measured strains and the curve obtained from the strain values estimated under the moving wheel load. The corresponding magnitude of the maximum strains and strain signal shapes were compared. It was found that the magnitude and shape of computed strains matched well the magnitude and shape of strain signals measured by the installed strain gages before any APT loading was applied. This indicated that the FEM analysis and the assumptions made modeled the undamaged composite pavement structures well.

The FEM model was then modified to include loss of support under the joint. Then the strains at the top fiber at the mid-span of the slabs were computed for several lineal extent of the loss of support area, which was considered to be the same along the transverse joint. The length of the loss of support area was estimated by interpolation from the obtained computed strains and the values of the corresponding strains measured during the APT loading. The evolution of the length of loss of support

underneath the slabs with the number of applied passes of the CISL machine was thus estimated.

The major findings of this study are:

- The 3-D finite element model built and the assumption made (linear elastic materials, fully bonded overlays) can predict very well the response of TWT and TCO pavements under wheel loading. This suggests that the calculation of pavement response using 3D finite element can be used effectively to estimate the effect of wheel loading on the performance of thin concrete overlays.
- Under the wheel loading applied by the APT machine, all pavements experienced loss of support in the subgrade under the joints which caused the increase of the maximum longitudinal strains at the mid-span of the slabs.
- The wheel loading did not cause any de-bonding between the concrete overlay and the existing pavement. This suggests that environmental factors (high daily or seasonal temperature gradients, presence of water at the interface, etc.) or improper surface preparation may be the causes for the loss of bonding between the PCC overlays and the existing pavement.
- The lineal extent of the loss of support can be successfully back-estimated from the values of the strains computed with the FEM model. The length of loss of support increased continuously up to a certain value after which it remained constant. At this point the flexural stiffness of the slabs prevented a further consolidation of the subgrade soil underneath the joints.

The following recommendations can be made from this research:

- The FE model with the assumption of linear elastic materials should be used for the effective estimation of the response of TCO and TWT pavement structures under wheel loading.
- The thin PCC overlays should be modeled as fully bonded to the under laying layer; TCO and TWT pavement structures should be modeled as monolithic structures.
- In the modeling of the deterioration of TCO and TWT pavements, it should be assumed that the length of loss-of-support increases with the applied traffic loading and then remains constant.
- Further studies should be conducted to better understand the behavior of these structures. The effect of the environment, subgrade soil type and, thickness of the existing distressed pavement on the performance of thin PCC overlays should be investigated.

REFERENCES

- AASHTO. (1993). *AASHTO Guide for the Design of Pavement Structures*, American Association of State Highway and Transportation Officials, Washington, DC.
- ACPA (1998). *Whitetopping- State of the Practice*. Engineering Bulletin EB210P, American Concrete Pavement Association, Skokie, Illinois.
- Barezinisky, R. (2003) Personal Communication, June 2003.
- Gisi, A. (2003) Personal Communication, June 2003.
- Gisi, A. (1985) "Portland Cement Concrete Overlay Over a Bituminous Pavement". In *Transportation Research Record No. 1040*, Transportation Research Board, Washington, D.C., pp. 12-17.
- Grogg, M. G., K.D. Smith, S.B. Seeds, T.E. Hoerner, D.G. Peshkin, and H.T. Yu. (2001) *HMA Pavement Evaluation and Rehabilitation*. Reference Manual, NHI Course No. 131063, National Highway Institute, Arlington, VA.
- Grove, J.D., G. K. Harris and B. J. Skinner. *Bond Contribution to Whitetopping Performance on Low Volume Roads. Construction Report*, Iowa Highway Research Board Project No. HR-341, Iowa Department of Transportation, January 1993.
- Huang, Y. J. (2003) *Pavement Analysis*. Prentice Hall, Second Edition, New Jersey.
- McCullough, B.F. and Rasmussen, R.O. (1999), *Fast Track Paving: Concrete Temperature Control and Traffic Opening Criteria For Bonded Concrete Overlays. Volume II: HIPERPAV User's Manual*, FHWA –RD-98-168. Federal Highway Administration, McLean, VA.
- Melhem, H.G. (1997), *Development of an Accelerated Testing Laboratory for Highway Research in Kansas*. Report No. FHWA-KS-97/5, Kansas Department of Transportation, Topeka, KS.
- Rasmussen, R.O., McCullough B.F., Ruiz, J.M., Mack, J. and Sherwood, J.A. (2002) "Identification of Pavement Failure Mechanisms at FHWA Accelerated Loading Facility Ultrathin Whitetopping Project", *Transportation Research Record*, No. 1816, Washington, D.C., pp 148-155.
- Rowden L. R. (1996). *Thin Bonded Concrete Overlay and Bonding Agents*. Report No. FHWA/IL/PR-123, Interim Report, Illinois Department of Transportation, Springfield, Illinois.

Sheehan, M. J., S. M.Tarr, and S. Tayabji (2004). *Instrumentation and Field Testing of Thin Whitetopping Pavement in Colorado and Revision of the Existing Colorado Thin Whitetopping Procedure*. Report No. CDOT-DTD-R-2004-12.: Colorado Department of Transportation., Denver, CO.

Smith K.D., Yu H.T. and D.G. Peshkin. (2002) *Portland Cement Concrete Overlays: State of the Technology Synthesis*. Publication No. FHWA-IF-02-045, Federal Highway Administration, McLean, VA.

Tarr, S.M., Sheehan, M. J. and Ardani A. (2000), "Mechanistic Design of Thin Whitetopping Pavements in Colorado". In *Transportation Research Record No. 1730*, Transportation Research Board, Washington, D.C., pp. 64-72.

Tarr, S.M., Sheehan, M. J. and Okamoto, P.A. (1998) *Guidelines for the Thickness Design of Bonded Whitetopping Pavement in the State of Colorado*. Final Report No. CDOT-DTD-R-98-10, Colorado Department of Transportation, Denver.

Zollinger D., Tayabji S., Smith K. and H.T.Yu (2001). *Repair and Rehabilitation of Concrete Pavement: State-of-the-Practice*. Volume 1, Report No. FHWA-01-C-00080.

